University of Valladolid
Department of Condensed Matter Physics, Crystallography and Mineralogy.

Templated Hydroxyapatite Nucleation and Growth at Physiological Conditions onto Self-assembled Elastin-Like Nanoparticles.

By

Mohamed Hamed Misbah
Department of
Condensed Matter Physics, Crystallography and Mineralogy
G.I.R. Bioforge

A Master Thesis Submitted in Partial Fulfillment of Requirements for the Degree of M.Sc. in Molecular Nanoscience and Nanotechnology

Supervisor

Prof. J. Carlos Rodríguez-Cabello

Professor of Condensed Matter Physics, Crystallography and Mineralogy

School of Industrial Engineering

University of Valladolid

2013

University of Valladolid
Department of Condensed Matter
Physics, Crystallography and Mineralogy.

Supervisor

Thesis title:

Templated Hydroxyapatite Nucleation and Growth at Physiological Conditions onto Self-assembled Elastin-Like Nanoparticles.

Researcher name: *Mohamed Hamed Misbah Elzehiri*

Supervisor: *Prof. J. Carlos Rodríguez-Cabello*
Professor of Condensed Matter Physics,
Crystallography and Mineralogy
School of Industrial Engineering
University of Valladolid

Supervisor Signature

University of Valladolid
Department of Condensed Matter
Physics, Crystallography and Mineralogy.

Referees Committee Discussion

Thesis title:

Templated Hydroxyapatite Nucleation and Growth at Physiological Conditions onto Self-assembled Elastin-Like Nanoparticles.

Researcher name: *Mohamed Hamed Misbah Elzehiri*

Referees Committee:

President	*Prof. José Antonio de Saja Sáez*	*Condensed Matter Physics, Crystallography and Mineralogy University of Valladolid*
Vocal	*Prof. Miguel Ángel Rodríguez Pérez*	*Condensed Matter Physics, Crystallography and Mineralogy University of Valladolid*
secretary	*Prof. Maria Luz Rodríguez Méndez*	*Physical Chemistry and Inorganic Chemistry. University of Valladolid*

Note

The present thesis is submitted to Valladolid University in partial fulfillment for the requirements of M. Sc. degree in Molecular Nanoscince and Nanotechnology. The courses during the academic years (2011-2013) are:

1er COURSE

LEVEL COURSE		
B0	M0	Introduction to the Master in Molecular Nanoscience and Nanotechnology.
BASIC COURSE		
B1	Nanoscience Fundamentals: Concepts of nanochemistry and nanophysics. Characterization techniques	
	M1	Fundamentals of Nanophysics.
	M2	Fundamentals of Nanochemistry.
	M3	Characterization Techniques for Nanoscience.
B2	Molecular nanostructures and nanomaterials: methods of preparation, properties and applications.	
	M4	Preparation methods I: Supramolecular chemistry and bottom-up approach.
	M5	Preparation methods II: Approximation down for nanofabrication.
	M6	Molecular nanomaterials

2nd COURSE

ADVANCED COURSE		
B3	M7	Use of supramolecular chemistry for the preparation of nanomaterials and nanostructures.
B4	Electronics and molecular magnetism: basic concepts, major developments and applications.	
	M8	Introduction to molecular electronics.
	M9	Unimolecular Electronics
	M10	Molecular nanomagnetism
B5	M11	Current Issues in Molecular Nanoscience and Nanotechnology.

ACKNOWLEDGEMENTS

In the name of ALLAH, the most Gracious and the most Merciful. Alhamdulillah, thanks and indebtedness are directed first and always to ALLAH for all his graves, without the power he gave me, the accomplishment of this work would have been certainly impossible.

Infinite thanks to my parents, thanks for their love and their support throughout my life. Thanks for both who tempered each other's advice to give me the right mix of keeping my feet on the ground and reaching for the stars (Be the best!).

Thank very much to my supervisor, Prof. J. Carlos Rodríguez-Cabello for all the orientation and support given and making me going in the right direction during this work.

Thanks to G.I.R. Bioforge group, in this group I learned a lot of things from the first day. Thanks to Prof. Matilde Alonso Rodrigo, Prof. F. Javier Arias, Dr. Ana, Dr. Mercedes, Dr. Alessandra, Dr. Luis. My gratitude to my colleagues who finished their PhD, Dr. Laura, Dr. Menchu, Dr. Rosa, and for who making their PhD with me, María, Israel, Guillermo, Alicia, Piña, Ito, Arturo. My gratitude to Rocio, Irene and Vanesa.

Thanks to the coordination of the master, Prof. M. Luz Rodriguez Mendez.

I didn't can forget my professors, Prof. H. Doweidar and Prof. G. El-Damrawi in glass research group- Physics department – Mansoura university- Egypt, thanks to him who learned me the basis of the scientific research and what scientific research mean.

My gratitude to my friends and colleagues in my first group, Glass research group. My gratitude to my friends in the physics department at Mansoura University in Egypt.

My gratitude to my friends in Egypt and in Spain. Thanks for all of the people who learned me anything in my life.

Thanks a lot to my family that mean everything in my life that means the world to me, my parents, my uncle-aunty, my brothers and my sister. I extend my respect to my parents, my parental and maternal grandparents and all elders to me in the family. Thank you my mother, my father, my uncle and my aunty for showing love and faith in me. Really I am very lucky with this supportive family.

M. Hamed Misbah

" No wealth is more useful than intelligence and wisdom; no solitude is more horrible than when people avoid you on account of your vanity and conceit or when you wrongly consider yourself above everybody to confide and consult; no eminence is more exalting than piety; no companion can prove more useful than politeness; no heritage is better than culture; no leader is superior to Divine Guidance; no deal is more profitable than good deeds; no profit is greater than Divine Reward; no abstinence is better than to restrain one's mind from doubts (about religion); no virtue is better than refraining from prohibited deeds; no knowledge is superior to deep thinking and prudence; no worship or prayers are more sacred than fulfillment of obligations and duties, no religious faith is loftier than feeling ashamed of doing wrong and bearing calamities patiently; no eminence is greater than to adopt humbleness; no exaltation is superior to knowledge; nothing is more respectable than forgiveness and forbearance; no support and defense are stronger than consultation."

Ali Ibn Abi Taleb

For my Parents

The present work was granted by the following research project:

Development of highly functional materials and systems from recombinamers having a complex molecular architecture.

Funded by: Ministry of Science and Innovation. National R + D + i 2008-2011.
MAT-2010-15310.
Entity: University of Valladolid.
Period: 2011 to: 2013.
IP Prof. J. Carlos Rodriguez Cabello

Contents

Abstract

Studying materials in the nanosize scale lead to develop new synthetic approaches and discover a lot of new properties, and therefore manipulating to develop new materials that are used for different applications. In the nanoscale, physics, chemistry, biology, material science and engineering converge toward the same principles and tools. In this work, nanoparticles that developed genetically have been used to form hydroxyapatites.

Polymers such as elastin-like polymers can be manipulated by the bottom-up approach to form nanoparticles and also by top-down to form patterns in scales of nanometers on the polymer hydrogel.

The first aim of this work is to synthesis a nanoparticles and characterizing it. These nanoparticles are synthesized from amphiphilic elastin-like copolymers that exhibit a lower critical solution temperature, (LCST), and under the effect of the environmental stimuli could show a transition from soluble phase to insoluble phase. Below this transition temperature, in aqueous solution, the polymers chains are hydrated and extended by the hydrophobic interaction. Above this transition temperature, the chains can be assembled to form a phase separated state and adopt a dynamic, regular and nonrandom structure.

Due to the self-assembly properties of thess amphiphilic elastin-like polymers at low temperature, recombinant DNA genetic engineering has been used to recombine it with SN_A15 fragment. The SN_A15 fragment is the first fifteen amino acid from salivary protein statherin wherein the two phosphoserine amino acid residues at positions 2 and 3 have been substituted by L- aspartic acid. This fragment has a negative charge and a helical structure in all solvents that has a high affinity to nucleate and promote the crystallization of hydroxyapatites. The amphiphilic block copolymer has been recombined with three and six fragments of SN_A15. These polymers have been characterized in ultra-pure deionized water by using differential scanning calorimetry and light

scattering; furthermore, have been characterized in the solid state by Fourier Transform Infrared Spectroscopy (FTIR).

The second aim of this work is using these nanoparticles as a template to form nanoparticles of calcium phosphates under physiological conditions. The elastin-like polymers assembled to nanoparticles that are able to form calcium phosphate in SBF at 37^{o}C. Electron microscopy used to study the formed nanoparticles of calcium phosphate by performing electron diffraction and elemental analysis over the nanoparticles. Also, the calcium phosphates formed have been investigated using X-ray to identify the formed phases of calcium phosphate. Furthermore; the formed nanocalcium phosphates and its effect on polymer structure have been studied by FTIR spectroscopy.

Chapter 1

Background

1.1 Introduction to nanoscince

Nanoscience is the since that study the phenomena and manipulation of materials at atomic, molecular and macromolecular scales, which is derived from the distance of a nanometre (nm), one-billionth of a meter, 10^{-9} m.

In physics and electrical engineering, nanoscience is related to the quantum behavior and the behavior of photons and electrons in the nanoscale structures.[1] In chemistry, nanoscince is associated with the size of polymer molecules[2], phase separated polymers[3-4], colloids[5] and micelles[6-7] etc... In biology and biochemistry, the nanostructures of components of the cell have to be interested structures from DNA and viruses to subcellular organelles and gap junctions that are nanostructures.[8-9] The properties of materials in smaller size are different from the properties in bulk size, where the properties of materials are size-dependent. The types of size-dependent are surface effects and quantum effects.[10]

1.1.1 Types of size-dependent effects on materials properties

1.1.1.1 Surface effects

Surface effects are so important because atoms at surfaces have fewer neighbors than atoms in bulk. Because of this lower coordination and unsatisfied bonds, surface atoms are less stabilized than bulk atoms. Also the fraction of atoms at the surface are depend on the size of the particles where the smaller the particle, the larger the fraction of atoms. The ratio between the surface area and the volume is defined as dispersion. The dispersion F on the surface of a sphere scale with the square of its radius r is inversely proportional

to the radius. The total number of atoms N in this sphere scales linearly with volume and so the dispersion F proportional to $N^{-1/3}$; Fig.1.1.[10]

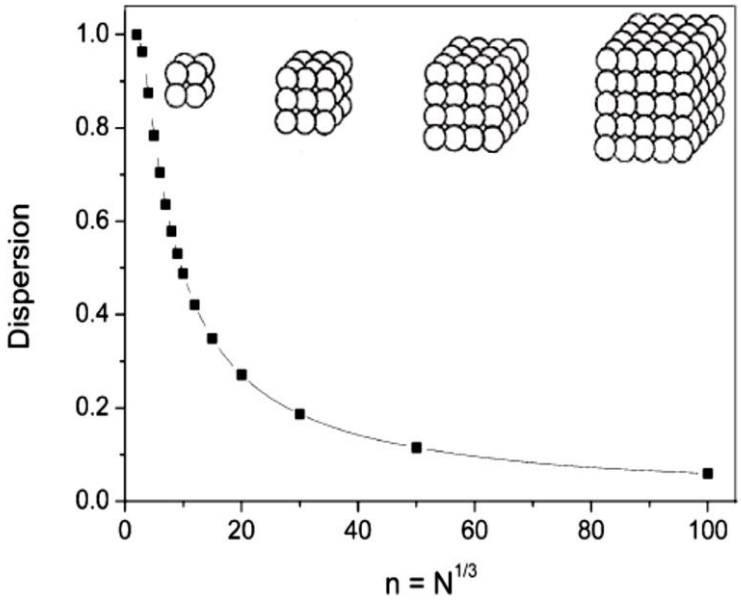

Fig.1.1: Evolution of the dispersion F as a function of n for cubic clusters up to n=100($N=10^6$). The structure of the first four clusters is displayed.[10]

1.1.1.2 Quantum effects

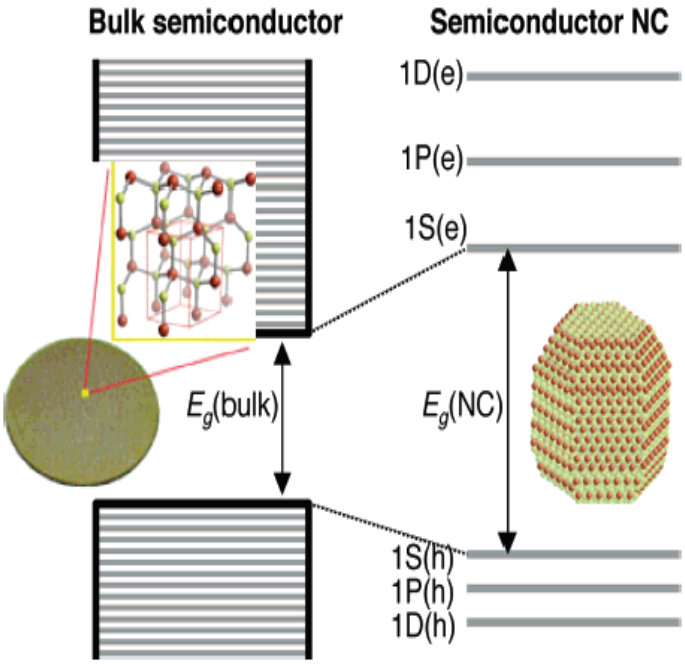

Fig.1.2: A bulk semiconductor has continuous condition and valence energy bands separated by a fixed energy gap, E_g, while a semiconductor NC is characterized by discrete atomic-like states and an NC size dependent energy gap.[1]

Quantum effects are dominating the behavior of matter at the Nano-scale particularly at the lower end. In a bulk semiconductor there are energy levels and so many close to each other formed a system of continuous energy called band. By contrast, the energy levels of electrons in the semiconductor nanoparticles are far apart, as shown in Fig.1.2.[1]

1.1.2 Manipulating nanoscience approaches

1.1.2.1 Top-Down approach

In this approach (physics); there are smaller pieces of matter is manipulated by photolithography and related techniques. This approach is subject to drastic limitations for dimensions smaller than 100 nm.[11,12] Therefore, "there is plenty of room at the bottom for further miniaturization" is for Richard Feynman[13] stated in a famous talk to the American Physical Society in 1959.

1.1.2.2 Bottom-up approach

This approach (chemistry) starts from nanoscale or subnanoscale objects to build up nanostructures.[14-15] This method includes the technique of molecular synthesis[15], polymer science[2], colloid chemistry[5] and the related areas for making structures with nanometer scales.

1.2 Polymers material

Polymers such as elastin-like polymers (ELPs) can be manipulated by the bottom-up approach to form nanoparticles[6, 16] and also by top-down to form patterns in scales of nanometers on the polymer hydrogel[12].

Polymers consist of large molecules, i.e. macromolecules. According to the basic IUPAC definition (Metanomski 1991): "A polymer is a substance composed of molecules characterized by the multiple repetition of one or more species of atoms or groups of atoms (constitutional repeating units) linked to each other in amounts sufficient to provide a set of properties that do not vary markedly with the addition of one or a few of the constitutional repeating units."[17]

A polymer can be a three-dimensional network or two-dimensional network or one-dimensional network.[18] There are many types of polymers including synthetic and natural polymers.

1.2.1 Synthetic polymers, for examples

- Plastics.[19-20]
- Elastomers - solids with rubber-like qualities.[21-22]
- Fibers.[23]

1.2.2 Natural biopolymers, for examples

- Polypeptides in proteins[24]-silk[25], Collagen[26], Keratin[27-28].
- Polysaccharides[24](Carbohydrates)[29] - Cellulose[30], Starch[31], Glycogen[32].
- Nucleic acids[33] - DNA[34] and RNA[35].

This study will be concentrated on the natural biopolymers, specifically elastin-like polymers that have amino acid as building blocks (polypeptides).

1.3 Natural amino acids

An amino acid is an organic compound containing an amino group and an acidic group, where there are 20 natural amino acids.[36] The amino acids that constitute proteins are all α-amino acids[37]. The "α-carbon" is bonded to four different groups: an amino group, a carboxylic acid, hydrogen, and the side chain as shown in the following schematic:

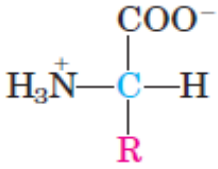

Because these are four different chemical groups, the α-carbon is chiral, (Stryer,1988).[38-39] For identifying the carbon in the amino acid, the "first" carbon of the amino acid is the carboxylate carbon. The next carbon is called the α-carbon, because it is in the position α- to the first carbon. The side chain is then bonded to the α-carbon. The side-chain carbons are given Greek letters in the order β, γ, δ, ε counting away from the α-carbon; for example, in Lysine amino acid as shown in the following schematic:[39]

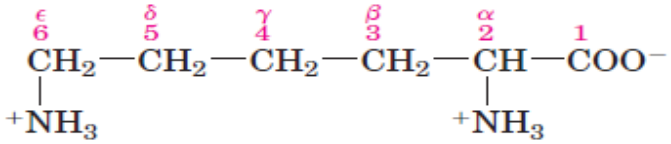

Lysine

The four different groups, a carboxyl group, an amino group, an R group, and a hydrogen atom, can occupy two unique spatial arrangements that are due to the tetrahedral arrangement of the bonding orbital around the α-carbon atom as shown in the following schematic:[39]

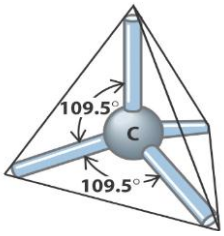

There are two possible stereoisomers where the α-carbon is the chiral center. All molecules with a chiral center are optically active, that is they rotate in a plane of polarized light. The two forms represent a class of stereoisomers called enantiomers as shown in Fig.1.3. The amino acid residues in proteins are L-stereoisomers. D-Amino acid residues have been found only in a few, generally small peptides, including some peptides of bacterial cell walls and certain peptide antibiotics.[38, 40-42]

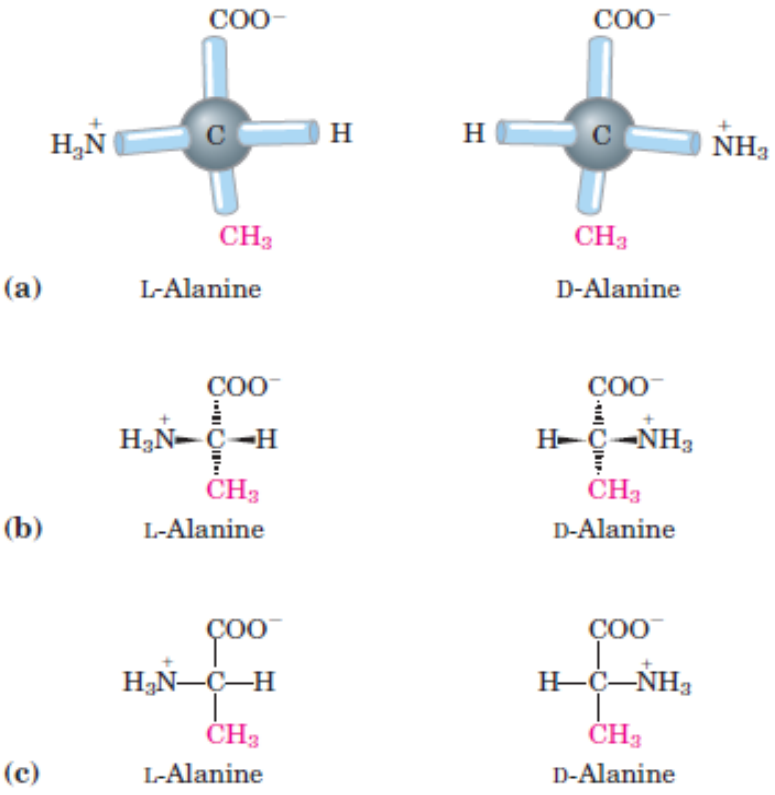

Fig.1.3: Stereoisomerism in α-amino acids. (a) The two stereoisomers of alanine, L- and D-alanine, are nonsuperimposable mirror images of each other (enantiomers). (b, c) Two different conversions for showing the configurations in space of stereoisomers. In perspective formulas (b) the solid wedge-shaped bonds project out of the plane of the paper, the dashed bonds behind it. In the projection formulas (c) the horizontal bonds are assumed to project out of the paper, the vertical bond behind. However, projection formulas are often used casually and are not always intended to portray a specific stereochemical configuration.[39]

1.3.1 Amino acids classified by R group

The following table shows the amino acids into five main classes based on the properties of their R groups (Table 1.1), in particular, their polarity, or tendency to interact with water at biological pH (near pH 7.0).

Table.1.1: properties and conventions associated with the common amino acids found in proteins:[39]

			pK_a values					
Amino acid	Abbreviation/ symbol	M_r	pK_1 (—COOH)	pK_2 ($—NH_3^+$)	pK_R (R group)	pI	Hydropathy index*	Occurrence in proteins (%)†
Nonpolar, aliphatic R groups								
Glycine	Gly G	75	2.34	9.60		5.97	−0.4	7.2
Alanine	Ala A	89	2.34	9.69		6.01	1.8	7.8
Proline	Pro P	115	1.99	10.96		6.48	1.6	5.2
Valine	Val V	117	2.32	9.62		5.97	4.2	6.6
Leucine	Leu L	131	2.36	9.60		5.98	3.8	9.1
Isoleucine	Ile I	131	2.36	9.68		6.02	4.5	5.3
Methionine	Met M	149	2.28	9.21		5.74	1.9	2.3
Aromatic R groups								
Phenylalanine	Phe F	165	1.83	9.13		5.48	2.8	3.9
Tyrosine	Tyr Y	181	2.20	9.11	10.07	5.66	−1.3	3.2
Tryptophan	Trp W	204	2.38	9.39		5.89	−0.9	1.4
Polar, uncharged R groups								
Serine	Ser S	105	2.21	9.15		5.68	−0.8	6.8
Threonine	Thr T	119	2.11	9.62		5.87	−0.7	5.9
Cysteine	Cys C	121	1.96	10.28	8.18	5.07	2.5	1.9
Asparagine	Asn N	132	2.02	8.80		5.41	−3.5	4.3
Glutamine	Gln Q	146	2.17	9.13		5.65	−3.5	4.2
Positively charged R groups								
Lysine	Lys K	146	2.18	8.95	10.53	9.74	−3.9	5.9
Histidine	His H	155	1.82	9.17	6.00	7.59	−3.2	2.3
Arginine	Arg R	174	2.17	9.04	12.48	10.76	−4.5	5.1
Negatively charged R groups								
Aspartate	Asp D	133	1.88	9.60	3.65	2.77	−3.5	5.3
Glutamate	Glu E	147	2.19	9.67	4.25	3.22	−3.5	6.3

*A scale combining hydrophobicity and hydrophilicity of R groups; it can be used to measure the tendency of an amino acid to seek an aqueous environment (- values) or a hydrophobic environment (+ values), see Chapter 11. From Kyte, J. & Doolittle, R.F. (1982) A simple method for displaying the hydropathic character of character of a protein. J.Mol. Biol. 157, 105-132.

†Average occurrence in more than 1,150 proteins. From Doolittle, R.F. (1989) Redundancies in protein sequences, in Prediction of protein Structure and the Principles of Protein Conformation (Fasman, G.D., ed.), pp. 599-623, Plenum Press, New York.

Fig.1.4 shows the structures of the 20 common amino acids and some of their properties are listed in Table 1.1. Within each class, there are gradations of polarity, size, and shape of the R groups.

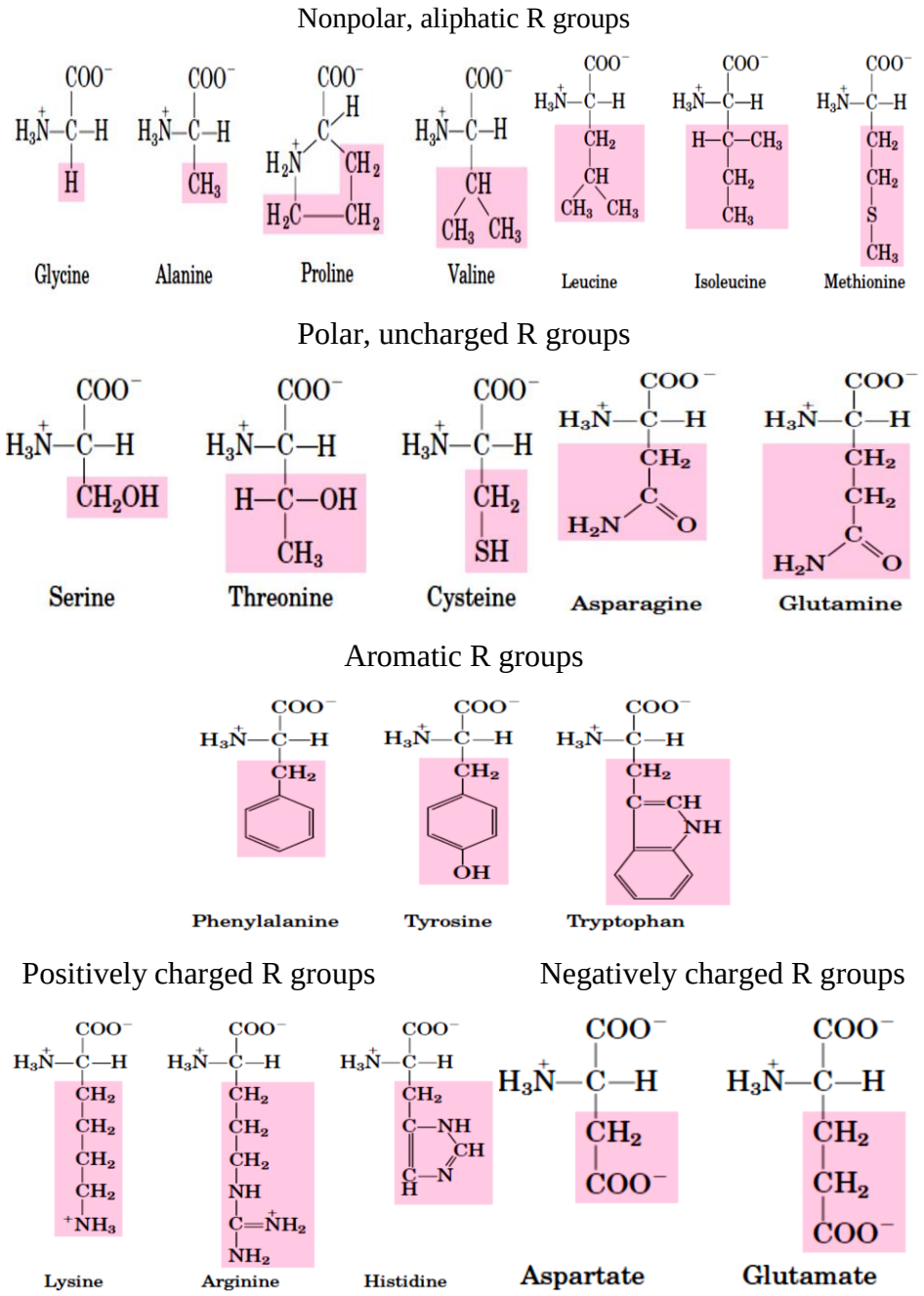

Fig.1.4: The 20 common amino acids of proteins. The structural formulas show the state of ionization that would predominate at pH 7.0. The undashed portions are those common to all the amino acids; the portions shaded in red are the R groups. Although the R group of histidine is shown uncharged, its pK_a (see table.1.) is such that small but significant of these groups are positively charged at pH 7.0.[39]

The amino acids are joined end to end through covalent linkage. The α-carboxyl group of the first amino acid reacts with the α-amino group of the next amino acid to generate a peptide bond and eliminate a water molecule as shown in Fig.1.5.

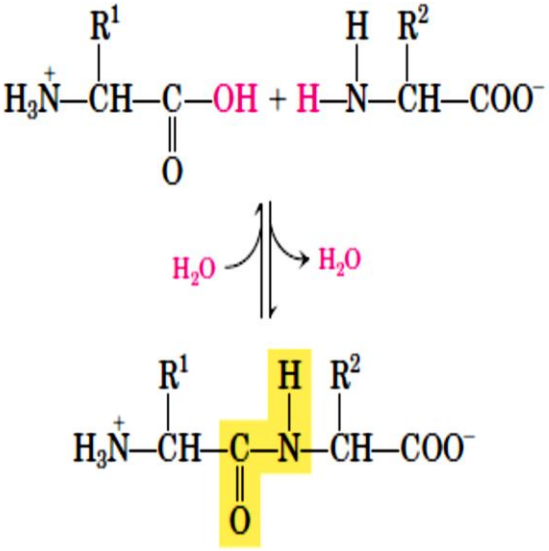

Fig.1.5: Formation of a peptide bond by condensation. The α-amino group of one amino acid (with R^2 group) acts as a nucleophile to displace the hydroxyl group of another amino acid (with R^1 group), forming a peptide bond (shaded in yellow). Amino groups are good nucleophiles, but the hydroxyl group is a poor leaving group and is not readily displaced. At physiological pH, the reaction shown does not occur to any appreciable extent.[39]

Fig.1.6 shows the structure of a pentapeptide that has two different ends, termed respectively the N-terminus and the C-terminus. A polypeptide chain consists of a regularly repeating part, called the 'main chain' or 'backbone', from which projects a variable part comprising the different side chains. Protein structure is divided into four levels complexity[43-44] as concluded in Fig.1.7.

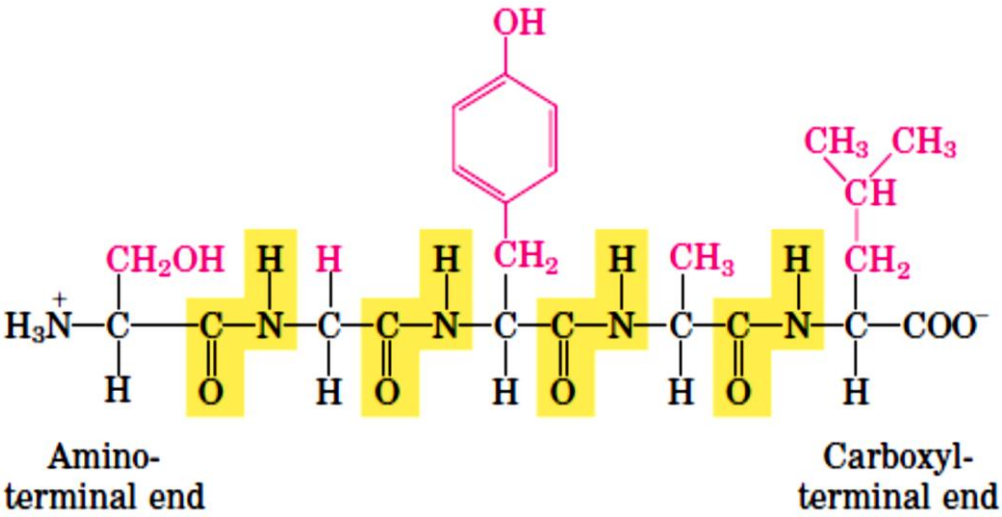

Fig.1.6: The pentapeptide serylglycyltyrosylalanylleucine, or Ser-Gly-Tyr-Ala-Leu. Peptides are named beginning with the amino-terminal residue, which by convention is placed at th left. The peptide bonds are shaded in yellow; the R groups are in red.[39]

1.3.2 Four levels complexity of protein structure

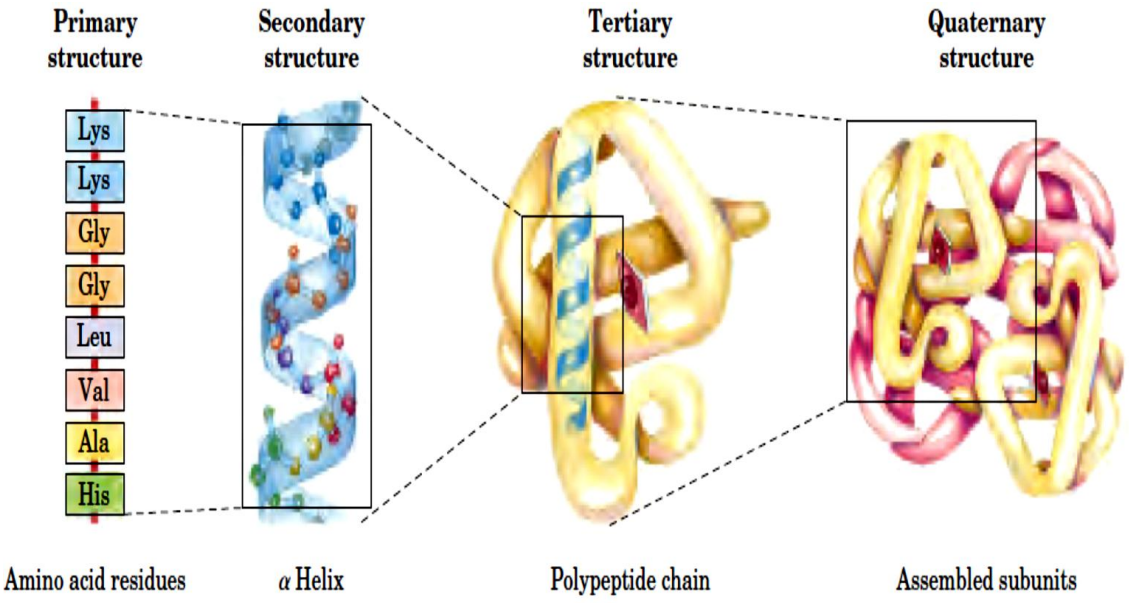

Fig.1.7: Levels of structure in proteins. The primary structure consists of a sequence of amino acids linked together by peptide bonds and includes any disulfide bonds. The resulting polypeptide can be coiled into units of secondary structure, such as an α-helix. The helix is a part of the tertiary structure of the folded polypeptide, which is itself one of the subunits protein, in this case hemoglobin.[39]

1.3.2.1 Protein primary structure

The primary structure of the protein is the linear sequence of amino acids that linked by the covalent bonds, mainly peptide bond and disulfide bond.[39, 43-45] The α-carbons of adjacent amino acid residue are separated by three covalent bonds, arranged as C_α-C-N-C_α. It is found from X-ray diffraction studies of crystals of the amino acids and of simple dipeptides and tripeptides that the peptide C-N bond is somewhat shorter than the C-N bond in a simple amine, and all the atoms associated with the peptide bond are coplanar, which mean that the carbonyl oxygen and the amide nitrogen are partially shared by two pairs of electrons. Furthermore, a small electric dipole produced due to the partial negative charge of oxygen and the nitrogen positive charge.[39, 46-47]

Theoretically, the planar peptide bond can take trans and cis configurations, Fig.1.8, but trans form is favored energetically than cis form. The rotation of the peptide bond CO-NH is restricted because of its partial double bond character due to the resonance (Fig.1.9a.). But for the single bonds that link each C_α atom to the N and C atoms of the peptide bonds show free rotation; the angle of rotation around the N–C_α bond is phi (ϕ) and the angle of rotation around the C_α–C bond from the C_α-atom is psi (Ψ).[39, 48]

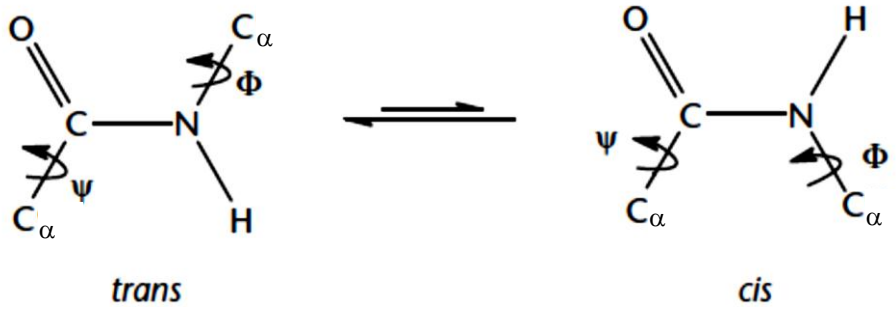

Fig.1.8: The configurations of trans and cis forms of the peptide bond CO-NH with the angle of rotation around the N–C_α bond is phi (ϕ) and the angle of rotation around the C_α–C bond from the C_α-atom is psi (Ψ).[48]

When the polypeptide is in its fully extended conformation and all peptide groups are in the same plane, both (ϕ) and (Ψ) can be defined as 180° (Fig.1.9b).[39] In principle, ϕ and Ψ can take any value between 180° and -180°, but the conformation at 0 of both ϕ and Ψ (Fig.1.9c) not permitted and this conformation is used as a reference point for determining the angle of rotation.[39]

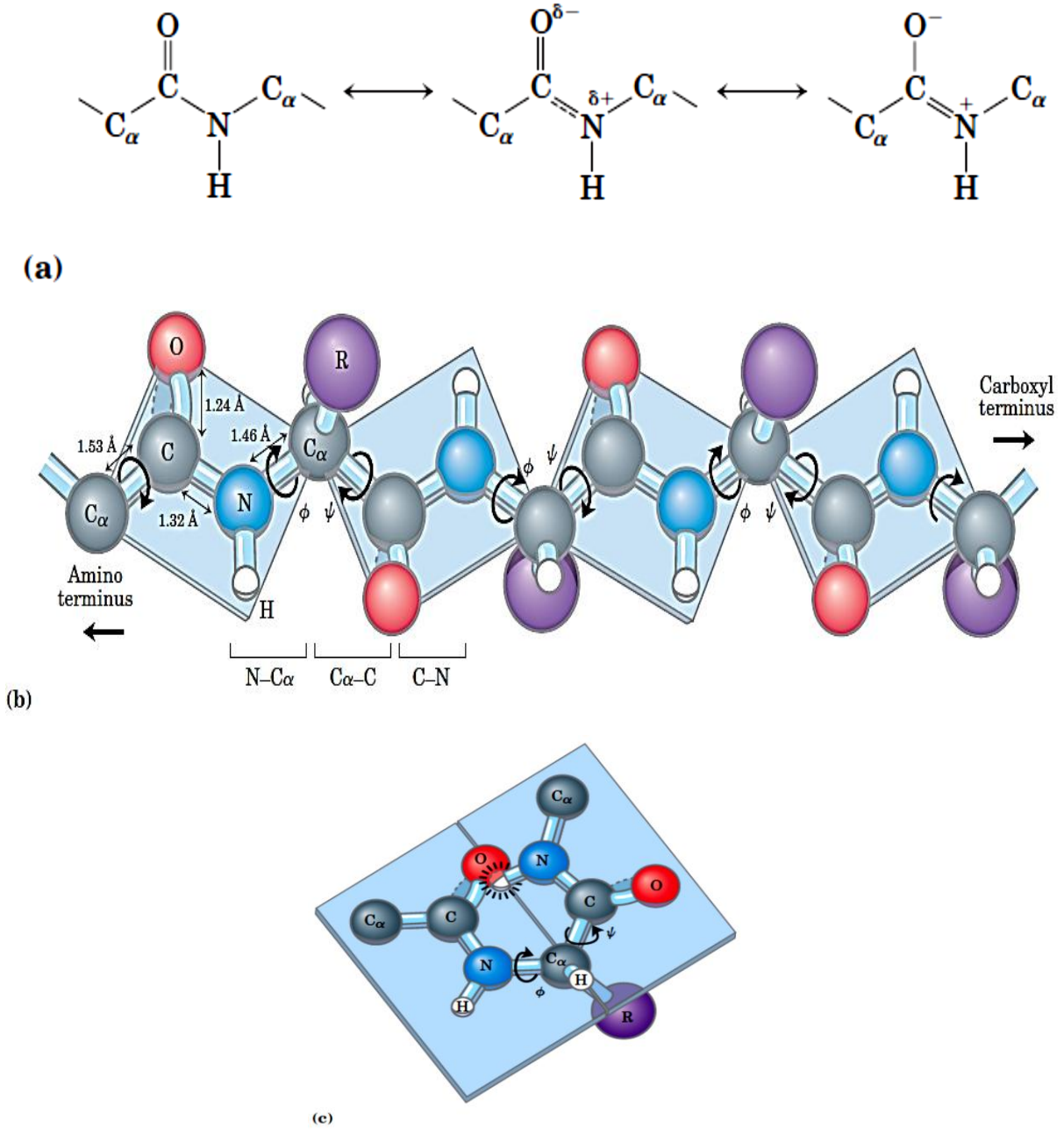

Fig.1.9: The planar peptide group. (a) Each peptide bond has some double-bond character due to resonance and cannot rotate. (b) Three bonds separate sequential α carbons in a polypeptide chain. The N-C_α and C_α-C bonds can rotate, with bond angles designed ϕ and Ψ,

respectively. The peptide C-N bond is not free to rotate. Other single bonds in the backbone may also be rotationally hindered, depending on the size and charge of the R groups. In the conformation shown, ϕ and Ψ are 180^o (or-180^o). As one looks out from theα carbon, the Ψ and ϕ angles increase as the carbonyl or amide nitrogen (respectively) rotate clockwise. (c) By convention, both ϕ and Ψ are defined as 0^o when the two peptide bonds flanking that α carbon are in the same plane and positioned as shown. In a protein, this conformation is prohibited by steric overlap between an α-carbonyl oxygen and an α-amino hydrogen atom. To illustrate the bonds between atoms, the balls representing each atom are smaller than the van der Waals radii for this scale. $1A^o$=0.1 nm.[39]

1.3.2.2 Protein Secondary Structure[39, 43-44, 48]

The side-chains of the amino acids of the proteins interact with one another or with the solvent to form the global structure of the protein, which is called Protein Secondary Structure. These interactions are non-covalent, that are;

1- Hydrogen bond that is resulted from hydrophilic amino acid, where the hydrogen atom that is connected covalently with an electronegative atom (donor) interact with another electronegativity atom (acceptor).
2- Electrostatic forces between net charges of opposite signs or between two dipoles.
3- Repulsion forces or van der Waals forces between electron orbitals of atoms.
4- Hydrophobic interactions, in which amino-acid residues, that engage in van der Waals interactions, have a tendency to repel with water and pack against each other.

The major two types of protein secondary structure are α-helices, and β-conformation.

1.3.2.2.1 The α-helix structure[39, 43, 48]

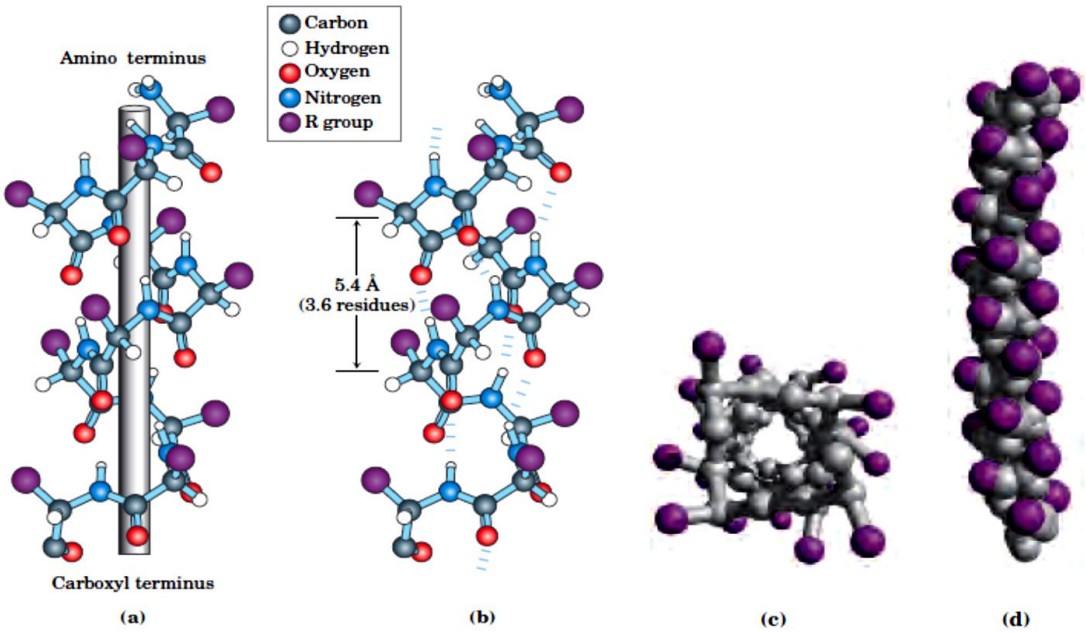

Fig.1.10. Four models of the α-helix, showing different aspects of its structure. (a) Formation of a right-handed α-helix. The planes of the rigid peptide bonds are parallel to the long axis of the helix, depicted here as a vertical rod. (b) Ball-and-sick model of a right-handed αhelix, showing the interaction hydrogen bonds. The repeat unit is a single turn of the helix, 3.6 residues. (c) The α-helix viewed from one end, looking down the longitudinal axis (derived from PDB ID 4TNC). Note the positions of the R groups, represented by purple spheres. This ball-and-sick model, used to emphasize the helical arrangement, gives the false impression that the helix is hollow, because the balls do not represent the van der Waals radii of the individual atoms. As the space-filling model (d) shows, the atoms in the center of the α-helix are very close contact.[39]

Fig.1.10 show a polypeptide chain arranged in a helical structure or α-helix structure. It is shown that the polypeptide backbone is tightly wound around an imaginary axis in the middle of the helix, and the R groups of the amino acids stand outward from the helical backbone. A single turn of the helix is the repeating unit which has a length of 5.4 Å. The helix is stabilized by hydrogen bonds with repeated torsion angle values of about -60^{o} for ϕ and -40^{o} to -45^{o} for Ψ. The hydrogen bond formed between the hydrogen atom that is

covalently bonded to the nitrogen atom of a peptide linkage and the carbonyl oxygen atom of the fourth amino acid from this peptide linkage (Fig.10b).

Each peptide bond possesses an individual dipole moment, and these dipoles are connected through the hydrogen bonds of the helix that resulting in a net dipole with a positive charge at the amino end and a negative charge at the carboxyl end as shown in Fig.1.11. The net dipole increases with the length of the helix.[39, 48]

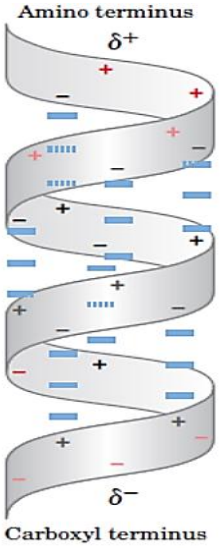

Fig.1.11: Helix dipole. The electric dipole of a peptide bond is transmitted along an α-helical segment through the intrachain hydrogen bonds, resulting in an overall helix dipole. In this illustration, the amino and carbonyl constituents of each peptide bond are indicated by + and – symbols, respectively. Non-hydrogen-bonded amino and carbonyl constituents in the peptide bonds near each end of the α-helical region are shown in red.[39]

1.3.2.2.2 The β-Conformation

The β-sheet structure[39, 43, 48]

A five to ten residues can form a strand of a rotation angle of -120^{o} for ϕ and of 140 for Ψ that is called β-strand. This β-strand is not stable structure and tend to interact with others β-strand of another region of the same polypeptide chain. These strands are interacted by hydrogen bonds forming β-sheet. The polypeptide chain backbone is arranged side by side by hydrogen bonds to form a pleated sheet that gives a zigzag polypeptide shape. The R groups of the amino acids stand outward from the zigzag structure in opposite directions as shown in Fig.1.12. Furthermore,

polypeptide chains can be arranged in a β-parallel sheets in which have the same amino to carboxyl orientations or β-antiparallel sheets in which have the opposite amino to carboxyl orientations.

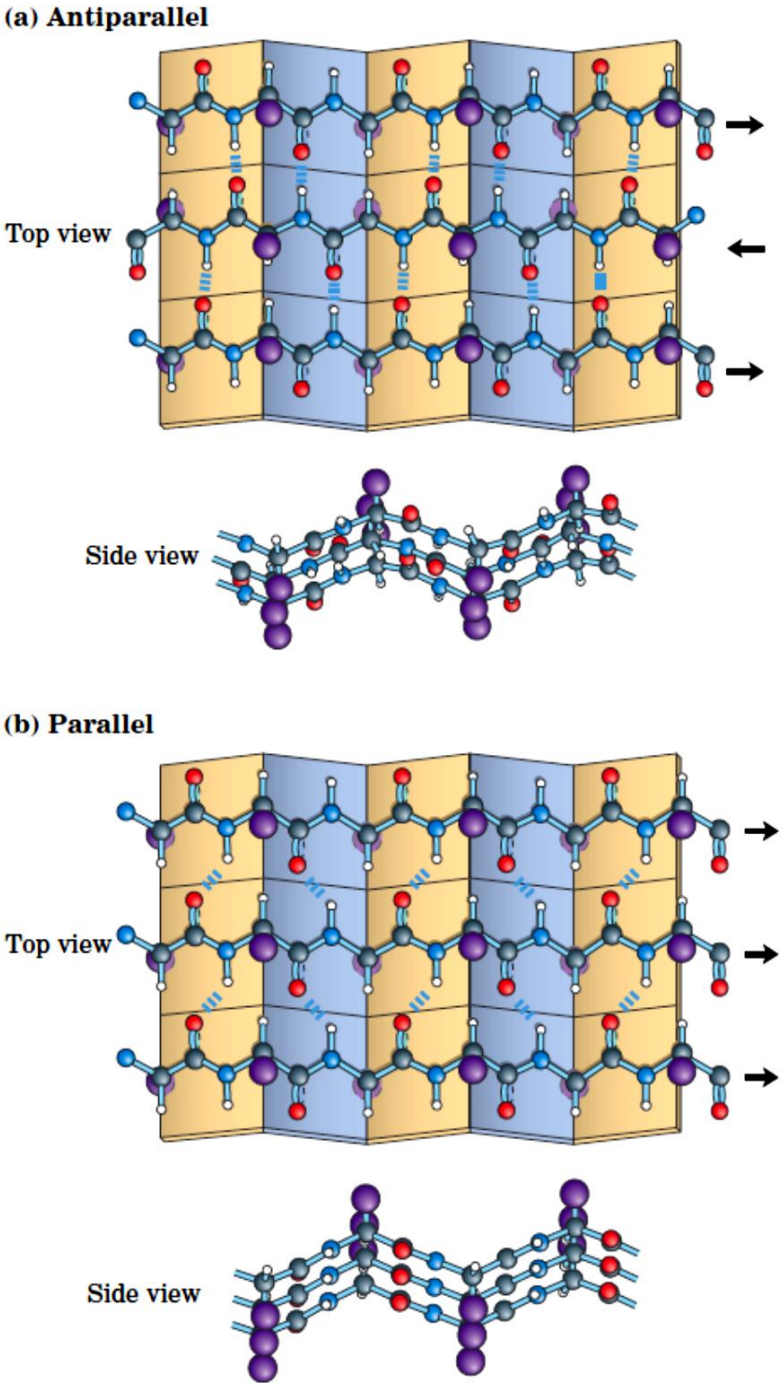

Fig.1.12: The β-conformation of polypeptide chains. These top and side views revels the R groups extending out from the β-sheet and emphasize the pleated shape described by the planes of the peptide bonds. (An alternative name for this structure is β-pleated sheet.) Hydrogen-bond cross-links between adjacent chains are also shown. (a) Antiparallel β-sheet,

in which the amino-terminal to carboxyl-terminal orientation of adjacent chains (arrows) is inverse. (b) Parallel β-sheet.[39]

The β-turn structure[39, 43]

At the ends of each segment of the β-sheet, there is a reverse turn or β-turn that makes the polypeptide chain turn back upon itself. There are amino acids are in turns or loops in which the polypeptide chain reverses their direction. These turns connect successive chains of α-helix or β-conformations. β-turns are the common turns that link two adjacent chains of an antiparallel β-sheet, which have a structure of 180^{o} turn where the carbonyl oxygen of amino acid residue form a hydrogen bond with the hydrogen atom, that bonded with the nitrogen atom, of the fourth amino acid residue, as shown in Fig.1.13.

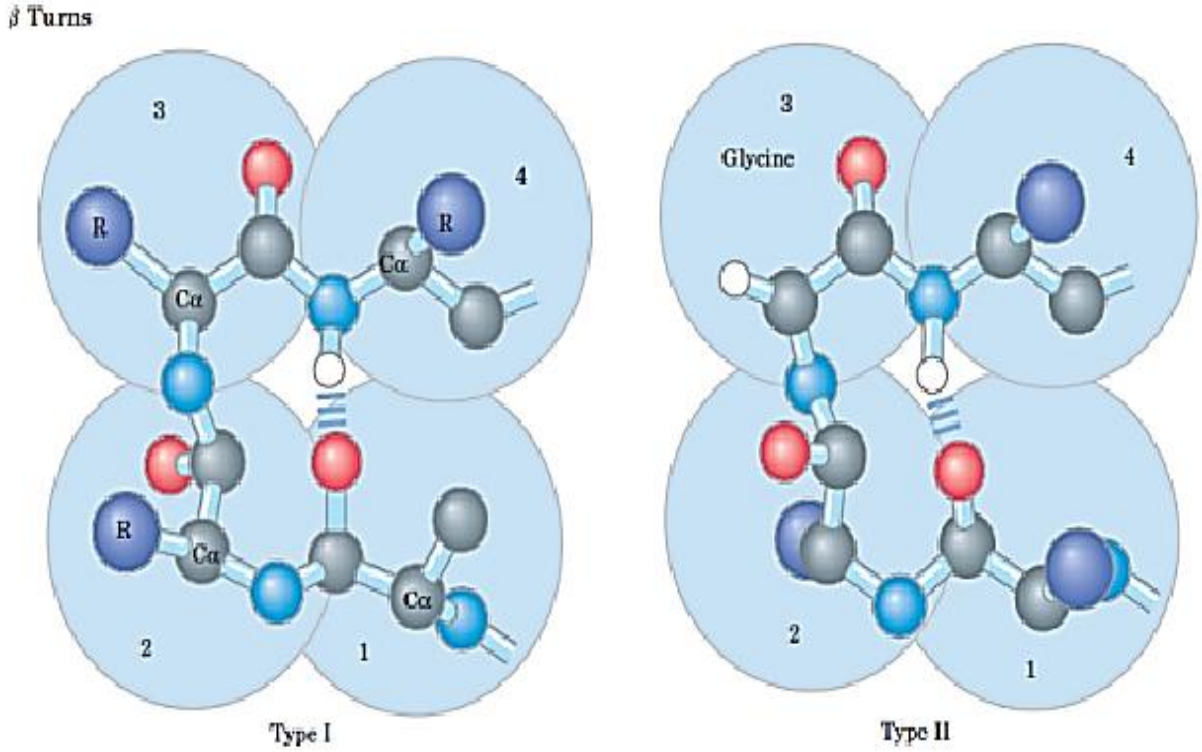

Fig.1.13: Structure of β turns. (a) Type I and type II β turns are most common; type I turns occur more than twise as frequently as type II. Type II β turns always have Gly as the third residue. Note the hydrogen bond between the peptide groups of the first and fourth residues of the bends. (Individual amino acid residues are framed by large blue circles.).[39]

1.3.2.3 Tertiary structure[39, 43-44, 48]

Tertiary structure of protein is the three-dimensional structure of proteins. The tertiary structure is determined by the packing of the secondary structure that is combined to form what is called domains, see Fig1.7. A single domain can have about 100-150 amino acid residues of about 25 Å diameter.

Protein structures can also be classified, by the types of structural motifs that formed the domains, into four main groups:

1- Proteins that have α-helices in an antiparallel or perpendicular arrangement.
2- Proteins, that have β-sheet where the β-strands are arranged in antiparallel manner.
3- α/β Proteins; that have β-sheets surrounded by α-helices.
4- α+β Proteins that are a combination of α and β motifs.

The tertiary level of structure refers to the spatial arrangement of a polypeptide chain through folding and coiling to produce a compact globular shape. The tertiary structure is essentially determined by the packing of the secondary structures, α-helices and β-sheets, which combine to form one or several units called ‘domains’. These combinations are limited in number, and some of them are especially frequent in proteins. They represent the fundamental elements of globular polypeptide chains in terms of three-dimensional structure as well as in terms of function. On average, a single domain consists of 100–150 amino acid residues, corresponding to a globule of about 25 Å diameters.

1.3.2.4 Quaternary structure[39, 43-44, 48]

When there are two or more separate polypeptide chains or subunits that are identical or different in some proteins, the structure that describes the spatial arrangement of these subunits in three-dimensional complexes is called quaternary structure, see Fig1.7.

1.4 Elastin like polymers (ELPs)

1.4.1 Definition of ELP

The amino acids that are arranged in the following sequences, LGGVG[49], GXGGX[50], APGVGV[51], AVGVP[52], KGGVG[53], LGAGGAG[54] and $VPGX_{aa}G$, in which X_{aa} can be any of the natural or synthetic amino acids except for Proline[55], sequence, they are called ELP. The most common ELP is $(VPGVG)_n$ that is considered a model for ELPs.[56]

1.4.2 The molecular basis of the inverse transition temperature of ELP

These polymers exhibit a lower critical solution temperature (LCST) and transition from soluble to insoluble in response to environmental stimuli.[55] This transition temperature is depending on the chemical composition, chain length, concentration, and architecture of the ELP in the solution.[57-59]

In aqueous solutions, before this transition temperature, the polymer chains are extended and hydrated by hydrophobic hydration (Fig.1.14a).[60-61] This hydration around its hydrophobic moiety is in ordered caged-like or clathrate structures surrounding the moieties of the polymer that are stabilized by hydrogen bonding (Fig.1. 14b).[60, 62]

After the transition temperature, the chains assemble to form a phase-separated state or to form a strong shrinkage and collapse of hydrogels.[60, 62-63] In this state, the polymer adopts a dynamic, regular, non-random structure, called β-spiral, formed by concatenation of adjacent type II β-turns and stabilized by intra-spiral, inter-turn and inter-spiral hydrophobic contacts (Fig.1.14c).[60, 64]

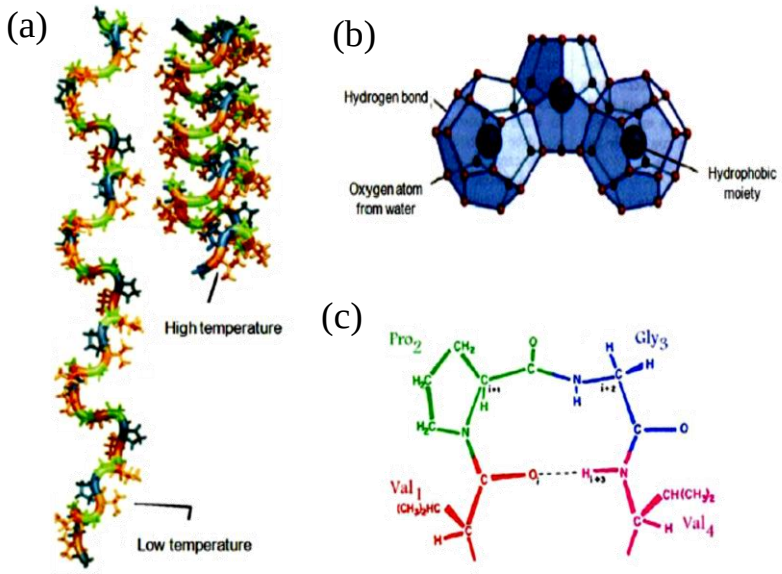

Fig.1.14: (a) schematic representation of the thermal transition of the ELPs between the extended state (low temperature) and the folded state (high temperature); (b) Water in clathrate-type structured state; (c) type II β-turn in the VPGVG pentapeptides.[65]

The transition temperature, T_t, can be measured by different techniques. The most used are turbidity measurements, also called measured of the "cloud point", or calorimetric methods that measure the heat flow during the transition. In Fig.1.15, the turbidity profile and the heat flow from a DSC measurement are plotted against the temperature.

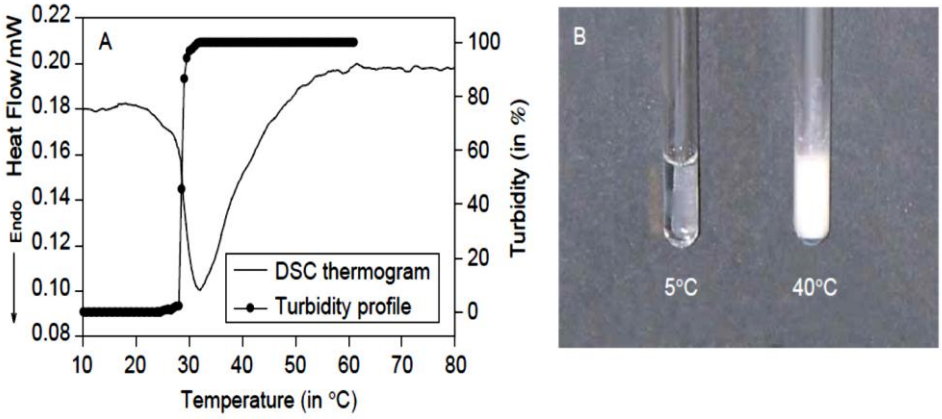

Fig.1.15. (A) Turbidity profile as a function of temperature for a poly(VPGVG) 5mg/ml sample dissolved in water and DSC thermogram of a 50mg/mL aqueous solution of the same polymer (heating rate 5°C/min). (B) Photograph of aqueous solution (5mg/mL) of this poly(VPGVG) below (5°C) and above (40°C) its T_t.[66]

1.4.3 Molecular structure of (VPGVG) ELP

Poly(GVGVP) or alternatively poly(VPGVG), is the parent elastic protein based polymer, has special advantages that can be used as the model system for studying and developing the principles of free energy transduction.[57]

According to Urry's model for ELP transition, the chains below their transition temperature start to form type II β-turn conformation as they closer to their transition temperature and then at the transition temperature they fold into a so called a β-spiral that is a helical arrangement of β-turns[67] as shown in Fig.1.16.

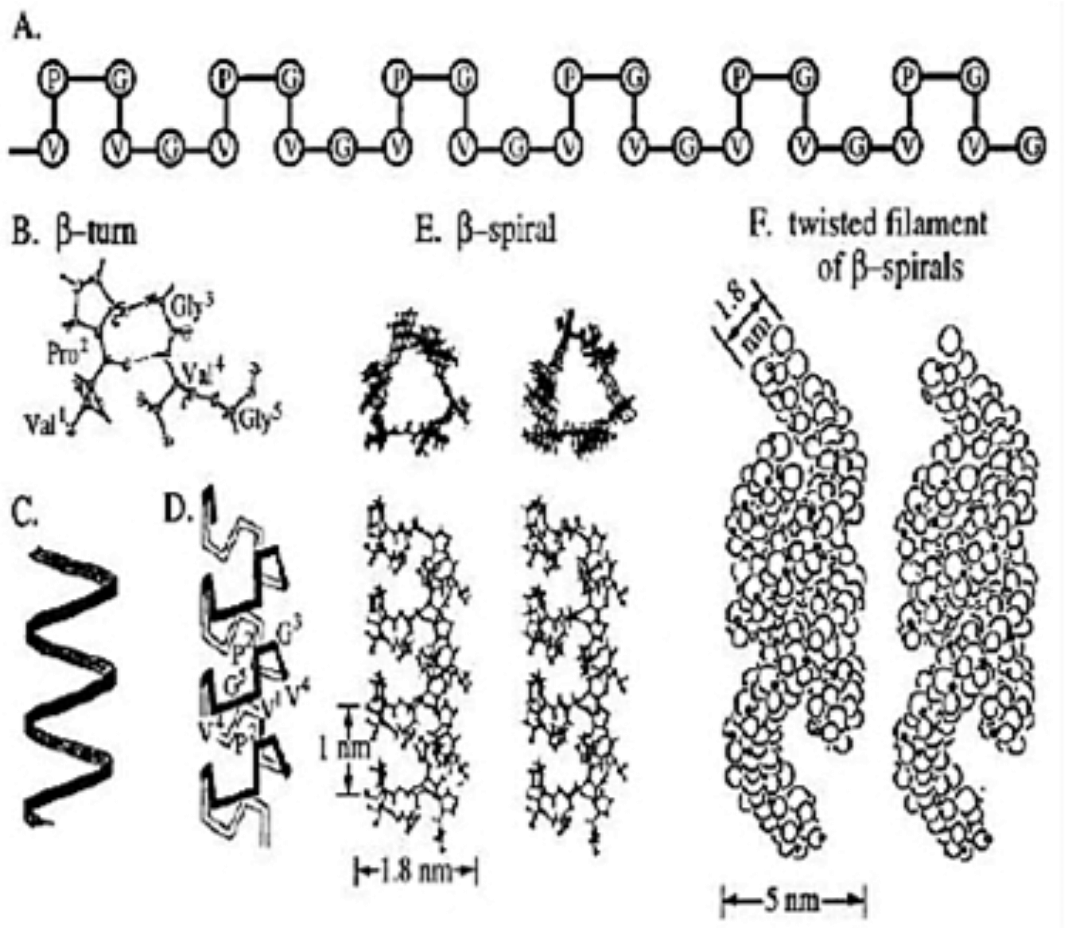

Fig.1.16: The formation of twisted filaments from folded ELP chains as suggested by Urry. The β-spiral formation from β-turns is belived to be precursor of ELP aggregation.[68]

Urry[69] showed that a polypentapeptide of $(VPGVG)_3$ in its crystalline state consists of three types II β-turns joined by V-G-V bridges. Depending on

these observations and on the (VPGVG) as the used elastin-like polypeptide, after that they employed circular dichroism (CD), NMR and dielectric relaxation studies to investigate the transition of unordered polypeptide chains at low temperatures to more ordered structures at temperatures above the transition temperature.[70-71] And then they suggested that this transition temperature is in accordance with their suggested phase diagram for ELP molecules[67] and there is a molecular change accompanied by the phase change in solution. But the later studies showed that the molecular structure change is a gradual process which starts at a temperature below the transition temperature.[72]

1.4.4 Hydrophobic nature of ELP

In general, as the mean polarity increases the transition temperature T_t increase. As well as, if the polymer chain has chemical groups that have two different states of polarity it will exhibit two different transition temperature values under the influence of an external stimulus.[60-61] As the Gibbs free energy, $\Delta G=\Delta H-T\Delta S$ and as the change in Gibbs-free energy, ΔG is zero, then $\Delta H=T_t\Delta S$ and then $T_t=\Delta H_t/\Delta S_t$. The ratio $\Delta H_t/\Delta S_t$ for a family of model proteins becomes dominated by differences in the interactions of the water solvent with a substituent residue of the protein-based polymer, that T_t depends on the hydrophobicity of the substituent residue as well as becomes a relative measure of the water numbers of hydrophobic hydration that change to bulk water during the transition.[57, 73] So that by increasing hydrophobicity lead to decreasing the transition temperature, T_t. Lowering transition temperature T_t to drive hydrophobic folding and assembly in the direct performance of mechanical work, or in hydrophobically shifting the properties of functional groups associated with the elastin like polymer or protein to achieve diverse energy outputs, that is defined as the ΔT_t-mechanism, and so this effect can be used to obtain interconvertible energy processes (Fig.1.17) .[55-56]

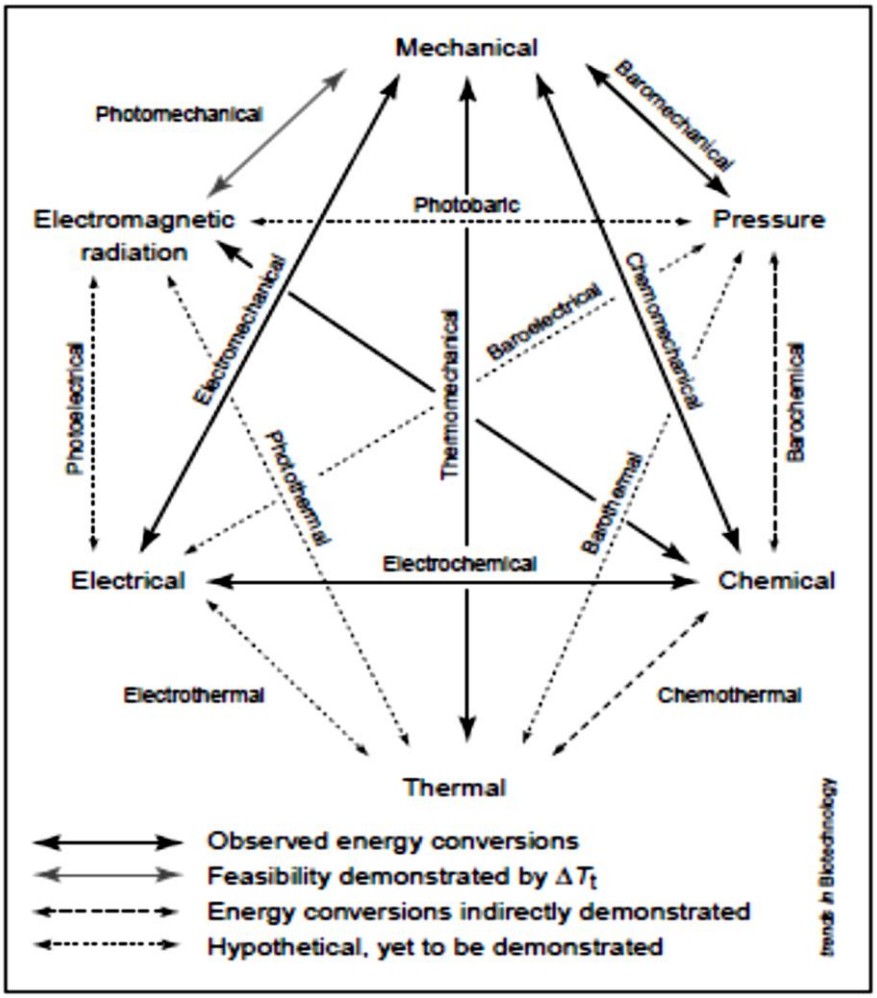

Fig.1.17: The ΔT_t hydrophobic paradigm for protein folding and function. The diagram indicates the pairwise interconversions of energies that are possible using molecular machines capable of inverse temperature transitions.[57, 74]

The hydrophobic paradigm, involving the inverse transition temperature, ITT, and the ΔT_t mechanism, for protein folding and function and the intrinsic capability of performing several energy interconversions allows new strategies for the development of ELP derivatives and working temperatures. Experimental studies on the ITT exhibited by ELPs and based on the factors that control hydrophobic folding and assembly of model proteins resulted in a set of five phenomenological axioms for the protein engineering of protein based polymers capable of inverse temperature transitions[62, 74]:

Axiom 1:

The temperature intervals for the hydrophobic folding and assembly transition of a host protein or protein based polymer with different guest substituents becomes a functional measure of their relative hydrophobicity.

Axiom 2:

Heating to raise the temperature from below, to above, the temperature interval for hydrophobic folding and assembly of macromolecules can drive contraction with the performance of mechanical work.

Axiom 3:

At a constant temperature, an energy input that changes the temperature interval for thermally-driven folding and assembly in a macromolecule can drive hydrophobic folding and self-assembly at a constant temperature.

Axiom 4:

Two or more different functional groups of a macromolecule, each of which can be acted upon by a different energy input that changes the temperature interval for hydrophobic folding and assembly, become coupled one to another by being part of the same hydrophobic folding and self-assembling domain, that is, the energy input acting on one functional constituent alters the property of another functional constituent as an energy output.

Axiom 5:

More hydrophobic domains make more efficient the energy conversions involving constituents undergoing conversion between more and less hydrophobic states.

The phase transition behavior and mechanical properties of ELPs depend critically on the identity of the residues X_{aa} and Y_{aa} in the polypentapeptide sequence [(Phe/Val/Ile)-Pro-Y_{aa}-X_{aa}-Gly]. There are two types of substitutions: those that adjust hydrophobicity and those that instill functionality.[75] This functionality depends on the conformational changes that some amino acids

undergo due to environmental conditions (residues like lysine, aspartic acid and glutamic acid).[75] However, this substitution is not straightforward with the risk of losing functionality. ELPs can accept substitutions in either of the two Valine positions. The first position in the polypentapeptide, reported so far, only accepts Val, Phe or Ile amino acids, as an example, APGVG rather than reversibly forming a viscoelastic coacervate, irreversibly forms a granular precipitate when the temperature is raised.[76] But a change from a Val to Ile leads to some structural changes; when comparing poly(VPGVG) with poly(IPGVG), with an extra CH_2 group per pentamer but still retaining β-branching, the transition temperature is lower in the latter case due to the increase in hydrophocity accompanied by an increase in the heat of the transition.[76] This last statement is a result of the increase in the endothermic heat, necessary to drive the transition, as it is required more energy to destructure the higher number of water structures from hydrophobic hydration. Additionally, reported so far, the last Gly does not accept any substitutions, i.e., the substitution of the fifth residue by an Ile or Ala residue, inserting extra CH_2 moieties in the side chain will lead to loss of elastic properties completely.[77]

Alterations in the fourth residue, X_{aa}, modulate the values of T_t in aqueous solution, depending on the polarity of the amino acid side chain. While X_{aa} accepts many isomorphic substitutions, Y_{aa} does not accept other amino acids than glycine or L- Ala.[60, 78] This is because, according to Urry, there is a type II β-turn per pentamer that involves the glycine of the basic VPGVG in the folded state of the polymer. The presence of bulky moieties of amino acids with L chiralty impedes the formation of the β-turn leading to non-functionality. Although the substitution of Yaa by L-alanine is the only possibility, reported so far, the resulting polymer shows significant different mechanical and thermal properties.[60]

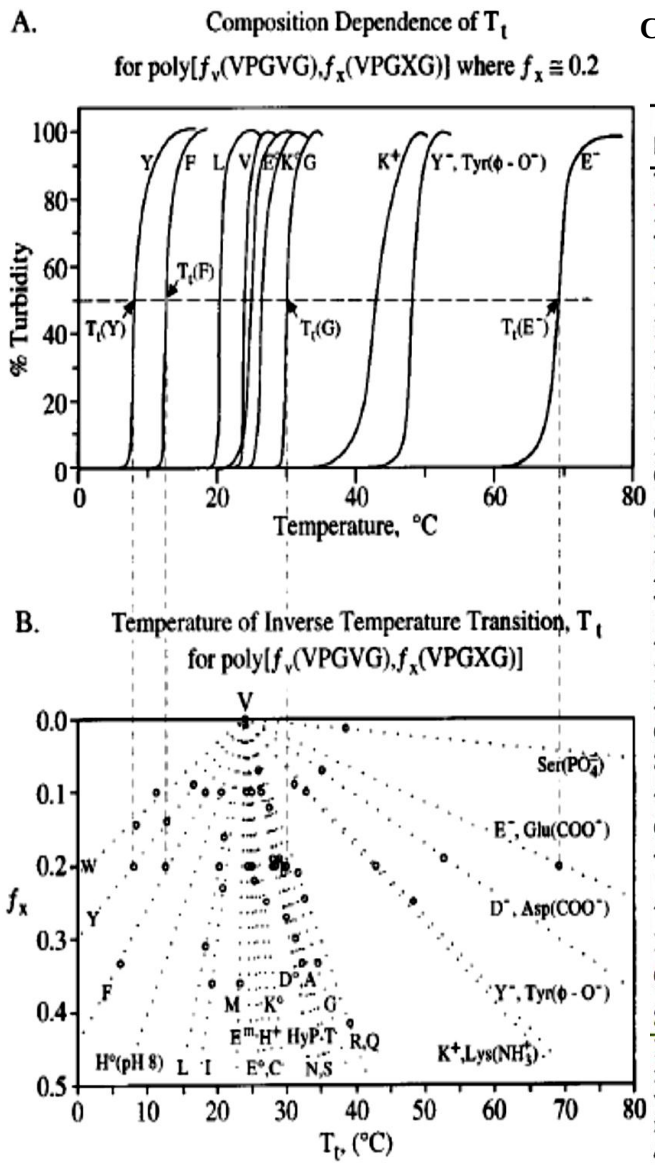

C

Residue X	$T_{b(t)}$°C	$\Delta G°_{HA}(\chi)$/kcal/mol pentamer
Trp	-105	– 7.00
Phe	-45	– 6.15
Tyr	-75	– 5.85
His°	-10(T_t)	– 4.80 (from graph)
Leu	5	– 4.05
Ile	10	– 3.65
Val	26	– 2.50
Met	15	– 1.50
His$^+$	30 (T_t)	– 1.90 (from graph)
Cys	30 (T_t)	– 1.90 (from graph)
Glu(COOH)	20 (2)	– 1.30 (– 1.50)
Pro	40	– 1.10
Ala	50	– 0.75
Thr	60	– 0.60
Asp(COOH)	40	– 0.40
Lys(NH_2)	40 (38)	– 0.05 (– 0.60)
Asn	50	– 0.05
Gly	55	0.00
Ser	60	+ 0.55
Arg	60 (T_t)	+ 0.80 (from graph)
Gln	70	+ 0.75
Tyr(ϕ-O$^-$)	140	+ 1.95
Asp(COO$^-$)	170 (T_t)	≈ + 3.4 (from graph)
Lys(NH_3^+)	(104)	(+ 2.94)
Glu(COO$^-$)	(218)	(+ 3.72)
Ser($PO_4^=$)	860 (T_t)	≈ + 8.0 (from graph)

Data within parentheses utilized microbial preparations of poly(30 mers), e.g., (GVGVP GVGVP GXGVP GVGVP GVGVP GVGVP)$_n$, with n ≈ 40. The notation (from graph) indicates that the value of T_t from Table 4 was used with the sigmoid curve of Fig. 13 to estimate $\Delta G°_{HA}(X)$. Adapted from Urry, 2004).

Fig.1.18: Data for developing the Tt-based Hydrophobicity. (A) Dependence of T_t on Amino Acid Composition for poly-[f_V(GVGVP),f_X(GXGVP)] where f_X=0.2. (X stands for the guest amino acid residue; f_X is the mole fraction of (GXGVP) pentamers, and f_V is the mole fraction of (GVGVP) pentamers, such that $f_X+f_V=1$). (B) Using the composition of the First Basis Set poly[f_V(GVGVP),f_X(GXGVP)], the value of T_t is plotted versus f_X, the mole fraction of pentamers containing the residue X. Extrapolation to f_X=1 gives the value of the temperature of inverse temperature transition, T_t, for poly(GXGVP). (C) Hydrophobic scale in terms of ΔG^o_{HA}, the change Gibbs free energy of hydrophobic association, for aminoacid residue (X) of chemically synthesized poly[f_V(GVGVP),f_X(GXGVP)], 40 mg/mL, Mw ≈ 100 kDa in 0.15 M NaCl, 0.01 M Phosphate, using the net heat of the inverse temperature transition, $\Delta Ht \approx \Delta G^o_{HA}$,, per (GXGVP), determined at f_X = 0.2 and extrapolated to f_X = 1.[77, 79]

In the hydrophobicity scale of amino acids, Trp > Tyr > Phe > Leu ≈ Ile ≈ Met > Val > Ala > Gly (Trp = Tryptophan, Tyr = Tyrosine, Phe = Phenylalanine, Leu = Leucine, Ile = Isoleucine, Met = Methionine, Val = Valine, Ala = Alanine, Gly = Glycine), when changing the 4th amino acid, X_{aa} by any other residue, the temperature of the reversible aggregation transition in water (described as coacervation) is inversely dependent on the mean hydrophobicity and the heat of the transition is found to be directly proportional to the mean residue hydrophobicity.[76] That is, as the polypeptide is more hydrophobic, the value of the T_t is lower, whereas as the polypeptide is more polar, the T_t is higher. By changing the guest residue, X_{aa}, it is possible to design polymeric materials with a particular T_t or to introduce temperature modulated switches. Accordingly, a hydrophobicity scale was proposed by Urry (Fig.1.18). In addition, when inserting a charged residue in the X_{aa} site, it is possible to obtain a functional polymer. By substituting this guest residue by a glutamic acid, it is possible to obtain a polymer responding to pH. On ionization of the glutamic acid side chains, the polymer chains become less hydrophobic and thus the transition temperature shift to higher temperatures.[77] Urry and co-workers observed that when the valine in the 4th position of $(VPGVG)_n$ is replaced with one out of five pentamers by a glutamic acid residue, the T_t shifts from 25 ºC at pH=2 and pH=7, in poly(VPGVG), to 25 ºC at pH=2 and 70 ºC at pH=7 in the modified polypentapeptide poly(VPGEG).[80]

1.5 Self-Assembly

Self-assembly is the process in which a well-defined, discrete supramolecular architecture is generated spontaneously from a given set components under thermodynamic equilibration.[81-85] Self-assembly concept has been coming from studying the molecular processes that is illustrated in Fig.1.19.

A self-assembly system is composed of a group of molecules or segments of macromolecules that interact with each other to change from some less ordered state (solution, disordered aggregate, or random coil) to a final state (crystal or folded macromolecule) which is a more ordered state. These interactions are weak compared to thermal energies and non-covalent; van der Waals and coulomb interactions, hydrophobic interactions, and hydrogen bonds but relatively weak covalent bonds (coordination bonds) are also appropriate for self-assembly.[86] The self-assembly of the molecules normally is carried out in solution or at an interface for the motion of molecules, and the molecules must be mobile. In solution, thermal motion is the major part of the motion required to bring the molecules in contact.[81-85] There are two types of self-assembly, static self-assembly and dynamic self-assembly.[87]

1.5.1 Static self-assembly

It involves systems that not dissipate energy and are global or local equilibrium systems. In this type, the formation of the ordered structure may require energy, although become stable after formation. For example; atomic, ionic and molecular crystal systems that used in materials and optoelectronics applications.[84,88] Also, phase-separated and ionic layered polymer system.[89] Another example, self-assembled monolayers system that used in microfabrication, sensors and nanoelectronics applications.[90]

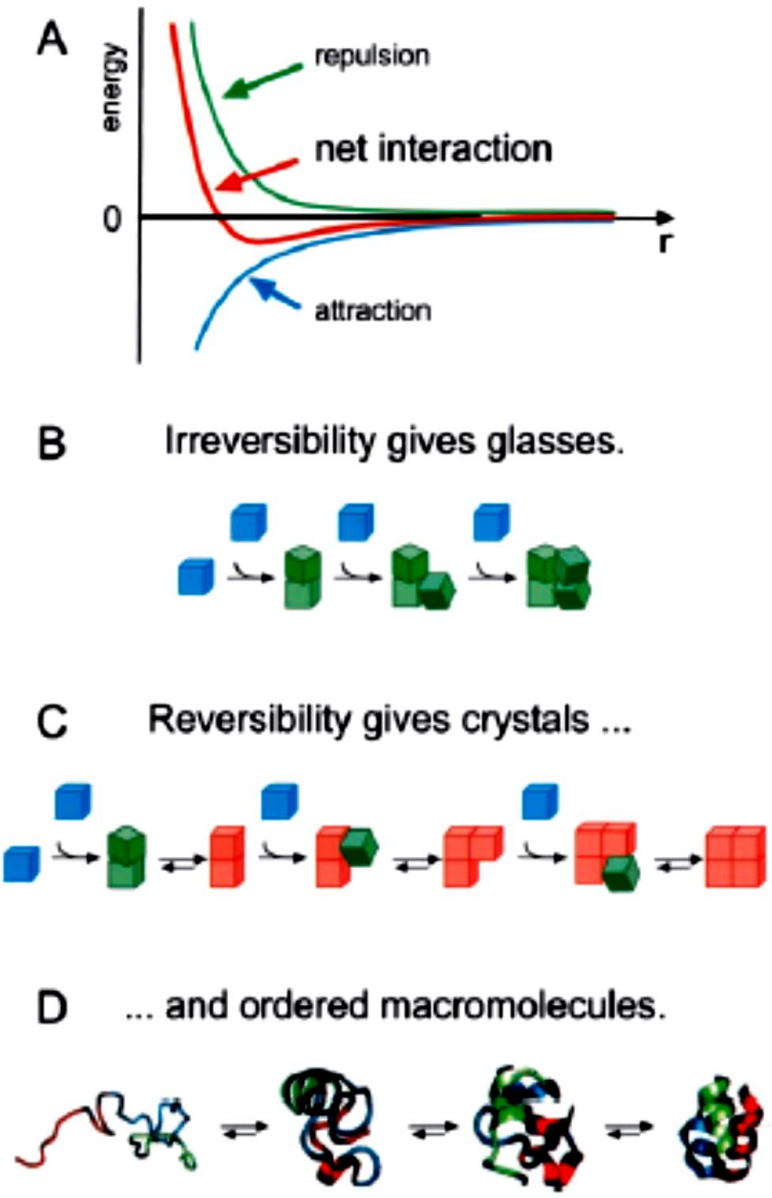

Fig.1.19: (A) Aggregation occurs when there is a net attraction and an equilibrium separation between the components. The equilibrium separation normally represents a balance between attraction and repulsion. These two interactions are fixed in molecular self-assembly but can be engineered independently in macroscopic self-assembly. (B and C) Schematic illustration of the essential differences between irreversible aggregation and ordered self-assembly. (B) Components (shown in blue) that interact with one another irreversibly form disordered glasses (shown in green). (C) Components that can equilibrate, or adjust their positions once in contact, can form ordered crystals if the ordered form is the lowest-energy form (shown in red). (D) Biology provides many examples of self-assembly (here, the formation of a protein, an asymmetric, catalytically active nanostructure); these examples will stimulate the design of biomimetic processes.[91]

1.5.2 Dynamic self-assembly

The system is dissipating energy. For example, Bacterial colonies.[92] Also, Oscillating and diffusion reactions that used in biological oscillations.[90, 93]

The important driving force for self-assembly is the amphiphilicity. Molecules that have polar and apolar elements tend to minimize unfavorable interaction, where in the polar solvent, by the self-assembly process, the hydrophobic moieties that repel with the aqueous solution and become shielded by the hydrophilic domains, and vice versa with nonpolar solvent.[94-95] A classic example is the block copolymers that connected covalently by flexible blocks,[96] and achieved a lot of structures and hierarchies[97] by incorporating a large number of flexible blocks or by blending,[98-100] by engineering the architectures,[101] or by incorporating rod-like moieties within the blocks[102-108]. In the block copolymer bibliography, separation of microphase is used.[3, 109]. In non-equilibrium thermodynamics, self-organization is used for dissipative non-equilibrium structure.[110] Static self-assembly, as called by Whitesides, refers to structures near thermal equilibrium.[87]

1.5.3 Self-assembly of recombinant polypeptides

Recombinant polypeptides, that incorporate functional sequences of the human elastin protein, are attractive as amphiphilic block copolymers with alternating hydrophobic blocks and cross-linking domains.[111-113] The hydrophobic domains, that can facilitate both self-aggregation and elastomeric functions[114], are rich in valine (V), proline (P), alanine (A) and glycine (G)[115] which are present in tetrapeptide, pentapeptide and hexapeptide tandem repeats, VPGG, VPGVG and VAPGVG, respectively [113, 116].

Linear AB diblock copolymers are the simple example of self-assembly of polymers with a large solubility difference between the two blocks.[117-118] For amphiphilic AB diblock copolymers, a spherical micelles can be formed by self-

assembling that consisted of a core made up of an insoluble block that is shielded from the solvent by a hydrated corona composed of a more soluble block.[117] Other structures such as cylindrical micelles, toroids, lamellar sheets, or vesicles can also be formed based on amphiphilicity of the blocks.[119]

The formation of these structures depends on the length of the A and B segments relative to each other as well their organization in the macromolecule as diblock or triblock copolymer. In Fig.1.20, are represented possible nano and microstructures as a result of the self-assembly process of amphiphilic block copolymers.

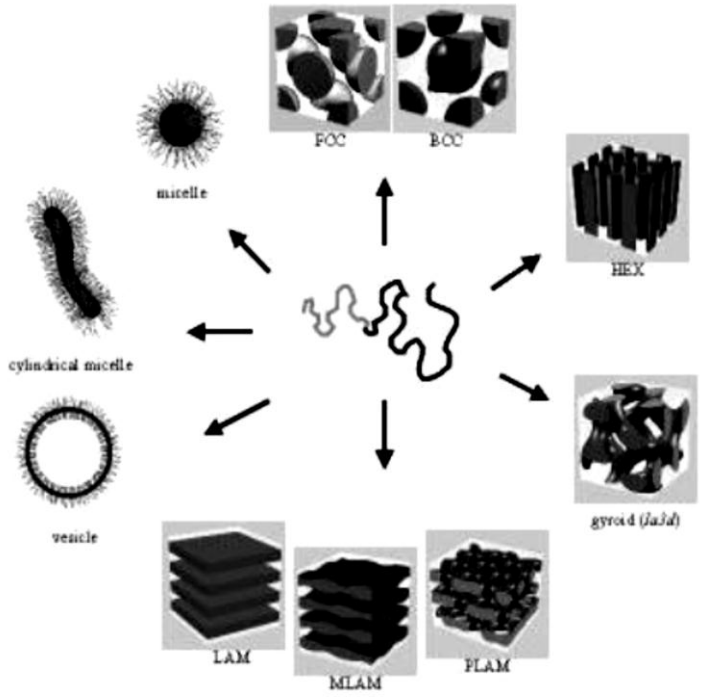

Fig.1.20: self-assembly nano- and micro-structures adopted by amphiphilic block copolymers.[119]

Other structural assemblies such as those obtained from tri-blocks[6, 120] and tetra-block[121] assemblies have been also prepared into highly desirable structures.

Chapter 2

Synthesis of Elastin-Like Polymer and Characterization Methods

2.1 Genetically Engineered Polypeptides

A highly repetitive nature of elastin like polymers (ELPs) has to be synthesized with a better candidate by the genetic engineering. The biosynthesis of a recombinant protein can be drafted in six main steps:

1- Design and construction of the codifying gene for the protein of interest and the cloning in a vector with tight control over transcription.
2- Vector insertion in bacterial cells suitable for cloning.
3- Analysis of the constructions inserted in the bacteria, in order to obtain a positive transforming into what concerns to gene sequence and size.
4- Transformation of a bacterial strain suitable for expression with the selected positive plasmid.
5- Bio production of the recombinant polypeptide.
6- Purification of the protein.

There are two approaches in genetically engineering for polypeptides synthesizing, concatemerization and directional ligation.

2.1.1 Concatemerization method

In concatemerization, two single stranded forward and reversed sequence DNAs has to be used for synthesizing a double-stranded DNA sequence with two well-defined identical sticky ends. Due to the same sticky ends on both sides of the gene, the ligation process resulted in a random distribution of different lengths of the gene. Then the ligated DNA sequence with different lengths are inserted into a vector DNA digested at the same cut sites as the two sticky ends of the annealed insert, see Fig.2.1.

Then the genes are separated based on their molecular weight that results in a range of gene sequences with different molecular weights. So this method is useful for obtaining different lengths of gene.[122]

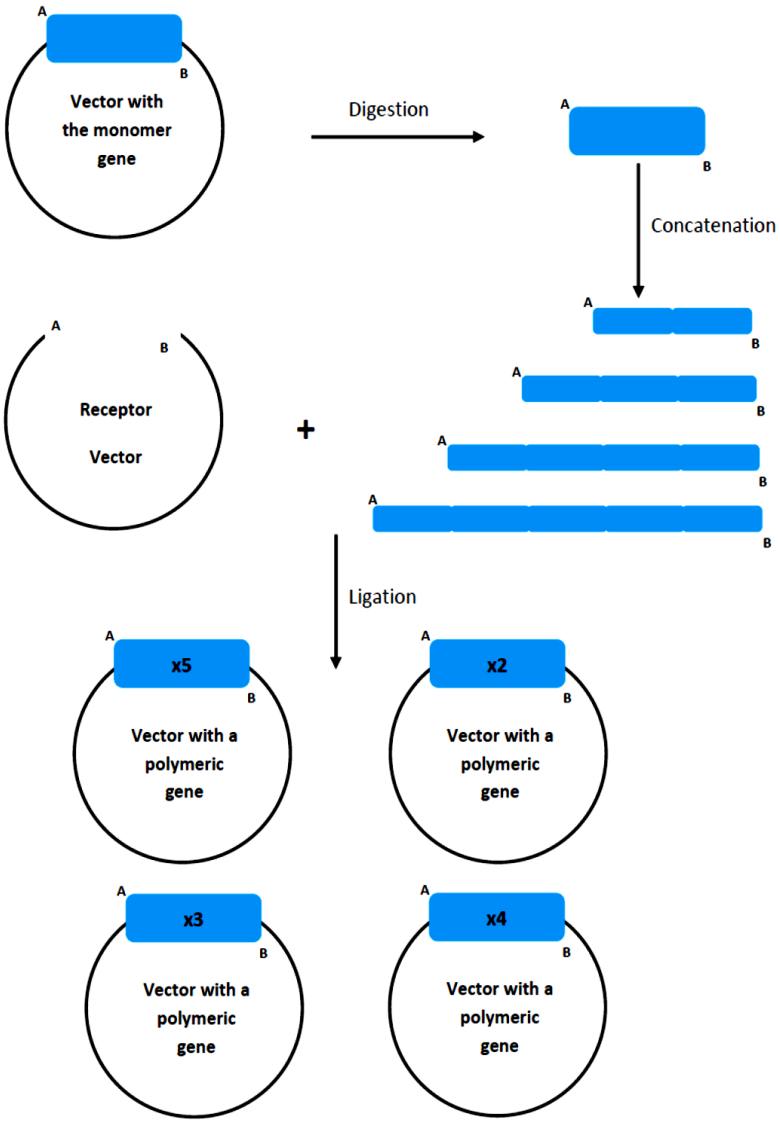

Fig.2.1: Schematics of the concatenation method.[123]

2.1.2 Directional ligation method

The second method of genetically synthesized engineering is recursive directional ligation (RDL), that is become more common after applying this method for synthesizing silk elastin-like proteins by Cappello et al.[124] In this method, a double-stranded DNA sequence with two different sticky ends is inserted into a vector which is doubly digested with the same two restriction

enzymes of the insert DNA sequence, see Fig.2.2, and then this plasmid amplified in vivo in a host bacterial cell.

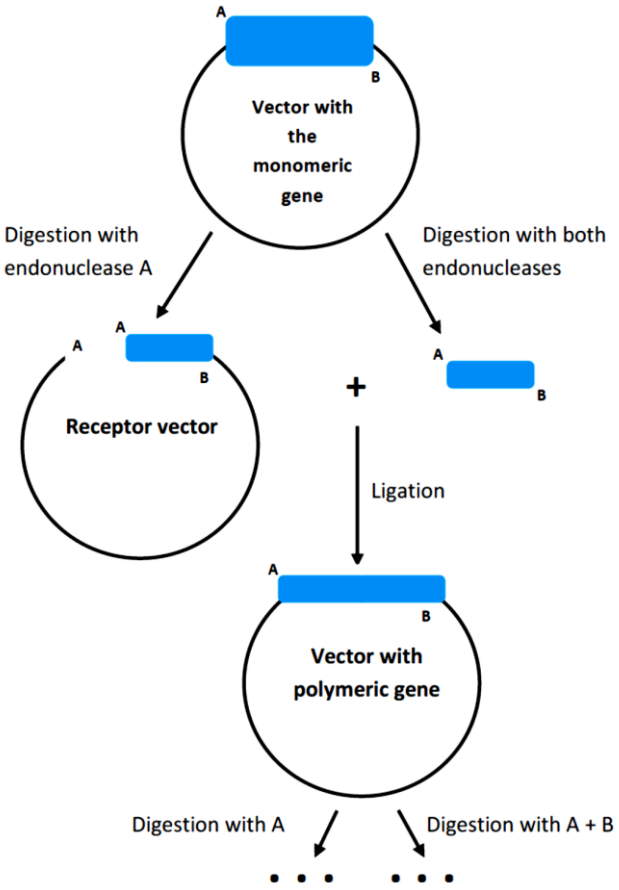

Fig.2.2: Schematics of the recursive-iterative method.[123]

2.2 Materials and Methods

2.2.1 Materials

2.2.1.1 Chemicals Reactive

All the reactive employed in this work are listed on Table2.1

Table2.1: Reactive employed and suppliers.

REACTIVE AND ABBREVIATION	BRAND
Acetone	Sigma Aldrich
Acrylamide	Amresco
Ammonium Persulfate (APS)	Sigma Aldrich
Ampicilin	Apollo Scientific
Bacto Agar	Invitrogen
Bromophenol blue	Sigma Aldrich
Chloridric Acid	Merck
Dimethyl Sulfoxide (DMSO)	Carlo Erba
D(+) Glucose	Merck
Ethanol	Merck
Ethylenediamine tetraacetic acid (EDTA)	Sigma Aldrich
Glycerol	Merck
Glycine	Invitrogen
Gel red	Biotium
Isopropanol	Invitrogen
Kanamicine	Invitrogen
Seakem Agarose	Cambrex
Sodium Chloride	Merck
Sodium Dodecyl Sulfate (SDS)	Sigma Aldrich
Sodium Hydroxide	Merck
Tetramethylethylenediamine (TEMED)	Sigma Aldrich
Tris(hydroxymethyl)aminomethane (Tris)	Sigma Aldrich
β-mercaptoethanol	Sigma Aldrich

2.2.1.2 Glass Materials

The glass materials have been washed and rinsed several times with distilled water.

2.2.1.3 Other Materials

Other laboratory materials like tips, microtubes, conical tubes, Eppendorf tubes, etc.., are bought sterile or are sterilized on an autoclave (Autester E-75) for 20 minutes, at 120ºC and one atmosphere.

2.2.1.4 Buffers

In this work, the following buffers have been used:

- ► PBS (pH 7.4): 5mM pH 7.4 phosphate buffer, 140mM NaCl
- ► TAE: 40mM Tris-acetate, 1mM pH 8 EDTA
- ► SB (sonication buffer): 20mM Tris-base, 2.5 mM pH 8 EDTA.
- ► Washing buffer: 20mM Tris pH7.5, 0.2M NaCl.
- ► Running buffer: 15.1g Tris-base, 71g Glycine, 5g SDS.

All the solutions are prepared using ultrapure de-ionized water (Millipore), and when necessary are sterilized in the autoclave.

2.2.1.5 Biological Materials

2.2.1.5.1 Bacterial strains

The Escherichia coli strains used in this work have the following genotypes:

- ► XL1-Blue (Stratagene): endA1 supE44 hsdR17 thi1 recA1 gyrA96 relA1 lac [F' proAB $lacI^q$ ZΔM15 Tn (Tet^r)].
- ► BL21 (DE3) (Novagen): F^- ompT hsdSB (r_B^- m_B^-) gal dcm (DE3).

2.2.1.5.2 Culture Media

The culture media used for bacteria growth and transformations are:

- ► LB (Luria-Bertani):(Pronadisa)

Formula in grams per liter of distilled water:

Tryptone (Pancrreatic digest of casine): 10g/l

Yeast extract: 5g/l

Sodium chloride: 10g/l

Final pH: 7.0±0.2at 25^{o}C and is sterilized on the autoclave.

- ► LB-agar, composition per liter: 15g of Agar in LB medium. Sterilization on autoclave.
- ► TB (Terrific Broth):

  Formula in grams per liter of distilled water:

  20g/l Yeast extract

  35g/l Tryptone

  3.3g/l Ammonium Sulphate

  6.5g/l potassium Dihydrogen Phosphate

  7.1g/l Disodium Hydrogen Phosphate

  0.5g/l Glucose

  2g/l Alpha lactose

  0.15g/l Magnesium Sulphate

  0.35g/l Auto Induction Medium Element Mix,

  Then sterilizing on autoclave.
- ► SOC Broth (Sigma Aldrich).

2.2.1.5.3 Endonucleases

The endonucleases used for this work are:

- ► DpnI, EarI, EcoRI, HindIII, SapI, XbaI (NewEngland Biolabs)
- ► Fast EcoRI, Fast HindIII, Fast XbaI, (Fermentas)
- ► T4 DNA ligase (NewEngland Biolabs, Fermentas)
- ► Shrimp Alkaline Phosphatase (S.A.P.) (NewEngland Biolabs)
- ► Antarctic Alkaline Phosphatase (NewEngland Biolabs)

In all cases the reactions were made according the manufacturer's instructions.

2.2.1.5.4 Vectors

a) Cloning Vector

Fig.2.3 represents the scheme of the pDrive cloning vector (Qiagen). In the scheme are represented the functional domains of the vector as the position of the Ear I endonuclease, also indicate the Ear I/Sap I restriction sites at position 3843bp, eliminated during mutagenesis.

pDrive Cloning Vector

Positions of various elements

Vector size (bp)	3851
Multiple cloning site	266–393
LacZ α-peptide	216–593
T7 RNA polymerase promoter	239–258
T7 transcription start	256
SP6 RNA polymerase promoter	398–417
SP6 transcription start	400
Ampicillin resistance gene	1175–2032
Kanamycin resistance gene	2181–2993
pUC origin	3668
Phage f1 origin	588–1043
Primer binding sites:*	
M13 forward (–20)	431–447
M13 forward (–40)	451–467
M13 reverse	209–224
T7 promoter primer	239–258
SP6 promoter primer	400–418

Fragments obtained by Ear I digestion:
1951+1262+637
or
1746+1262+637+215+insert

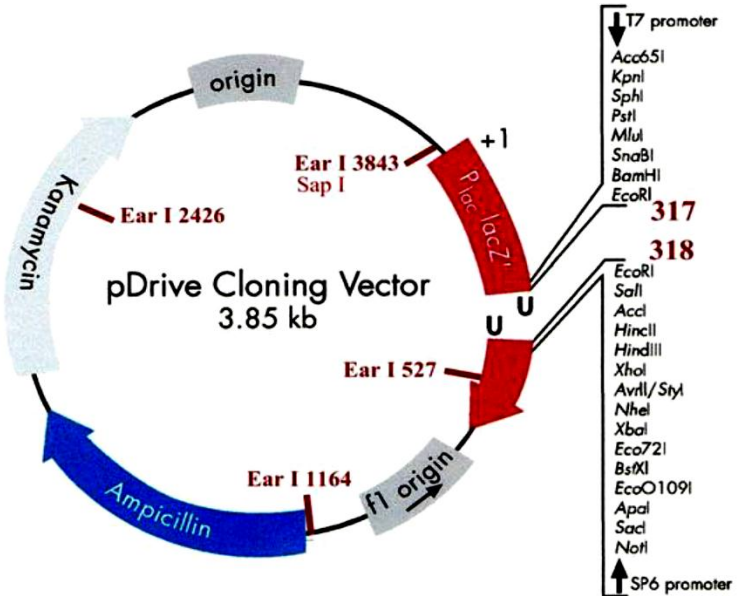

Fig.2.3: Scheme of the pDrive cloning vector

b) Expressing Vector

pET10: is used for protein production which is modified from pET-9a, Fig.2.4, (Novagen Ca.No.69431-3), in Bioforge group by M. Pierna

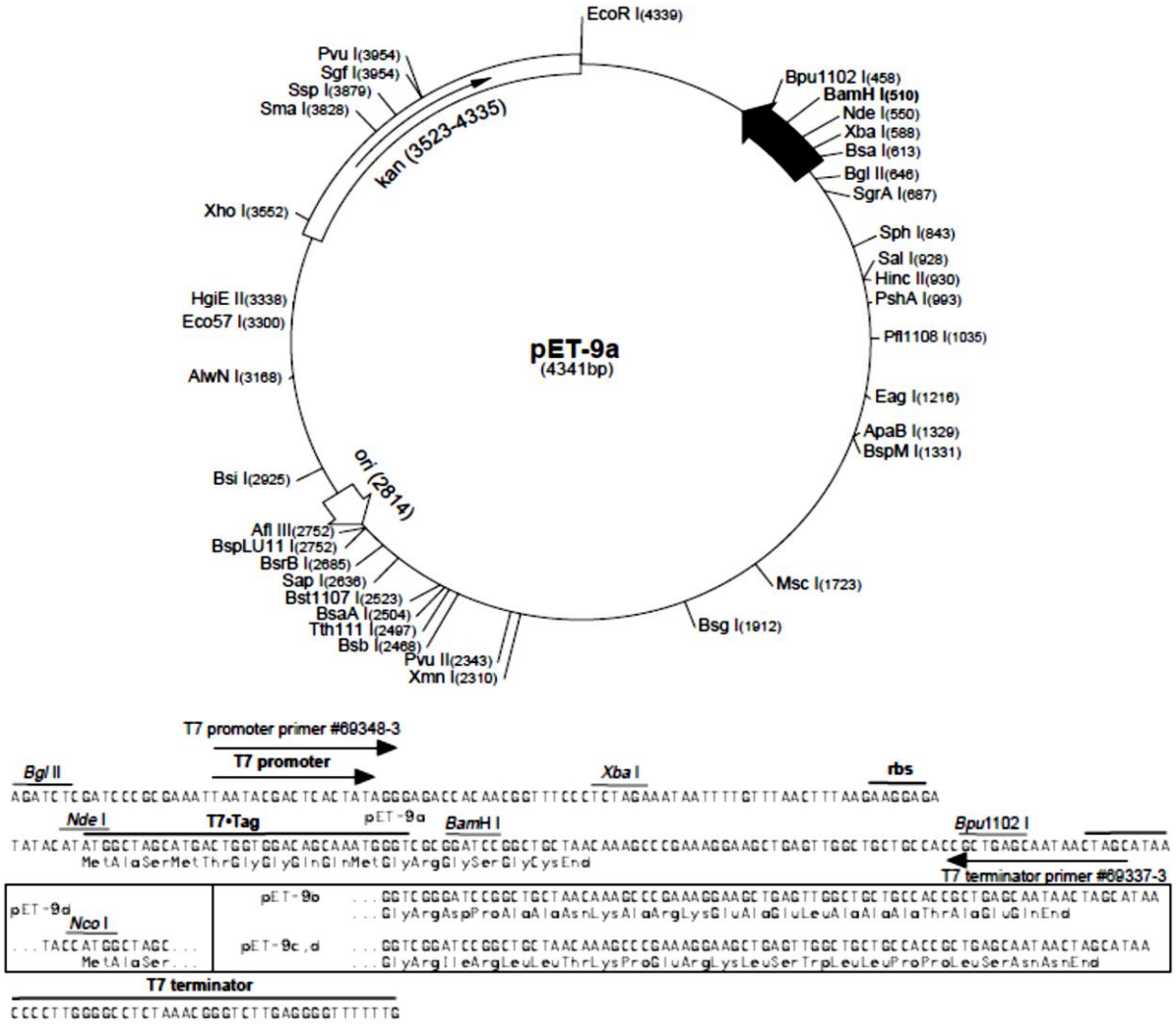

Fig.2.4: Scheme of pET-9a-d cloning/expressing region.

2.2.1.5.5 DNA materials

1- $E_{50}I_{60}$ DNA has been recombined by Carmen Garcia-Arevalo in Bioforge group.[65]

2- DNA of (DDDEEKFLRRIGRFG) $_{1, 3, 6}$ amino acids that have been prepared in Bioforge group by A. RIBEIRO.

c) Other reagents

1- QuantumPrep® Plasmid Kit (Biorad).

2- PureLink™ Quick Gel Extraction Kit (Invitrogen).

2.2.2 Methods

Recombinant DNA molecules are defined as either molecules that are constructed outside living cells by joining natural or synthetic DNA segments to DNA molecules that can replicate in a living cell.[125]

The DNA of amino acid sequences of $E_{50}I_{60}$ with DNA of amino acid sequences of $(SN_A15)_3$ and also with amino acid sequences of $(SN_A15)_6$ have to be recombined and transformed.

The amino acid sequence of $E_{50}I_{60}$ elastin like polymer is

$$[((VPGVG)_2(VPGEG)(VPGVG)_2)_{10}\text{-}(VPGIV)_{60}]$$

and for $(SN_A15)_3$ is

$$(DDDEEKFLRRIGRFG)_3$$

and for $(SN_A15)_6$ is

$$(DDDEEKFLRRIGRFG)_6$$

The DNA of $E_{50}I_{60}$, the DNA of $(SN_A15)_3$ and DNA of $(SN_A15)_6$ have been transformed, using the following steps:

2.2.2.1 Transformation of XL1-Blue cells

An aliquot of 50µl of cells (stored at -80 ^oC) is thawed on ice and β-mercapthoethanol is added to a final concentration of 25mM. After mixing gently with the tip, the cells are kept on ice for 10 minutes and shaking gently each two minutes. A 10µl from the cells and 0.7µl of plasmids that have the DNA to be colonized are mixed in pre-chill 14-mlBD Falcon polypropylene round-bottom tubes on ice for 20 minutes (A volume of ligation lower than the 10% of the initial cell volume).

A heat shock is applied to the cells in 42^oC water bath for 30 seconds where the duration of the heat pulse is critical. A SOC Broth volume 9 times higher than the starting volume is added to the suspension (180µl), and the bacteria are incubated one hour at 37^oC with shaking at 225- 250rpm. Then, 50-

200µl of the mixture plated in LB agar plate containing the appropriate antibiotic which are incubated for 16-20 hours at 37 ^{o}C.

A single colony is isolated from the LB agar plate and used to inoculate 5ml of LB medium containing the appropriate antibiotic and is grown at 37^{o}C with shaking at 225- 250rpm for 16-20 hours.

2.2.2.2 Plasmid purification

For plasmid purification, the "Quantum Prep Plasmid Mini, Midi and Maxiprep" from BioRad kits have been used following the manufactures instructions. These methods are based on bacteria alkaline lyses[126] followed by a partial purification and selective DNA adsorption to a silica gel. And the eluted DNA is stored under -20^{o}C until using.

2.2.2.3 DNA Agarose gel electrophoresis

To separate and check the appearance and size of DNA fragments from a plasmid; fragments resulting from an enzymatic digestion with endonucleases; it used the agarose gel electrophoresis.

Different concentrations in 1x TAE, are applied according to the sizes of the DNA fragments and the kind of gel, analytical or preparative (Table 2.2). The gels are prepared adding in an Erlenmeyer flask the quantity of agarose and a volume of buffer according to the gel concentration and size. The agarose is melted in the microwave, after weight and hydration, until the formation of a gel. Once melted, the flask with the gel is weighted again and ultrapure de-ionized water (Millipore) is added until reach the initial weight, maintaining the initial concentration and gel uniformity. After cooling down to 60ºC the gel is casted in a horizontal tray with a comb.

Table 2.2: Optimal resolution for linear DNA.

Fragment size in base pair (bp)	Agarose final % 1x TAE
800-10000	0.8
400-8000	1
300-7000	1.2
200-4000	1.5
100-2000	2

2.2.2.4 DNA fragment analysis

The DNA is cut at the desired position using the Ear I and Sap I endonucleases, then performing electrophoresis analysis. The samples are applied adding 0.20 volumes of 5x loading buffer [(30% (v/v) glycerol, 0.1% (w/v) SDS, 0.05% (w/v) bromophenol blue, 0.05% xilen cianol, 50mM Tris pH 8, 0.05mM EDTA)]. A fixed voltage, between 2 and 7 V/cm according to each sample, is applied.

Last, the gel is stained for 10 to 30 minutes in a Gel Red nucleic acid stain solution, and the DNA bands are visualized by exposition to UV light in a Viber Lourmat, TFX-20M transilluminator.

Picture image:

Images were taken with the Kodak "Gel Logic 100 imaging System" digital camera. Visualization and manipulation were made using the "Kodak 1D image Analysis" and "Paint Shop pro Version 9.00" (Jasc software) programs.

The stained agarose gels were photographed over the UV light trans-illuminator, using an appropriated filter. The polyacrylamide gels stained with Cooper Chloride were placed over a dark surface.

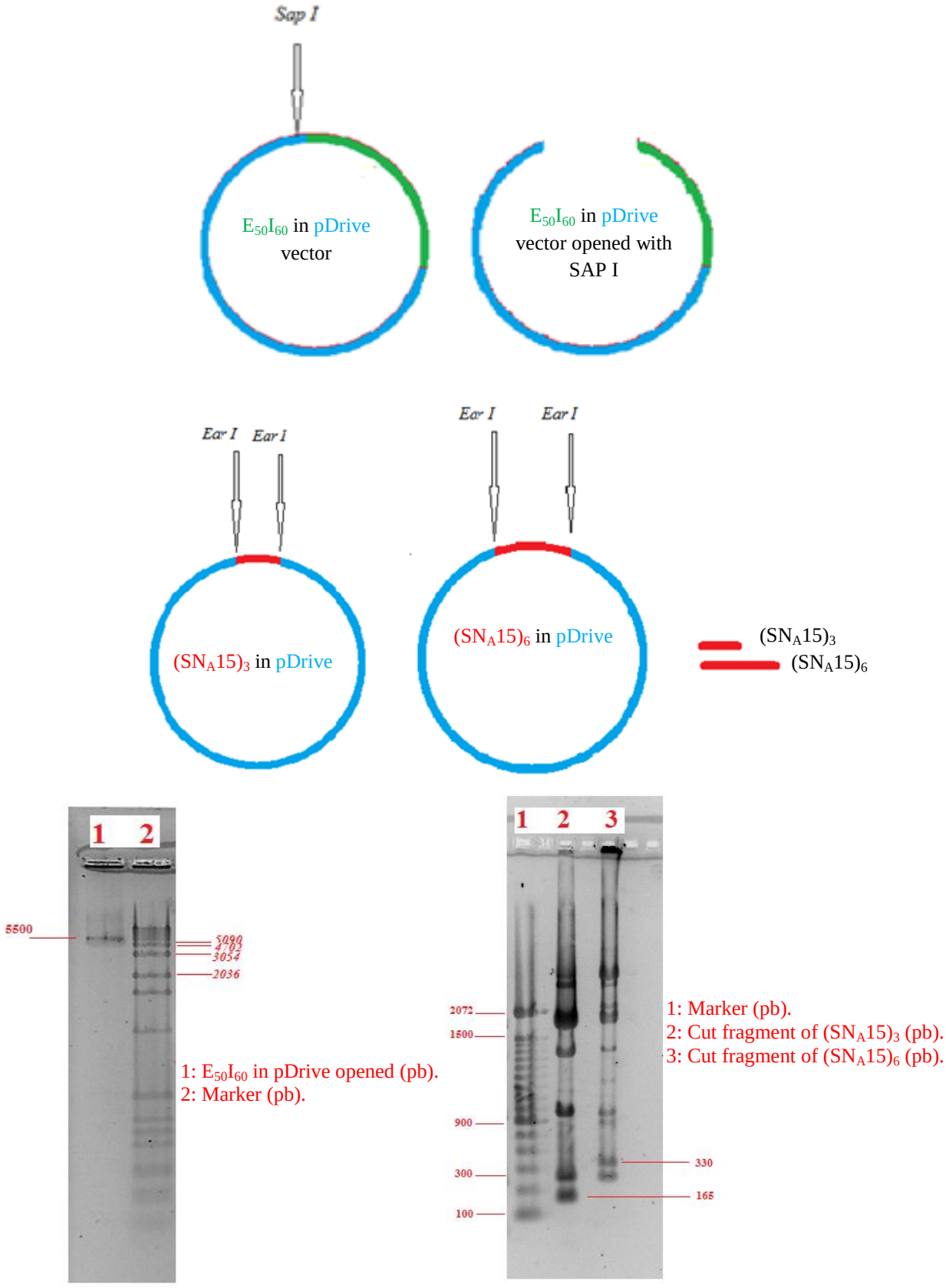

Fig.2.5: Electrophoresis analysis for DNA of $E_{50}I_{60}$ in opened pDrive vector at 5500pb and $(SN_A15)_3$ at 165pb and $(SN_A15)_6$ at 330pb DNA cut fragments.

From electrophoresis experiment, it is found that a Sap I enzyme open the DNA of $E_{50}I_{60}$ in pDrive vector at the desired position and Ear I enzyme for $(SN_A15)_3$ and $(SN_A15)_6$ DNA, see Fig.2.5. Making gel for obtaining more amounts DNA of $E_{50}I_{60}$ in pDrive, and also for $(SN_A15)_3$ and $(SN_A15)_6$ DNA.

2.2.2.5 DNA fragments purification from an agarose gel

The target DNA band is first separated and visualized in an agarose gel of an appropriated concentration and stained with Gel Red nucleic acid stain solution. Secondly, the band is extracted from the gel with the help of a scalpel. Minimum quantity of agarose should be cut during band extraction.

An approach that has been used for fragment purification is the "Pure Link Quick Gel Extraction kit" system. Following the manufacturer's instructions the DNA is purified by adsorption to silica gel membrane[127], and eluted with elution buffer. And the eluted DNA is stored under -20^{o}C until using.

2.2.2.6 Recombination between DNA of $E_{50}I_{60}$ in pDrive vector and DNA of $(SN_A15)_3$ and also Recombination between DNA of $E_{50}I_{60}$ in pDrive vector and DNA of $(SN_A15)_6$

First, opening the pDrive vector recombined by the DNA of $E_{50}I_{60}$ using Sap I enzyme then dephosphorylation of the opening plasmid that has sequence of $E_{50}I_{60}$.

The dephosphorylation has to be performed in 50µl of opening DNA of $E_{50}I_{60}$ in pDrive vector with 5.7µl Buffer (NEB buffer for Antartch) and 0.5µl Antartch enzyme in an Eppendorf, then putting the Eppendorf at 37^{o}C for 30 minutes, and then inactivate 5 minutes at 65^{o}C.

Second, making a ligation between the DNA of $(SN_A15)_3$ with disphosphorylated DNA of $E_{50}I_{60}$ in pDrive vector, and a ligation between the DNA of $(SN_A15)_6$ with the disphosphorylated DNA of $E_{50}I_{60}$ in pDrive vector.

The ligation has been performed in 6µl of the disphosphorylated DNA of $E_{50}I_{60}$ in pDrive vector with 4µl from DNA of $(SN_A15)_3$ and 0.8µl from T4DNA ligase using 1.2µl from the buffer, Fig.2.6a, then making electrophoresis experiment for examining the ligated fragments with a gel of concentration 1.8% of agarose. The electrophoresis analyses are shown in Fig.2.6b.

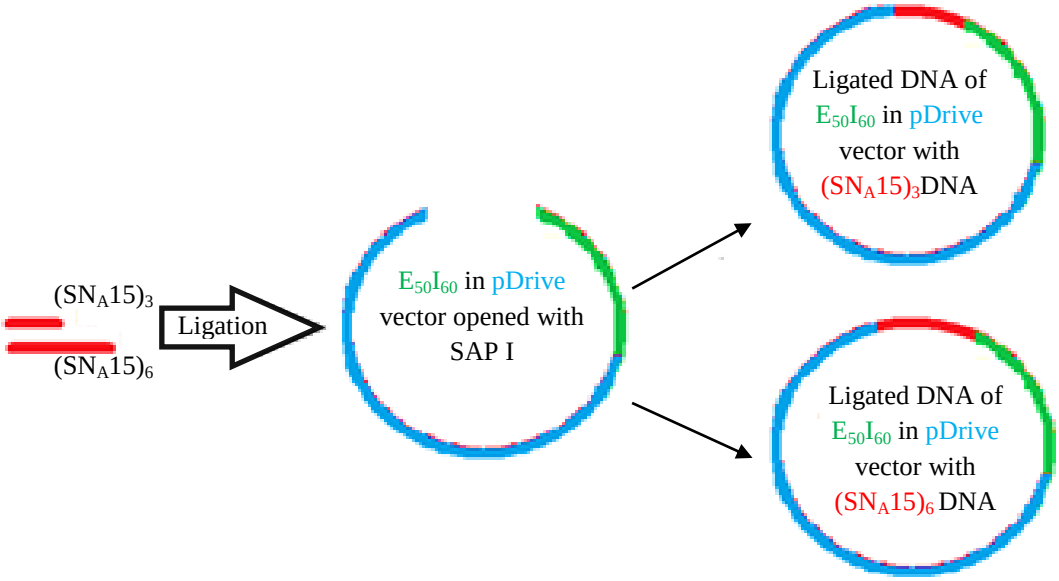

(a)

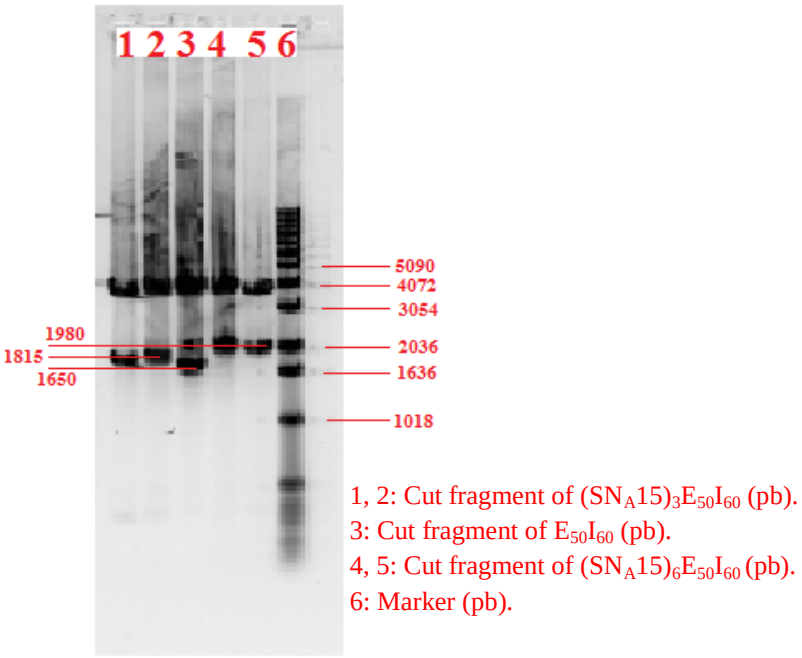

(b)

Fig.2.6: (a) Schematics of the ligated DNA of $E_{50}I_{60}$ in pDrive vector with $(SN_A15)_3$ and for ligated DNA of $E_{50}I_{60}$ in pDrive vector with $(SN_A15)_6$ DNA. (b) Electrophoresis analysis for ligated DNA of $E_{50}I_{60}$ with $(SN_A15)_3$ and for ligated DNA of $E_{50}I_{60}$ with $(SN_A15)_6$ DNA, that cut with endonuclease.

Then making another gel to cut and obtain a more amount of ligated DNA of $(SN_A15)_3E_{50}I_{60}$ in pDrive vector and of ligated DNA of $(SN_A15)_6 E_{50}I_{60}$ in pDrive vector. Then these DNAs are introduced in expressing vectors for producing the proteins.

2.2.2.7 Inserting DNA of $(SN_A15)_3E_{50}I_{60}$ in pET10 expression vector and also inserting DNA of $(SN_A15)_6E_{50}I_{60}$ in pET10 expression vector

First, cutting the fragments of the DNA of $(SN_A15)_3E_{50}I_{60}$ from $(SN_A15)_3E_{50}I_{60}$ pDrive vector and opening pET10 expression vector using the appropriate enzymes then put them overnight at 37^{o}C. Then putting a 1μl of Dpn I endonuclease in the DNA of $(SN_A15)_3E_{50}I_{60}$ and performing the electrophoresis experiment for cutting the DNA of $(SN_A15)_3E_{50}I_{60}$. Then, making purification of cut $(SN_A15)_3E_{50}I_{60}$ DNA and purifying DNA from gel, then Store the purified DNA at 4^{o}C for immediate use or at -20^{o}C until using. Also the same for the DNA of $(SN_A15)_6E_{50}I_{60}$

For inserting the DNA of $(SN_A15)_3E_{50}I_{60}$ and the DNA of $(SN_A15)_6E_{50}I_{60}$ in the pET10 expression vector, the dephosphoralation and ligation are applied as in 2.5.6 using the appropriate enzymes and appropriate conditions.

Then making electrophoresis, of 1.8% agarose concentration, experiment using Hin III and Xba I enzymes for cutting the plasmid of $(SN_A15)_3E_{50}I_{60}$pET10 and also the plasmid of $(SN_A15)_6E_{50}I_{60}$pET10, the electrophoresis analyses are shown in Fig.2.7.

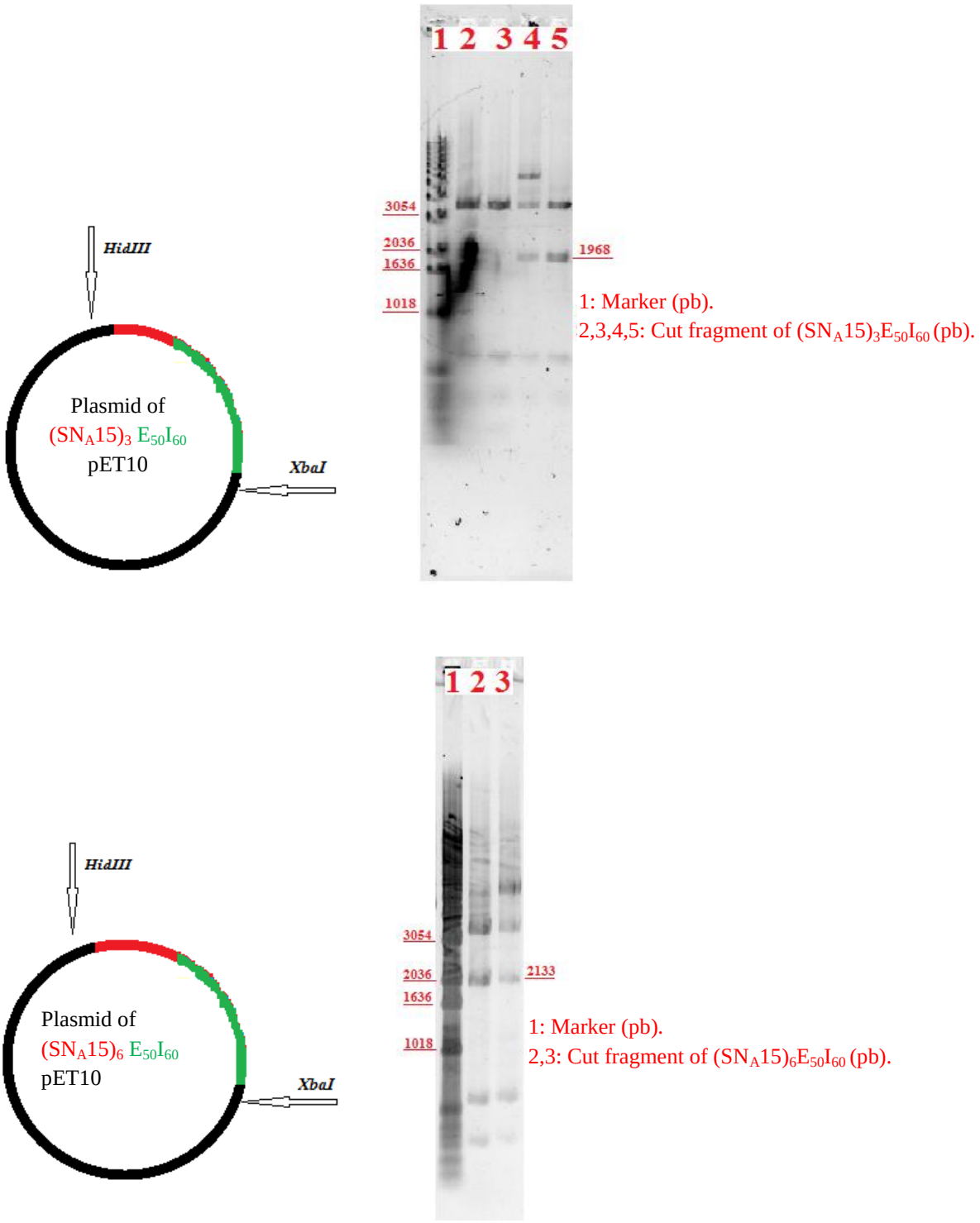

Fig.2.7: Electrophoresis analysis for cut plasmid of $(SN_A15)_3E_{50}I_{60}$pET10 and also for cut plasmid of $(SN_A15)_6E_{50}I_{60}$pET10.

2.2.2.8 Transformation of $(SN_A15)_3E_{50}I_{60}$pET10 plasmid and $(SN_A15)_6E_{50}I_{60}$pET10 plasmid for obtaining $(SN_A15)_3E_{50}I_{60}$ and $(SN_A15)_6E_{50}I_{60}$ proteins

Making a transformation of $(SN_A15)_3E_{50}I_{60}$pET10 plasmid and $(SN_A15)_6E_{50}I_{60}$pET10 plasmid, using the following steps:

1- Thaw on ice one vial of One-Shot cells per transformation.
2- Add 5 to 10ng of DNA, in a volume of 1 to 5μl, to the cells and mix by tapping gently. Do not mix cells by pipetting.
3- Incubate the vial on ice for 30 minutes.
4- Incubate for exactly 30 seconds in the 42^{o}C bath and quickly place on ice.
5- Remove the vial from 42^{o}C bath and quickly place on ice.
6- Add 250μl of pre-warmed SOC Broth medium to the vials. Note; SOC Broth is a rich medium; practice the good sterile technique to avoid contamination.
7- Place the vial in a micro-centrifugation rack and secure with tape. Place the rack on its side in a shaking incubator and shake the vial at 37^{o}C for 1 hour at 225rpm.
8- Plate 20 to 200μl each of the transformation reactions onto two LB plates containing the appropriate antibiotic and 34μg/ml chloramphenicol (if using BL21Star (DE3) pLysS). Plate two different volumes to ensure well-spaced colonies on at least one plate. The remaining transformation reaction may be stored at 4^{o}C and plated out the next day, if needed.
9- Invert the plates and incubate at 37^{o}C overnight.
10- Making inoculum select a one clone for making a production of proteins, and put the clone in a falcon that contains 5ml of LB +250 μl

of glucose +5µl of Kamicina as interest antibiotic. Also another control falcon is prepared.

2.2.2.9 Glycerol Stock Preparation

To maintain and store the clones with interest, glycerol stocks were made. The selected colonies are grown at 37ºC with shaking (250rpm) on LB or LB with 0.5% of glucose (for the expression strains), until reach an OD600=0.6-0.8. At this point, 0.1 volumes of 80% sterile glycerol are added, and the cells are kept on cryovials at -80ºC.

2.2.2.10 Recombinamer's Expression on TB medium

Making a production of six Liters of TB with the interest antibiotic, and put the culture in a shaking at 37°C overnight. The analyses of total protein fractions were made with standardized culture medium volumes according to the number of cells estimated by absorbance at 600nm.

2.2.2.11 Total Protein Fraction Analysis

To analyze the total protein fraction composition, 1ml of culture media with the grown bacteria is taken. Bacteria are spin down by one minute cold centrifugation at 12000xg. The precipitation suspended in 100mQ. The samples are applied adding 0.20 volumes of 5x loading buffer [Tris 1M pH6.5: 1.56 ml, SDS: 0.5g, Glycerol: 2.5ml, β-mercaptoethanol: 1.25ml, Bromophenol Blue 2%: 16µl].

A sample is put at 95°C for 5 minutes and after centrifuge at 1200xg for 5 minutes and then a 5µl of sample is loaded on a polyacrylamide gel.

2.2.2.12 Protein Polyacrylamide Gel Electrophoresis

The protein polyacrylamide gel electrophoresis in the presence of sodium dodecyl sulfate – SDS-PAGE – is made following the protocol for discontinuous systems described by Laemmli.[128]

A “MiniVE vertical electrophoresis system” from Hoefer (Amersham Pharmacia Biotech, Pittsburg, USA) electrophoretic system is employed to perform the polyacrylamide electrophoresis.

The total percentage of acrylamide (%T) in the resolving gels varies according to the size of the polypeptides that we want to separate. For proteins which molecular weight is between 90 and 100kDa usually are employed gels of 10% T, if working with proteins with molecular weights between 60 and 80kDa usually are employed gels of 12%T; if working with smaller sizes are employed gels of 15%T. The composition of resolving and stacking gel for a gel 12%T is presented in table 2.3:

Table 2.3: Composition of the resolving and stacking gel in a gel 12%T.

	Resolving Gel	Stacking Gel
mQ	3.25ml	1.583ml
Tris 1.5 M pH 8., 8	1.88ml	----------
Tris 0.5 M pH 6.8	----------	0.625ml
Acrylamide 40%	2.25ml	250µl
SDS 10%	75µl	18.75µl
APS 10%	37.5µl	18.75µl
TEMED	3.75µl	2.35µl

*both gels are prepared in ultrapure de-ionized water (Millipore).

The proportion of acrylamide and bis-acrylamide only varies for the resolving gel with others percentage of T. Besides, the addition of SDS, proteins may optionally be briefly heated to near boiling in the presence of a reducing agent, such as 2-mercaptoethanol (β-mercaptoethanol), which further denatures the proteins by reducing disulfide linkages, thus overcoming some forms of tertiary protein folding, and breaking up quaternary protein structure (oligomer subunits). This is known as reducing SDS-PAGE, and is most commonly used. Non-reducing SDS-PAGE (no boiling and no reducing agent) may be used when the native structure is important in further analysis (e.g. enzyme activity). The denatured proteins are subsequently applied to one end of a layer of

polyacrylamide gel submerged in a running buffer (25mM Tris-base pH 8.3, 192mM glycine and 0.1% (w/v) SDS).

A constant electric current of 20mA per gel, is applied across the gel, causing the negatively-charged proteins to migrate across the gel towards the anode. The electrophoresis is finished when the bromophenol-blue of the loading buffer reaches the end of the polyacrylamide gel.

2.2.2.13 Protein Polyacrylamide Gel Electrophoresis Staining

Following electrophoresis, the gel is stained allowing visualization of the separated proteins. For staining, the Cooper method performed following Lee's[129] method; consisting in 10 minutes gel incubation on a 0.3M chloride cooper solution, then agitation with distilled water for 5 minutes.

After staining, different proteins appear as distinct bands within the gel. It is common to run molecular markers of known molecular weight in a separate lane in the gel, in order to calibrate the gel and determine the weight of unknown proteins by comparing the distance traveled relative to the marker.

2.2.2.14 Bacteria Disruption

The cells have to be centrifuged and washed with washing buffer, then are suspended in the sonication buffer for rupturing with interrupter (sonication method). Cell suspension is kept at 4^{o}C and 10μg/ml of PMSF protease inhibitor that dissolved in isopropanol has to be added to the cells.

Bacteria are disrupted by sonication cycles of 2 seconds pulse each 5 seconds at 100W, in a Sonicator 3000 from Misonix (Veron Hill, USA). During sonication, the samples are kept on ice to avoid protein denaturation. Then the suspension is centrifuged for 30 minutes at 4^{o}C at 12000xg; the supernatant corresponds to soluble fraction and the precipitation corresponds to the insoluble fraction.

2.2.2.15 Purification of the Recombinant Protein-based Polymers

Recombinamers purification is based on the Elastin like-polymers smart nature and in the inverse temperature transition. The soluble fraction is purified without pH modification by adding 1M of NaCl. The purification is depending on cold-warm centrifugation cycles of the supernatant. First, the sample is heated at 42°C for 1.5 to 2 hours, and centrifugation at 40°C at 12000xg. The precipitation is suspended in 2ml of cold mQ water per lire of culture and agitated overnight. This procedure is repeated two more times. The electrophoresis experiment has to be performed after purification to see that the proteins are purified. The electrophoresis analysis of $E_{50}I_{60}$, $(SN_A15)_3E_{50}I_{60}$ and $(SN_A15)_6E_{50}I_{60}$ are shown in Fig.2.8.

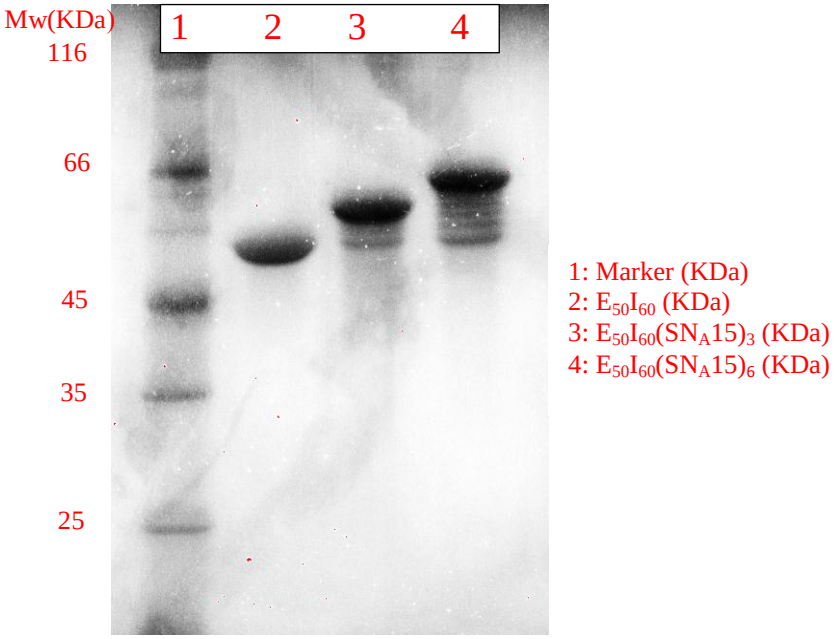

Fig.2.8: Electrophoresis analysis of $E_{50}I_{60}$, $(SN_A15)_3E_{50}I_{60}$ and $(SN_A15)_6E_{50}I_{60}$ elastin like polymers.

Then the dialysis process has to be performed to isolate the salts from the proteins, and the suspension is then lyophilized and stored at -20°C.

After lyophilizing, the molecular weight of the polymer has to be determined using Matrix-assisted laser desorption ionization (MALDI) time-of-flight (TOF) mass spectrometry (MS).

2.3 Characterization methods

2.3.1 MALDI-TOFMS

Matrix-assisted laser desorption ionization (MALDI) time-of-flight (TOF) mass spectrometry (MS) is a technique used for obtaining absolute molecular weights of synthetic polymers. The general principle of the Mass Spectroscopy is separating and detecting gas-phase ions. In MALDI-MS, the sample has to be embedded in the crystalline structure of small organic compounds and deposited on a conductive sample support. A nanosecond laser beam irradiates the crystals where the laser energy causes structural decomposition of the irradiated crystal and a particle cloud is generated, and the ions are extracted by an applied electric field. Following acceleration through the electric field, the ions drift through a field-free path and then to be detected. Ion masses (mass-to-charge ratios [m/z] are calculated by measuring their TOF, which is longer for larger molecules than for smaller molecules.[130-132]

2.3.2 Fourier Transform Infrared Spectroscopy (FTIR)

FTIR analysis was conducted with a BRUKER TENSOR 27, USA FTIR spectrophotometer. For each spectrum, a 128-scan interferogram was collected at single beam absorption mode with a 2 cm^{-1} resolution and a 1 cm^{-1} interval from the 4000 to 600 cm^{-1} region. Spectral calculations were performed by the OPUS (version 4.2) software (MATTSON INSTRUMENT, INC.).

2.3.3 Differential Scanning Calorimetry

Differential scanning calorimetry, DSC, experiments were done on a Mettler Toledo 822e DSC with liquid-nitrogen cooler and calibrated with indium. Solutions with polymer concentrations of 50 mg/ml in mQ solutions at different pH were placed in a 40 μL sealed aluminum pan, and an equal volume of SBF was placed in the reference pan. Before the experiment, samples were held at -5 C for 5 min. Measurements were run from -5 to 60 at 5^{o}C/min.

2.3.4 Light scattering

Light scattering measurement was performed using a BI-200SM multiangle goniometer (Brookhaven Instrument, Holtsville, NY) with a 33mWHe−Ne vertically polarized laser at a wavelength of 632.8 nm and a digital correlator (BI-9000AT). Dynamic light scattering is used to determine the effect of temperature on elastin like polymer and then determine inverse transition temperature. The mean hydrodynamic radius has been calculated. For the DLS measurements monitored at a scattering angle of 90°, $(SN_A15)_3E_{50}I_{60}$ and $(SN_A15)_6E_{50}I_{60}$ solutions at a concentration of 25μM was filtered and introduced into glass cells and stabilized for 10 min at the desired temperature (5−40°C) in a thermostated Decalin bath.

2.3.5 X-ray diffraction (XRD)

Powder X-ray diffraction (XRD) patterns were recorded with radiation CuKα of 1.5406A^o, position-sensitive detector 2θ (10 to 70^o), diffractometer (BRUKER D8 DISCOVER A25). The crystalline phases were determined from a comparison of the registered patterns ICDD powder diffraction file (PDF2).

2.3.6 Electron microscopy

Transmission electron microscopy specimens were prepared by depositing on a TEM copper grids coated with an amorphous carbon film for TEM examinations. The examinations were conducted in HRTEM systems (JOEL-JEM 2200FS) with a maximum acceleration voltage of 200 kV equipped with energy dispersive X-ray analysis detector. The microscope is provided with an energy filter in column, Ω-type was acquired applying a 16 eV. Zero loss images were taken to increase contrast. X-ray spectra were acquired in STEM mode by scanning an electron beam over a nanoparticle using the Oxford INCA EDX system. Live Counting time was 100 s. To characterize the phosphate phases the Ca/P ratios derived from the background subtracted intensities were used.

Chapter 3

Properties of Recombinant Polymers $(SN_A15)_3E_{50}I_{60}$ and $(SN_A15)_6E_{50}I_{60}$

3.1 Molecular weight of $(SN_A15)_3E_{50}I_{60}$ and $(SN_A15)_6E_{50}I_{60}$ ELPs

Molecular weights of polymers have a great effect on their physical and mechanical properties, so that it is important to study the molecular weight of the polymer. The Molecular weight of lyophilized elastin-like polymer has been characterized by MALDI-TOF.

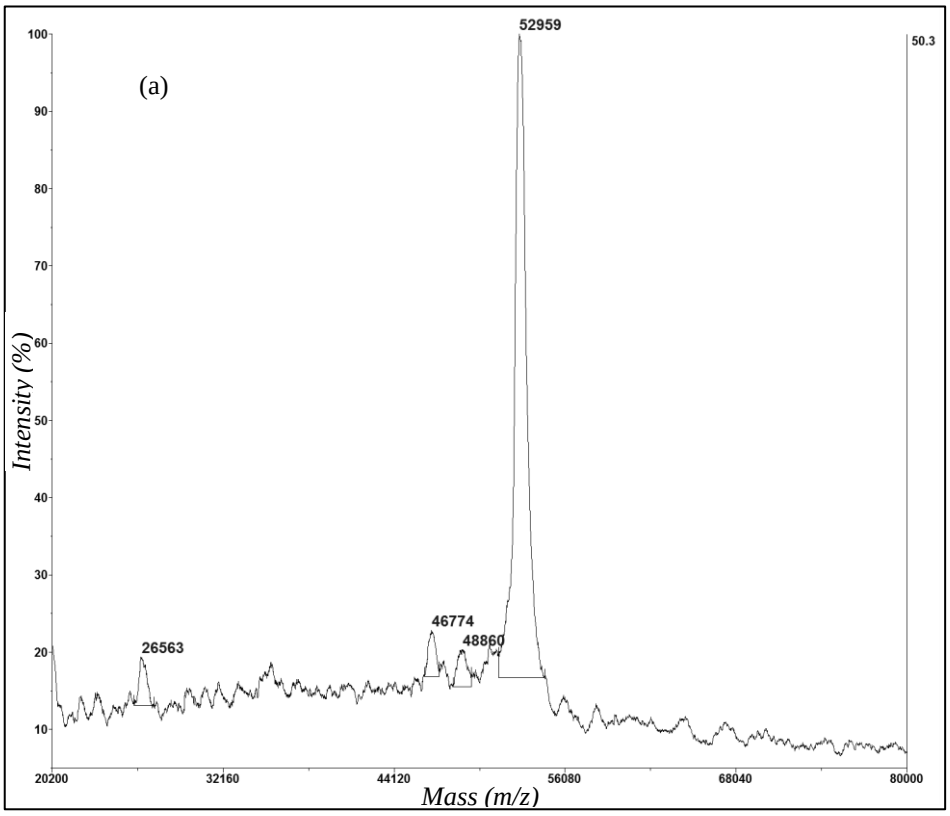

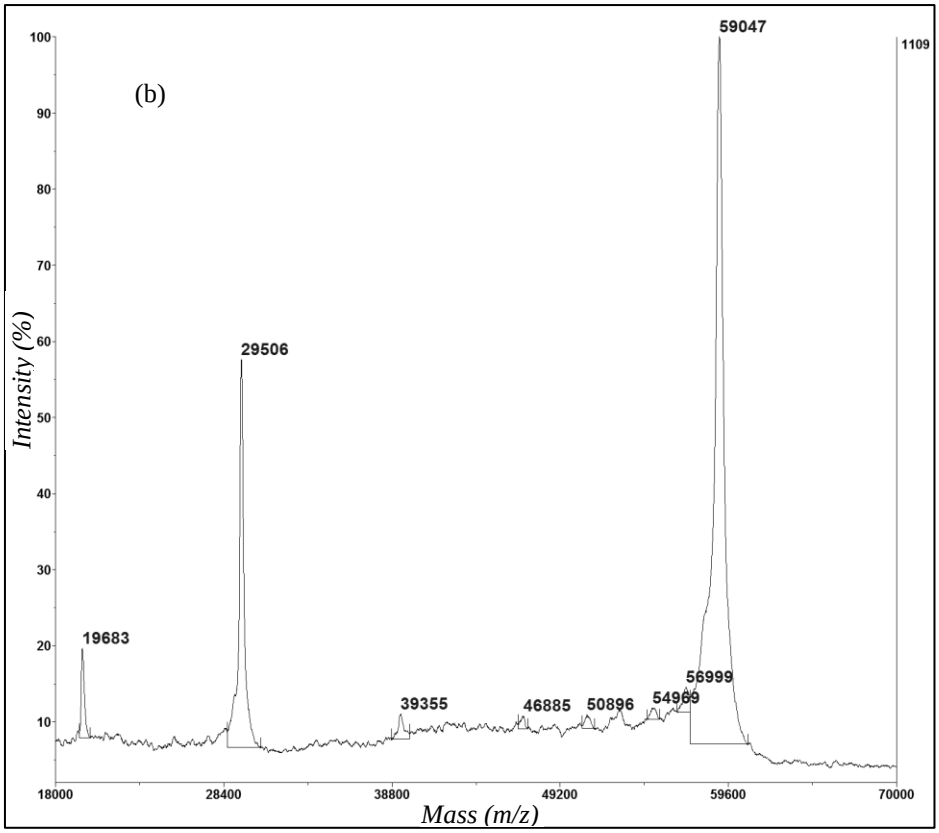

Fig.3.1: (a) MALDIT-TOF of $(SN_A15)_3E_{50}I_{60}$ ELP. (b) MALDIT-TOF of $(SN_A15)_6E_{50}I_{60}$ ELP.

Fig.3.1 shows the molecular weights of purified $(SN_A15)_3E_{50}I_{60}$ and $(SN_A15)_6E_{50}I_{60}$ ELPs that are 52.959 kDa and 59.047 kDa respectively. These values are in coincidence to theoretical values 52.92 kDa and 58.85 kDa for $(SN_A15)_3E_{50}I_6$ and $(SN_A15)_6E_{50}I_{60}$ ELPs respectively. The difference found between the theoretical and the experimental values are within the experimental error, confirming the rightness of the techniques employed to obtain the set of co-recombinamers. The analysis confirms that the polymer is nearly mono-disperse, that means all molecules nearly have the same molecular weight.

3.2 FTIR of polymer $E_{50}I_{60}$, $(SN_A15)_3E_{50}I_{60}$ and $(SN_A15)_6E_{50}I_{60}$ ELPs in solid state

Infrared spectroscopy is one of the most important analytical techniques available for characterization of material structure. The advantage of infrared spectroscopy is studying any sample in any state. Liquids, solution, pastes, powders, films, fibers, gases and surfaces can be studied by Infrared spectroscopy. Infrared spectroscopy technique based on the vibrations of the atoms within a molecule, where the spectrum is obtained by passing infrared radiation through a sample and determining what is the fraction is absorbed at particular energy. Every peak has its specific absorbed energy in the spectrum which is corresponding to the frequency of a vibration of a part of a sample molecule. Biological systems such as nucleic acids, peptides, proteins, lipids, bio-membranes, animal tissues, microbial, cells, plants and clinical samples can be studied by infrared spectroscopy.[133-138]

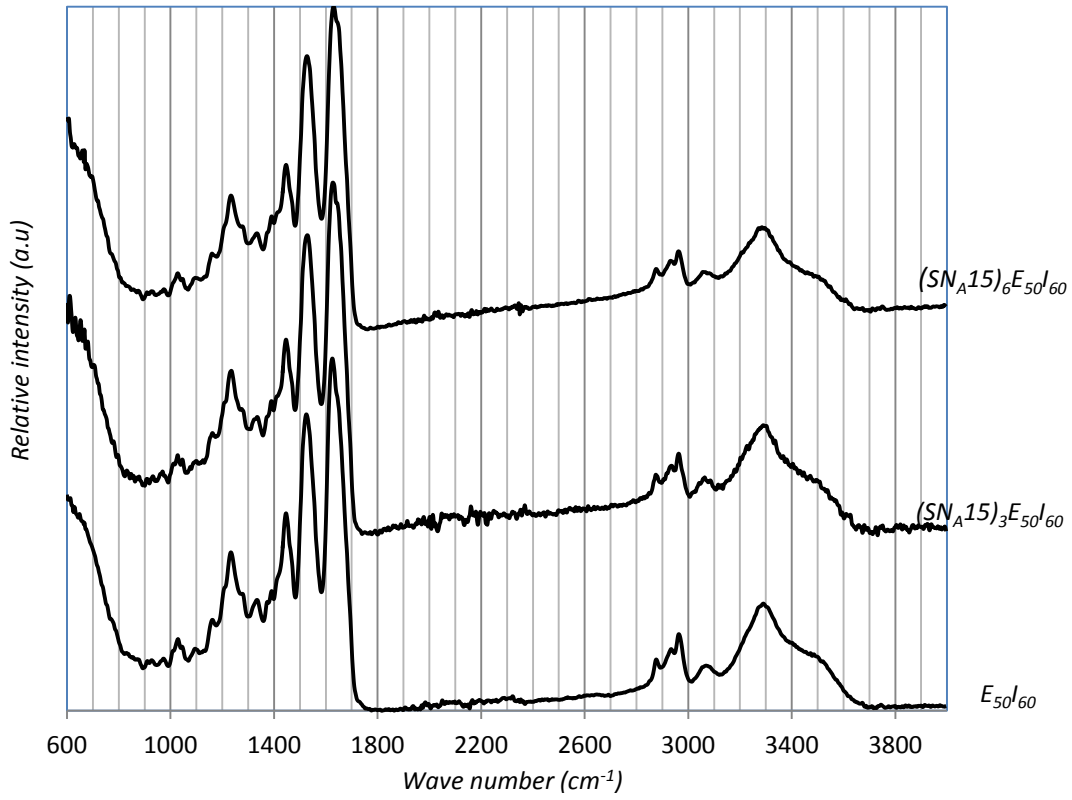

Fig.3.2: FTIR of $E_{50}I_{60}$, $(SN_A15)_3E_{50}I_{60}$ and $(SN_A15)_6E_{50}I_{60}$ ELPs in solid state.

Fig. 3.2 shows FTIR spectrum of $E_{50}I_{60}$, $(SN_A15)_3E_{50}I_{60}$ and $(SN_A15)_6E_{50}I_{60}$ ELPs. The band at 3500 is due to corresponding to the stretching vibrations of free OH, ν(OH), groups. The band at 3292 assigned to NH stretching (Amide A) while the band at 3072 is due to NH stretching (Amide B).[52, 139] The peak around 1628 cm^{-1} is assigned to (Amide I). Also the asymmetric starching mode of side chain COO^- groups, $\nu_{as}(COO^-)$ can absorb in the 1550 to 1610 cm^{-1} region.[140-144] The peak at 1521 cm^{-1} is due to CN stretching and NH bending (Amide II).[142, 144] The peaks between 1400-1500 cm^{-1} is attributed to absorptions arising from CH_3 asymmetric bending, CH_2 scissoring and COO^- symmetric stretching vibrations [Glu, $\nu_s(COO^-)$ 1404 cm^{-1}, Asp, $\nu_s(COO^-)$ 1402 cm^{-1}].[143-147] Amide III 1229-1301 cm^{-1} is due to CN stretching, NH bending.[141, 144]

3.3 Transition temperature of $E_{50}I_{60}$, $(SN_A15)_3E_{50}I_{60}$ and $(SN_A15)_6$ $E_{50}I_{60}$ ELPs as a function of pH

Calorimetry is a technique used for measuring thermal properties of materials to characterize the properties of materials under the effect of temperature and also used to determine the enthalpy associated with the interested process. [148-149]

The most popular calorimetry is the differential scanning calorimetry (DSC). In DSC, the physical properties of sample change are characterized by measuring the temperature against time; or in other words, DSC is a thermal analysis instrument that determines the temperature and heat flow associated with material transitions as a function of time and temperature.[150-151] DSC measures a heat quantity that is radiated or absorbed by the sample on the basis of a temperature difference the reference material and the sample material.[150-151] DSC can be classified into two types on the basis of operation mechanism: heat flux DSCs and power compensated DSCs.[151]

In the heat flux DSC, the sample material is enclosed in a pan and an empty reference pan are placed on a thermoelectric disk surrounded by a furnace.[151-152] The heat capacity of the sample produces a temperature difference between the sample and the reference pan that is measured by area thermocouples, and the heat flow is determined by the thermal equivalent of Ohm's law:

$$q=\Delta T/R$$

where q is the sample heat flow, ΔT is the temperature difference between the sample and the reference, and R is the resistance of thermoelectric disk.[152]

In power compensated DSC, the sample and the reference pan are placed in separate furnaces with separate heaters that are maintained at the same temperature.[151, 153] The difference in thermal power required to keep them at the same temperature is measured as a function of temperature or time.[151]

DSC is commonly used for determine thermal transition temperatures (T_t) and melting points of the samples that are in solutions, solid, or mixed phases such as suspensions.[154] DSC is capable of elucidating the factors that contribute to the stability of biomolecules.[155] For example, van der Waals, hydrophobic, electrostatic interactions, hydrogen bonds, hydration of the exposed residues, conformational entropy and the physical environment (such as pH, buffer, ionic strength, excipients).[156]

Fig.3.3 shows the behavior of the three polymers in mQ with increasing of pH. The transition temperature increase as the pH increase until about pH=7 and then decrease. The adding hydroxyl ions, OH^-, lead to COOH deprotonated of Glutamic acid E and have a negative charge COO^-. The formation more of COO^- in E block and also in $(SN_A15)_{3,6}$ fragment led to destructur of the hydrophobic hydration waters and exist a competition for hydration between apolar and polar residues, referred to as apolar-polar repulsive free energy of hydration[57]. This competition effect on the folding properties of polymer and then effect on the whole transition temperature of polymer.

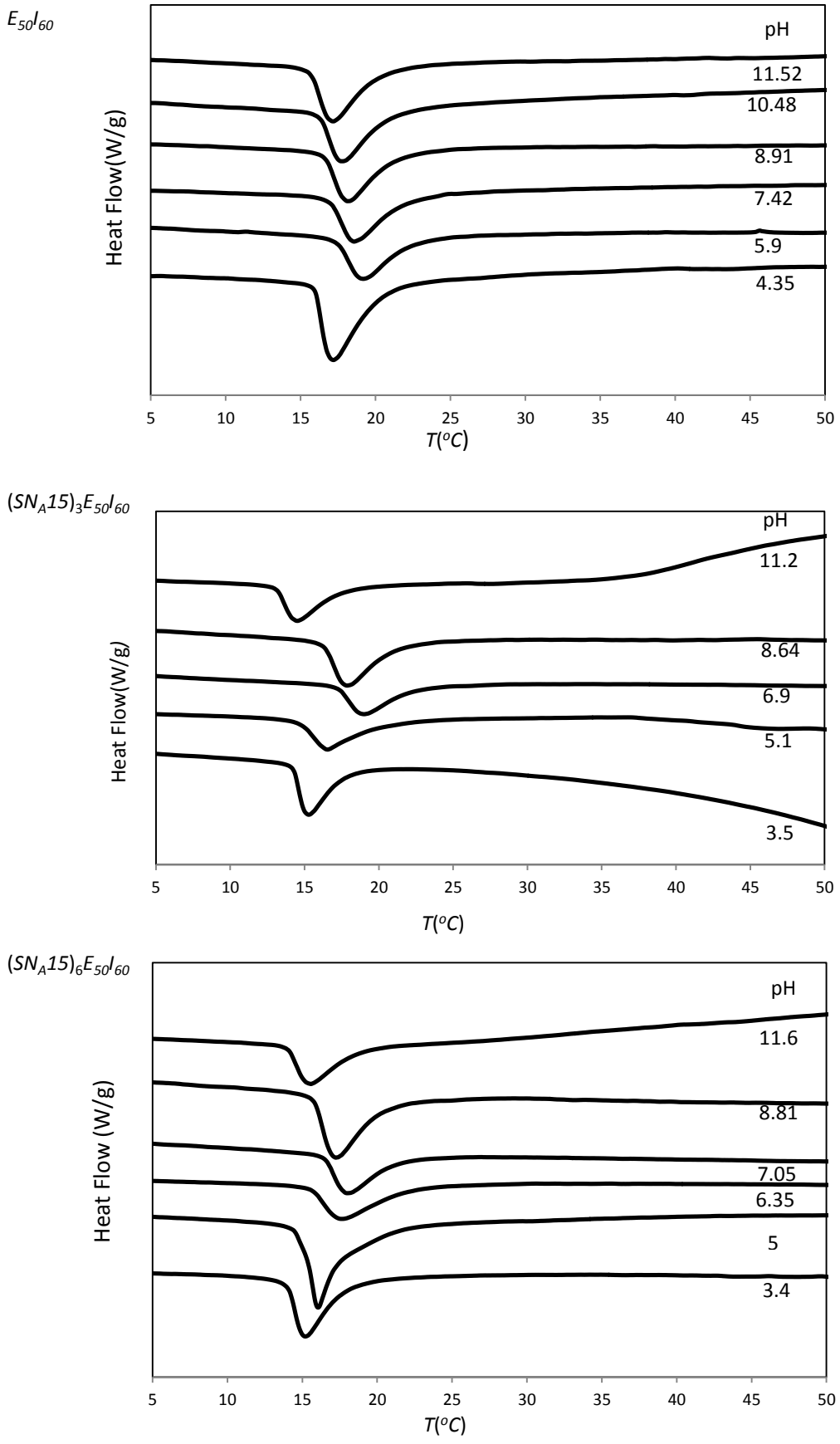

Fig.3.3: DSC of $E_{50}I_{60}$, $(SN_A15)_3E_{50}I_{60}$ and $(SN_A15)_6E_{50}I_{60}$ ELPs at concentration of 50mg/ml in mQ.

3.4 Dynamic Light Scattering of $E_{50}I_{60}$, $(SN_A15)_3E_{50}I_{60}$ and $(SN_A15)_6E_{50}I_{60}$ ELP nanoparticles

Light scattering spectroscopy is a non-destructive method for determining structure and dynamics of polymer solutions. Dynamic Light Scattering (DLS) is known as Photon Correlation Spectroscopy. Dynamic Light Scattering uses the intensity and the scattered light from a solution to characterize the size, shape, and interactions among the particles in a solution.[157-158] The autocorrelation of the temporal fluctuations in scattered light intensity due to the Brownian motion of particles in a dilute solution is evaluated to determine the intensity weighted average translational diffusion coefficient of the particles and then calculating the average hydrodynamic radius.[159]

When a coherent beam of a light incident on a dilute solution of macromolecules such as suspension of colloidal particles, polystyrene or latex microspheres, or proteins, the incident light beam scattered by each illuminated particle in all directions as a result of the solvent refractive index is different from that of the solute.[160-161]

If the light scattered from stationary particles, then the scattered light at each direction would be constant. But in reality, the particles in solution are in Brownian motion[162], that has led to fluctuations of the scattered intensity pattern on the detection plane. In Dynamic or quasi-elastic light scattering, the intensity fluctuation is measured rather than the average light intensity as in static light scattering. When incident light is scattered by a moving macromolecule or particle, the frequency of the scattered light will be higher or lower than the frequency of the original incident light due to the Doppler Effect depending on whether the particle moves away from or towards the detector.[160] Because the Brownian motion or diffusion of the particles in the suspension is the cause of the fluctuations so that the analyses of the intensity fluctuations in terms of a

time correlation function can provide information about the diffusion process.[163-165]

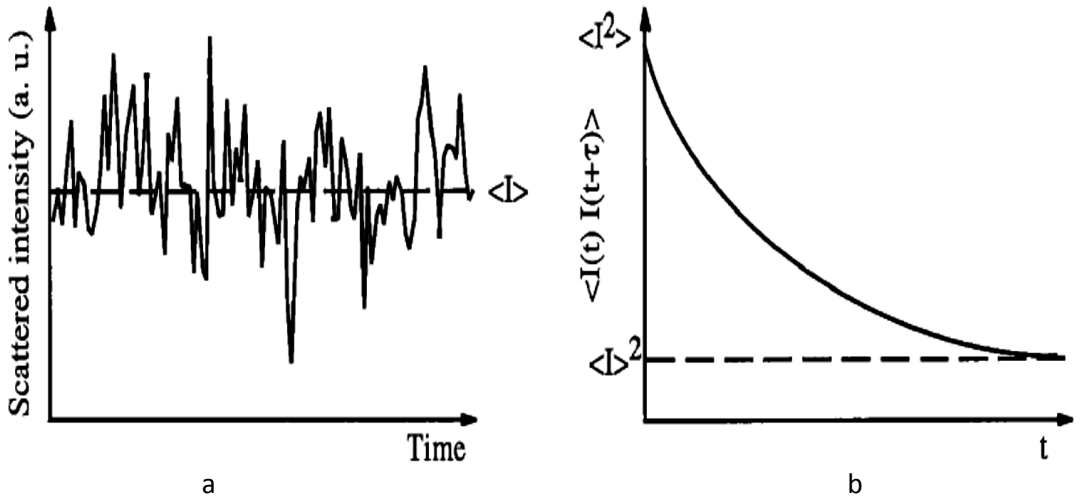

Fig. 3.4: Fluctuations in the scattered intensity (a) and the intensity auto-correlation function(b).[166]

Fig.3.4a show the time dependence of the scattered intensity that is the intensity values at two times separated by τ, I (t) and I (t + τ), in general, have different values. If τ is very small compared to the characteristic time of the fluctuations, I (t) and I (t + τ) will be very close, they are somehow correlated, while with increasing separation in time τ, the correlation will decrease. The correlation measured is so-called intensity auto-correlation function.[166]

$$\langle I(t_0)I(t_0+\tau)\rangle = \lim_{T\to\infty}\frac{1}{T}\int_{t_0}^{T} I(t)I(t+\tau)\,dt$$

The intensity correlation function and its relation to the temporal fluctuations in intensity is shown in Fig.3.4b. The correlations start with a maximum value of $\langle I^2\rangle$ and decay in the course of time $\langle I\rangle^2$ with characteristic decay time τ_a. In Dynamic light scattering, the normalized first-order electric filed correlation function used to determine the fluctuations in the amplitude of the electric field.[163, 166-167]

$$g_1(q,\tau) = \frac{\langle E_S(q,t)E_S^*(q,t+\tau)\rangle}{\langle |E_S(q,t)|^2\rangle}$$

This function is related to the diffusion coefficient of particles, but in Dynamic Light Scattering experiment, second-order intensity auto-correlation function is measured instead of electric fields.[159, 163, 166-168]

$$g_2(q,\tau) = \frac{\langle I_S(q,t)I_S(q,t+\tau)\rangle}{\langle |I_S(q,t)|^2\rangle}$$

that is related to the first-order electric field correlation function by the Siegert-relation:[163, 166, 169]

$$g_2(\tau) = 1 + b\, g_1(\tau)^2$$

Here, b is the coherence factor of the measurement instrument which is dependent on the detector area, the optical alignment and the scattering properties of the system. The determined diffusion coefficients can be converted to a hydrodynamic aggregate radius by Stokes-Einstein.[159, 163, 167]

$$D = \frac{k_B\, T}{6\pi\eta\, R_h}$$

where K_B is Boltzman's constant, T is temperature, η is the viscosity of the suspension medium and R_h is the hydrodynamic radius.

The solution behavior of thermally driven amphiphilic polymer $E_{50}I_{60}$, $(SN_A15)_3E_{50}I_{60}$ and $(SN_A15)_6E_{50}I_{60}$ ELPs were investigated in mQ at pH=7, as shown in Fig.3.5, which shows the formations of nanoparticles by hydrophobic interactions. The autocorrelation functions obtained from Dynamic Light Scattering at a scattering angle of 90° analyzed using the CONTIN fitting. Dynamic light scattering measurement was performed in mQ with a concentration of 25 μM of polymer $E_{50}I_{60}$, $(SN_A15)_3E_{50}I_{60}$ and $(SN_A15)_6E_{50}I_{60}$ ELPs as a function of the temperature to investigate the aggregation temperature.

The scattered light intensity can determine the inverse transition temperature of elastin like polymers. Before the inverse transition temperature, the chains of elastin like polymer are hydrated and extended. After this transition temperature, the polymer shows self-assembling behavior where the hydrophobic block form the core of the nanoparticles and the hydrophilic block forming the outer shell of nanoparticles.

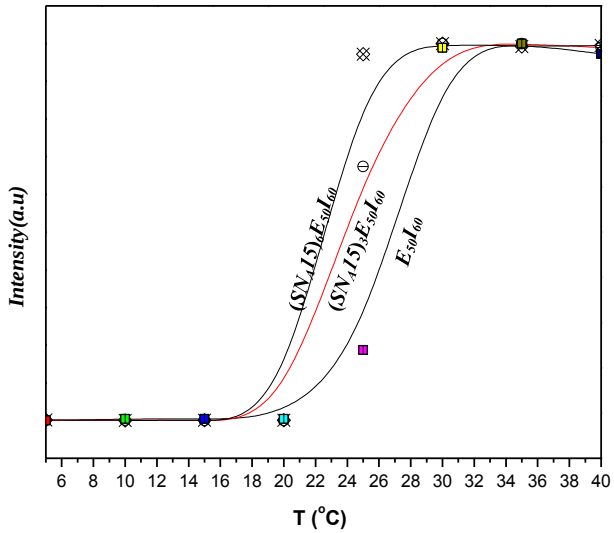

Fig.3.5: The scattered light of aqueous 25μM of $E_{50}I_{60}$, $(SN_A15)_3E_{50}I_{60}$, $(SN_A15)_6E_{50}I_{60}$ ELPs in mQ solution as a function of the temperature.

Fig.3.5 show that the transition temperature of aqueous 25μM of $E_{50}I_{60}$, $(SN_A15)_3E_{50}I_{60}$, $(SN_A15)_6E_{50}I_{60}$ ELPs in mQ solution are 27, 24, and 22.5 ^oC respectively. This means that as the increase the molecular weight leads to decrease transition temperature. It is found that these nanoparticles have around 200-300nm of radius in mQ after the transition temperature.

Chapter 4

Biomimetic Mineralization and Nanostructured Calcium Phosphate Formed by $(SN_A15)_3E_{50}I_{60}$ Elastin-like Polymer Nanoparticles

4.1 Biomimetic mineralization

The process by which the crystal nucleation and growth has been controlled by bioorganic molecules, that form inorganic minerals of skeletons, shells, teeth, etc., are called biomineralization.[170-171] In the biomineraliztion process, the inorganic precipitates are formed under full control of an organic tissue matrix.[171-172] The controlling biomineralization process involves manipulation of local concentrations of the precipitants, the presence of nucleating surfaces and the presence of inhibitors in solution that bind to a specific face on the growing mineral.[170-171] The mineralization processes are controlled by the catalytic action of acidic macromolecules such as proteins or polypeptides that have a high percentage of aspartic acid and phosphoserine residues in their sequences.[171, 173-176]

Salivary statherin is a highly acidic and has 43 amino acid residues that has a high affinity for calcium phosphate minerals that functions as an inhibitor of primary and secondary crystallization of the biomineral hydroxyapatite.[176-178] The primary role of the salivary statherin protein is to regulate the re-mineralization of hydroxyapatite (HAP) by nucleating and growing of hydroxyapatite. It is indicated that the sequence (1-15) of salivary statherin has a negative charge and a helical conformation.[176-178] The SN_A15 fragment is the first 15 amino acids from salivary statherin wherein the two phosphoserine amino acid residues at positions 2 and 3 have been substituted by L-Aspartic amino acid residues. This fragment has a negative charge and a helical structure in all solvents.[176] The positive calcium ions are bound to these negative charges

that gains positive surface charge for this amino acid, and then the negative phosphate groups in the fluid bind to the positive charge of the calcium ions to form a calcium phosphate nucleus, or embryo crystals.[176, 179] When the degree of supersaturation of calcium ions and phosphate groups are high, the Hydroxyapatite (HA) $Ca_{10}(PO_4)_6(OH)_2$ phase, which is thermodynamically more stable, is formed with intermediate precursor polymorphous such as Amorphous Calcium Phosphate (ACP), Octacalcium phosphate (OCP), $Ca_8H_2(PO_4)_6 \cdot 5H_2O$, or Dicalcium Phosphate Dehydrate (DCPD) $CaHPO_4 \cdot 2H_2O$ that are hydrolysis to HA.[179-181]

Biomimetic mineralization is a mimicking for synthetic minerals using advanced materials that have complex shapes, hierarchical organization and controlling size, shape and polymorph under the physiological conditions.[170-171, 180, 182] Therefore, amphiphilic organic molecules that show self-assembling properties are used to develop inorganic materials with complex architectural features in the nanometer range.[183-186] These amphiphilic organic molecules have been assembled into complex three-dimensional supramolecular aggregates that are used to form inorganic solids from soluble precursors.[183, 187-188] Synthetic and natural amphiphilic organic molecules such as surfactants, phospholipids and organic phase polymers are attractive for fabricating complex synthetic microstructures.[189-191] Organic phase macromolecules play several roles such as biomineralization modulators through amorphous calcium phosphate stabilization, mineralization acceleration, and mineraliztion inhabitation,[192-196] also as nanoscale adhesives[197-198] and as cell binding mediators[199].

In this bio mimicking mineralization work the elastin-like polymer $(SN_A15)_3E_{50}I_{60}$ ELP are used to form nanoparticles in Simulated Body Fluid (SBF) solution, where the hydrophobic block I_{60} is shielded by the hydrophilic block E_{50} which is attached by a peptide bond with the $(SN_A15)_3$ amino acid fragments that also hydrophilic. Where;

SN_A15= [DDDEEKFLRRIGRFG]

E_{50}= [$((VPGVG)_2$-(VPGEG)-$(VPGVG)_2)_{10}$]

I_{60}= [$(VPGIG)_{60}$]

$(SN_A15)_3E_{50}I_{60}$=

$(DDDEEKFLRRIGRFG)_3$ [$((VPGVG)_2(VPGEG)(VPGVG)_2)_{10}$] $(VPGIG)_{60}$],

4.2 Biomimetic mineralization method

SBF at pH=7.4 solution was prepared according to previously published procedures.[200] Polymer was dissolved in SBF of concentration was 0.5 mg/ml and stored at 4 ^oC overnight. Then, the solution was incubated at 37 ^oC for a one week. The SBF could not be exchanged because this would have led to loss of the elastin like polymer nanoparticles. Therefore, only pH values were checked. After one week, the solution is centrifuged and the precipitated are washed by ultrapure de-ionized water and then a sample from precipitation are suspended in ultrapure de-ionized water for Transmission electron Microscope (TEM) and Scanning transmission electron microscope (STEM) analysis. The rest of precipitation is dried and examined by Powder X-ray diffraction (XRD) patterns and FTIR spectrum.

4.3 Characterization of $(SN_A15)_3E_{50}I_{60}$ ELP nanoparticles and formed Nanostructured calcium phosphate:

The solution behavior of thermally driven amphiphilic $(SN_A15)_3E_{50}I_{60}$ ELP was investigated in SBF at pH=7.4 as shown in Fig.4.1, which shows the formations of nanoparticles due to hydrophobic interactions. The autocorrelation functions obtained from Dynamic Light Scattering at a scattering angle of 90° analyzed using the CONTIN fitting. Dynamic Light Scattering measurement was performed in SBF solution with a concentration of 25μM of $(SN_A15)_3E_{50}I_{60}$ ELP as a function of the temperature to investigate the

aggregation temperature. The scattered light intensity shows an initial temperature of aggregation about 14°C and the inverse transition temperature about 19°C. The polydispersity are nearly the same after the inverse transition temperature.

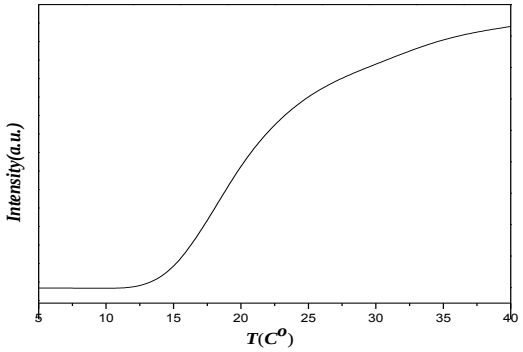

Fig.4.1: The scattered light of aqueous 25 μM of $(SN_A15)_3E_{50}I_{60}$ ELP in SBF solution as a function of the temperature.

Before the inverse transition temperature, the chains of elastin like polymer are hydrated and extended. After this transition temperature, the polymer shows self-assembling behavior where the hydrophobic block form the core of the nanoparticles and the hydrophilic block forming the outer shell of nanoparticles. These nanoparticles have a hydrodynamic radius of about 55 nm after the transition temperature.

Fig.4.2a shows representative STEM of $(SN_A15)_3E_{50}I_{60}$ ELP nanoparticles after one week of incubation of the former ELR dissolved (0.5 mg/ml) in SBF at 37°C. Table 4.1 shows the corresponding energy-dispersive X-ray spectroscopy (EDXS) data of $(SN_A15)_3E_{50}I_{60}$ ELP nanoparticles after one week of incubation of the former ELP dissolved (0.5 mg/ml) in SBF at 37°C calculated from spectrum in Fig.4.2b.

The detected elements are Ca, P, O and C, among which the C was revealed by $(SN_A15)_3E_{50}I_{60}$ ELP nanoparticles and grid supporting the nanoparticles which means that there are only calcium phosphates and a few of Mg.

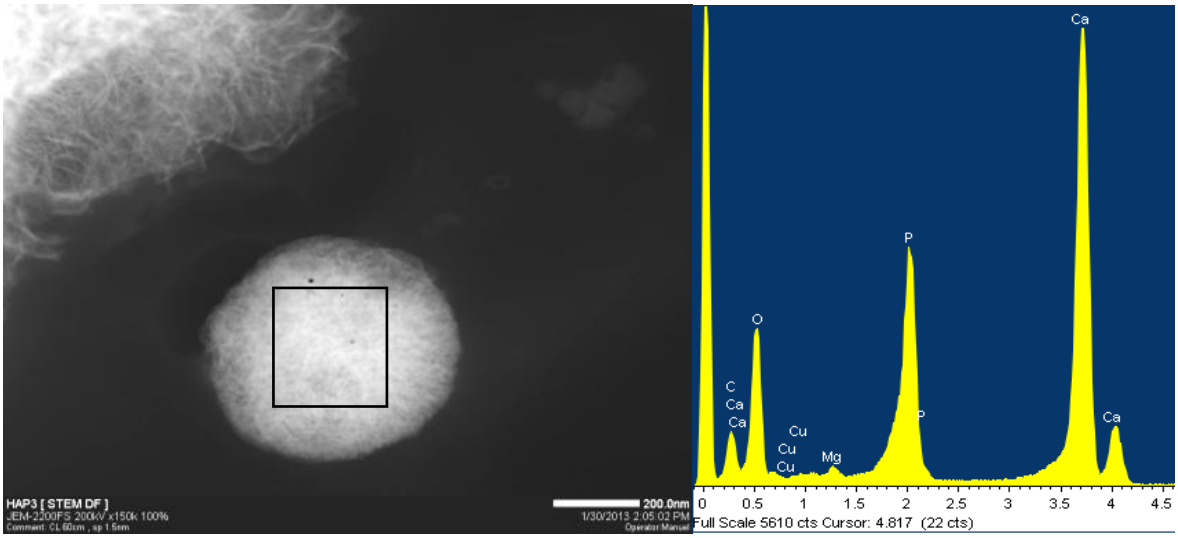

(a) (b)

Fig.4.2: (a) STEM of $(SN_A15)_3E_{50}I_{60}$ ELP nanoparticles after one week of incubation of the former ELP dissolved (0.5 mg/ml) in SBF at 37°C. (b) Elemental analysis over the indicted rectangular area over the nanoparticles in (a).

Table.4.1: The corresponding energy-dispersive X-ray spectroscopy (EDXS) data of $(SN_A15)_3E_{50}I_{60}$ ELP nanoparticles after one week of incubation of the former ELP dissolved (0.5 mg/ml) in SBF at 37°C calculated from spectrum in Fig.4.2b.

Element	Peak	Area	k	Abs	Weight%	Weight%	Atomic%
	Area	Sigma	factor	Corrn.		Sigma	
C K	4358	167	2.208	1.281	8.36	0.30	18.30
O K	12273	249	1.810	1.289	19.43	0.34	31.92
Mg K	1062	116	1.085	1.030	0.81	0.09	0.87
P K	28334	424	0.992	0.993	18.92	0.26	16.06
Ca K	73770	495	0.935	0.983	46.00	0.32	30.17
Cu K	7137	158	1.366	0.979	6.48	0.14	2.68

The Ca/P ratio on the nanoparticle is 1.87, in another nanoparticles Ca/P =0.95 as shown in Fig.4.3 and shown from calculated data Table.4.2. The difference in Ca/P ratio from the theoretical Ca/P ratio of HA is means there is a nonstochiometric apatite or ACP as seen from the broad X-ray diffraction peak.

Electron diffraction and HRTEM are used to examine the structure of the formed calcium phosphate on the $(SN_A15)_3E_{50}I_{60}$ ELP nanoparticles.

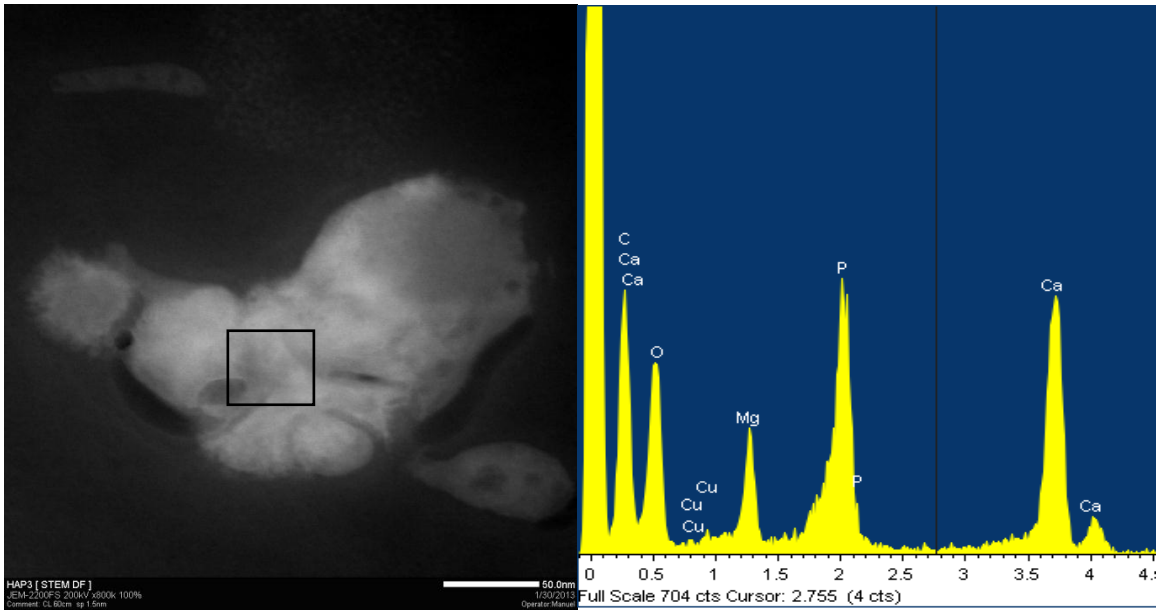

(a) (b)

Fig.4.3: (a) STEM of $(SN_A15)_3E_{50}I_{60}$ ELP nanoparticles after one week of incubation of the former ELP dissolved (0.5 mg/ml) in SBF at 37°C. (b) Elemental analysis over the indicted rectangular area over the nanoparticles in (a).

Table.4.2: The corresponding energy-dispersive X-ray spectroscopy (EDXS) data of $(SN_A15)_3E_{50}I_{60}$ ELP nanoparticles after one week of incubation of the former ELP dissolved (0.5 mg/ml) in SBF at 37°C calculated from spectrum in Fig.4.3b.

Element	Peak Area	Area Sigma	k factor	Abs Corrn.	Weight%	Weight% Sigma	Atomic%
C K	2343	106	2.208	1.270	29.83	1.04	50.79
O K	1553	90	1.810	1.206	15.39	0.80	19.67
Mg K	1196	71	1.085	1.027	6.05	0.36	5.09
P K	3438	147	0.992	0.992	15.35	0.62	10.14
Ca K	4552	127	0.935	0.980	18.95	0.55	9.67
Cu K	2384	87	1.366	0.976	14.43	0.53	4.64

The diffraction patterns show dots, regions or circles originating from the sample area illuminated by the electron beam depend on the material structure; nanocrystals show distinguished dots in the diffraction patterns, polycrystalline material show common centered circles and the amorphous materials show diffused circles.[201-202]

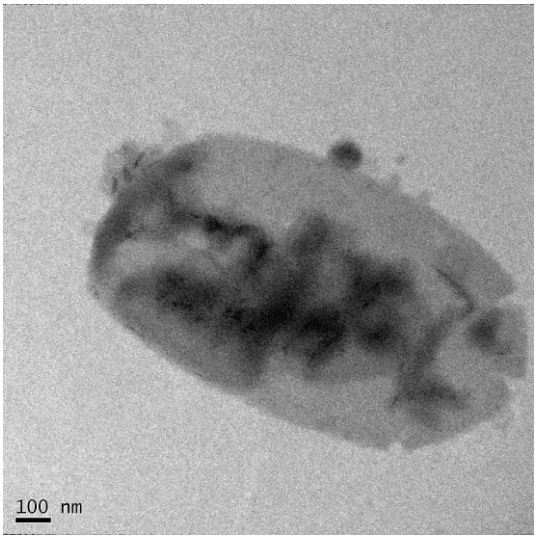

(a)

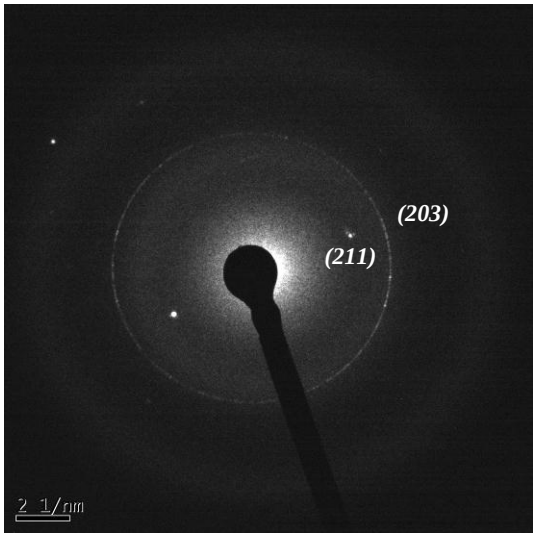

(b)

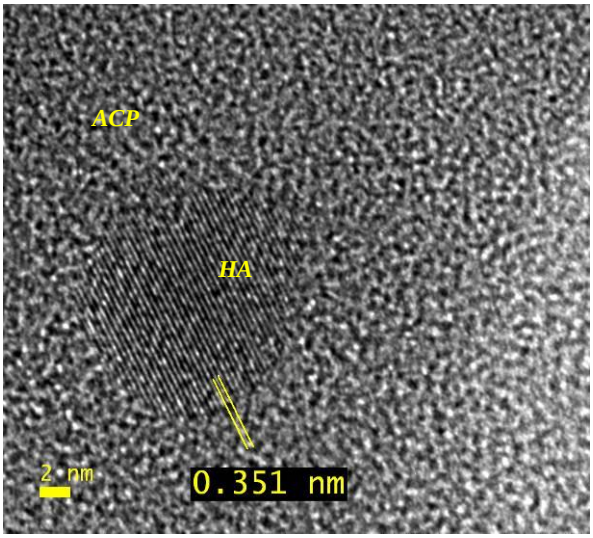

(c)

Fig.4.4: (a) TEM image of $(SN_A15)_3E_{50}I_{60}$ ELP nanoparticles after one week of incubation of the former ELP dissolved (0.5 mg/ml) in SBF at 37^{o}C. (b) Corresponding electron diffraction of formed calcium phosphate on nanoparticles. (c) HRTEM of HA nanosphere surrounded by ACP.

Fig.4.4a show a TEM image of $(SN_A15)_3E_{50}I_{60}$ ELP nanoparticles after one week of incubation of the former ELP dissolved (0.5 mg/ml) in SBF at 37^{o}C and Fig.4.4b show its corresponding diffraction pattern for nanosize crystalline nuclei of calcium phosphate which means these aggregates were polycrystallites. This ring corresponding to the HAP (203) plane, also the inner plane is due to the HAP (211) plane. Under HRTEM, Fig 4.4c, it is found that there is a nanosphere of the HA of about 14 nm that is surrounded by ACP precipitation. This nanosphere has d= 0.351nm that is matched to (201) plane of HAP.

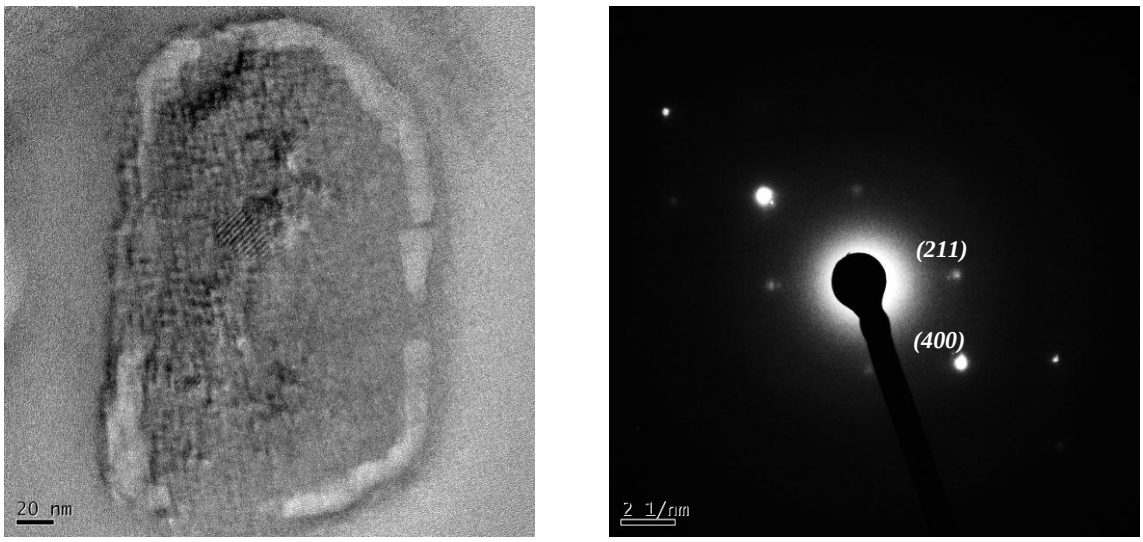

(a) (b)

Fig.4.5 (a) TEM image of $(SN_A15)_3E_{50}I_{60}$ ELP nanoparticles after one week of incubation of the former ELP dissolved (0.5 mg/ml) in SBF at 37^{o}C. (b) Corresponding electron diffraction of nanoparticles in (a).

Fig.4.5a shows TEM image of $(SN_A15)_3E_{50}I_{60}$ ELP nanoparticles after one week of incubation of the former ELP dissolved (0.5 mg/ml) in SBF at 37^{o}C and Fig.4.5b shows their corresponding electron diffraction. The electron diffraction is corresponding to (211) and (400) planes that are corresponding to HA.

Fig.4.6a show TEM image of a single crystal that is examined by the electron diffraction and the lattice fringes are corresponding to (002) or (302) and (321) faces of HA, Fig.4.6b. HRTEM of this single crystal, Fig.4.6c, reveals

that there are amorphous and crystalline regions of calcium phosphate, where crystallized units were surrounded and linked by ACP. This means that ACP is formed in the nucleating process and also it used for ordering the nanocrystallites of calcium phosphate to form more stable phases of calcium phosphate.

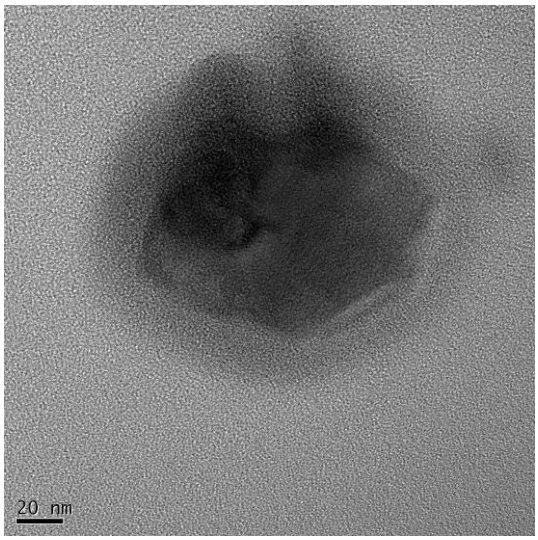

(a)

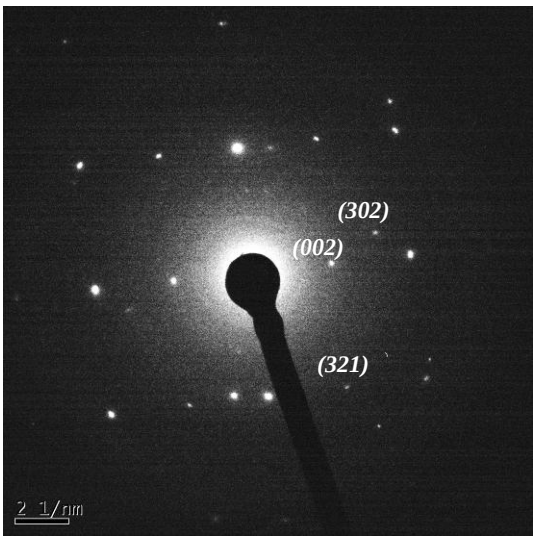

(b)

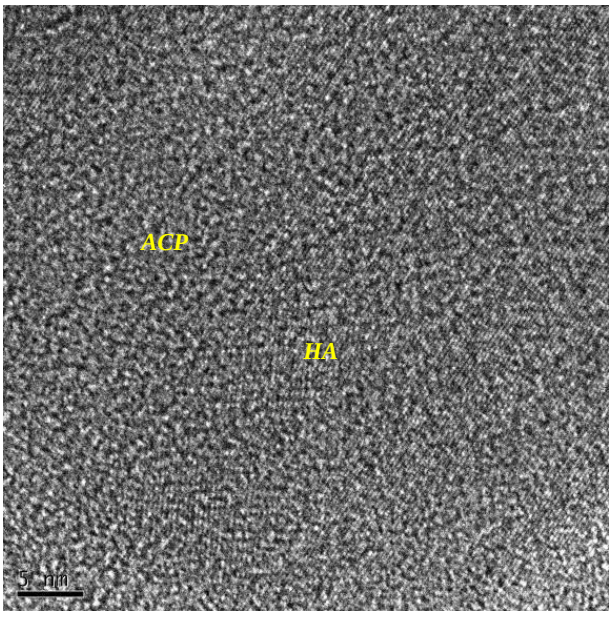

(c)

Fig.4.6: (a) TEM image of a formed nanocalcuim phosphate crystal. (b) Corresponding electron diffraction nanocrystal in (a). (c) HRTEM of nanocrystal in (a)

Fig.4.7 shows X-Ray diffraction of the dried solid residue found after one week of incubation of the former ELP dissolved (0.5 mg/ml) in SBF that show peaks at 27.698°, 30.254°, 31.873° and 34.468°. The existence of a broad band in the X-ray diffraction is due to the presence of ACP or from a collection of disordered crystals of nanometer dimensions.

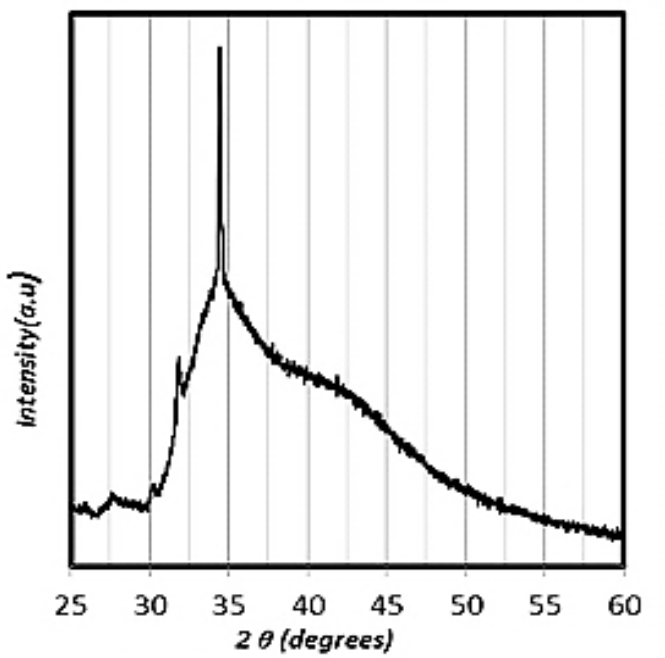

Fig.4.7: X-Ray diffraction of the dried solid residue found after one week of incubation of the former ELP dissolved (0.5 mg/ml) in SBF at 37°C.

The peak at 2θ=31.873° of d_{hkl}=0.281nm is near to the d_{hkl}=0.282nm of (211) plane of HA. While the intensive peak at 34.468° of d_{hkl}= 0.260nm is near to the d_{hkl}=0.261nm of (200) plane of DCPD and also near to the d_{hkl}= 0.263nm of (202) plane of HA phases. That is mean as well as the ACP, the DCPD may be formed as a precursor for HA formation and these peaks have d_{hkl} are near to the d_{hkl} of HA phases.[179, 201, 203]

Fig.4.8a show FTIR spectrum of $(SN_A15)_3E_{50}I_{60}$ ELP in solid state and Fig.4.8b show FTIR spectrum of the dried solid residue found after one week of incubation of the former ELP dissolved (0.5 mg/ml) in SBF at 37°C.with formed calcium phosphate. The peak around 1628 cm^{-1} is assigned to (Amide

I), also the asymmetric stretching mode of side chain COO^- groups, $\nu_{as}(COO^-)$ can absorb in the 1550 to 1610 cm^{-1} region.[140-144] The peak is shifted to higher wavelength 1650 cm^{-1} due to the effect of forming calcium phosphate on COO^-.

The peak at 1521 cm^{-1} is due to CN stretching and NH bending (Amide II)[142, 144] are shifted to higher wavelength 1531 cm^{-1} that is due to formed calcium phosphate. The peaks between 1400-1500 cm^{-1} is attributed to absorptions arising from CH_3 asymmetric bending, CH_2 scissoring and COO^- symmetric stretching vibrations [Glu, $\nu_s(COO^-)$ 1404 cm^{-1}, Asp, $\nu_s(COO^-)$ 1402 cm^{-1}].[143-147] The peak at 1405 cm^{-1} that is due to COO^- become more intense in the formed calcium phosphate with polymer, that is due to the binding of calcium phosphates. The region from 1229-1301 cm^{-1} is due to Amide III (CN stretching, NH bending).[141, 144]

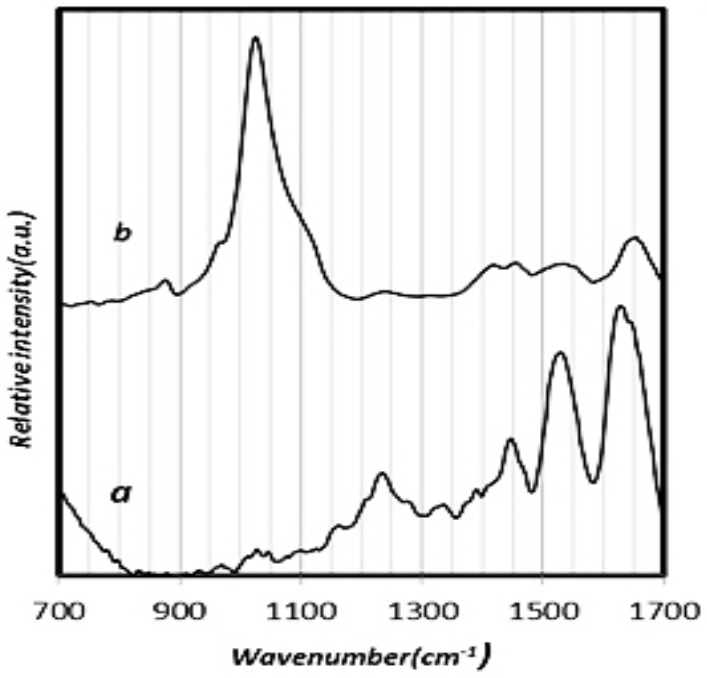

Fig.4.8: FTIR of (a) $(SN_A15)_3E_{50}I_{60}$ ELP in solid state and (b) the dried solid residue found after one week of incubation of the former ELP dissolved (0.5 mg/ml) in SBF at 37°C.

The region from 900-1200 cm^{-1} has been deconvoluted to four bands, 965, 1020, 1058, and 1096 cm^{-1}. Bands at 965, 1058, and 1096 cm^{-1} assigned to molecular vibrations of the phosphate (PO_4^{3-}) moiety in an apatitic/ stoichiometric environment of HA, while the band at 1020 cm^{-1} is attributable to

nonstoichiometry apatite.[204-205] This concept was supported by the lower Ca/P molar ratios measured by elemental analysis of formed calcium phosphate on the $(SN_A15)_3E_{50}I_{60}$ ELP nanoparticles.

Conclusion

The materials in nanosize have extraordinary properties that can be used in different applications. One of these materials is elastin-like polymers that are composed of natural amino acids. These materials have the properties of self-assembly and can form nanoaparticles in aqueous solutions at low temperatures. In this work $E_{50}I_{60}$ elastin like polymer has been recombined with the $(SN_A15)_{3,6}$ amino acid fragment of salivary statherin protein. This fragment (1-15) of salivary statherin has a negative charge and a helical conformation so that it can be used for biomemtic mineralization. These polymers form nanoparticles in aqueous solution at the temperature of the body such that the hydrophobic I_{50} block forms the core of the nanoparticle while the hydrophilic block E_{60} that recombined with the $(SN_A15)_{3,6}$ amino acid fragment forms the corona of the nanoparticles.

The transition temperature of $E_{50}I_{60}$, $(SN_A15)_3E_{50}I_{60}$, $(SN_A15)_6E_{50}I_{60}$ elastin-like polymers increase until pH=7 and then decrease for more pH. The increase of transition temperature is resulting from the formation more of COO^- in E block led to the destructur of the hydrophobic hydration waters and there is a competition for hydration between apolar and polar residues, referred to as apolar-polar repulsive free energy of hydration. This competition effect on the folding properties of polymer and then effect on the whole transition temperature of polymer.

Dynamic light scattering show that these polymer form nanoparticles of radius with 200 to 250 nm in mQ and about 50-60 nm in Simulated body Fluid solution. When the $(SN_A15)_3E_{50}I_{60}$ elastin-like polymer dissolves in SBF solution, nanoparticles of $(SN_A15)_3E_{50}I_{60}$ elastin-like polymer nanoparticles are used as a template for nucleating and forming nanocalcuim phosphate.

The formed HA and ACP have been studied by elemental analysis and by HRTEM which means that the ACP has been used as a precursor for HA

formation. The broad band in X-ray diffraction assigned to the formed ACP or polycrystallites of calcium phosphate. The formed calcium phosphate has an effect on the structure of the polymer that leads to the absorption peak of C=O and ν_{as} (COO^{-}) shifted to higher wavelength. Also the ν_{s} (COO^{-}) absorption peak become more intense due to the effect of calcium ions. The formed calcium phosphates are of regions that are stoichiometric and other regions that are nonstoichiometric calcium phosphate that is observed from FTIR spectroscopy and also by X-Ray diffraction.

References

1. Klimov, V. I., Mechanisms for Photogeneration and Recombination of Multiexcitons in Semiconductor Nanocrystals: Implications for Lasing and Solar Energy Conversion. *The Journal of Physical Chemistry B* **2006,** *110* (34), 16827-16845.
2. Park, C.; Yoon, J.; Thomas, E. L., Enabling nanotechnology with self assembled block copolymer patterns. *Polymer* **2003,** *44* (22), 6725-6760.
3. Hamley, I. W., *The Physics of Block Copolymers*. Oxford ; New York : Oxford University Press: 1998.
4. Elaissari, A., *Colloidal Polymers: Synthesis and Characterization.* . In: Surfactant Sci. Ser.: 2003; Vol. 1151.
5. Daniel, M.-C.; Astruc, D., Gold nanoparticles: assembly, supramolecular chemistry, quantum-size-related properties, and applications toward biology, catalysis, and nanotechnology. *Chemical Reviews-Columbus* **2004,** *104* (1), 293.
6. Martín, L.; Castro, E.; Ribeiro, A.; Alonso, M.; Rodríguez-Cabello, J. C., Temperature-Triggered Self-Assembly of Elastin-Like Block Co-Recombinamers:The Controlled Formation of Micelles and Vesicles in an Aqueous Medium. *Biomacromolecules* **2012,** *13* (2), 293-298.
7. Gohy, J.-F., Block Copolymer Micelles. In *Block Copolymers II*, Abetz, V., Ed. Springer Berlin Heidelberg: 2005; Vol. 190, pp 65-136.
8. Bamford, D. H., Virus structures: Those magnificent molecular machines. *Current Biology* **2000,** *10* (15), R558-R561.
9. Service, R. F., *Nanotechnology. Biology offers nanotechs a helping hand*. Science. ;298(5602):2322-3.: 2002 Dec 20.
10. Roduner, E., Nanoscopic materials size-dependent phenomena. **2006**.
11. Wang, Y.; Xia, Y., Bottom-Up and Top-Down Approaches to the Synthesis of Monodispersed Spherical Colloids of Low Melting-Point Metals. *Nano Letters* **2004,** *4* (10), 2047-2050.
12. Martin, L.; Alonso, M.; Moller, M.; Rodriguez-Cabello, J. C.; Mela, P., 3D microstructuring of smart bioactive hydrogels based on recombinant elastin-like polymers. *Soft Matter* **2009,** *5* (8), 1591-1593.
13. Feynman, R. P., there is plenty of room at the bottom *Engineering and Science* **1960,** *23*, 22–36.
14. LIEBER; #160; M., C., *Nanoscale science and technology: Building a big future from small things*. Materials Research Society: Warrendale, PA, ETATS-UNIS, 2003; Vol. 28, p 6.
15. Hecht, S., Welding, Organizing, and Planting Organic Molecules on Substrate Surfaces—Promising Approaches towards Nanoarchitectonics from the Bottom up. *Angewandte Chemie International Edition* **2003,** *42* (1), 24-26.
16. Rodríguez-Cabello, J. C.; Martín, L.; Alonso, M.; Arias, F. J.; Testera, A. M., "Recombinamers" as advanced materials for the post-oil age. *Polymer* **2009,** *50* (22), 5159-5169.
17. GEDDE, U. W., *Polymer physics*. Chapman & Hall. 2-6 Boundary Row, London SEl 8HN, UK 1995.
18. Bower, D. I., *An Introduction to Polymer Physics*. Cambridge University Press, New York: 2002.
19. Bueche, F., The Viscoelastic Properties of Plastics. *The Journal of Chemical Physics* **1954,** *22* (4), 603-609.
20. Demaid, A.; Spedding, V.; Zucker, J., Classification of plastics materials. *Artificial Intelligence in Engineering* **1996,** *10* (1), 9-20.

21. Maurer, J. J., CHAPTER 6 - Elastomers. In *Thermal Characterization of Polymeric Materials*, Edith, T., Ed. Academic Press: 1981; pp 571-708.
22. Petrović, Z. S.; Ferguson, J., Polyurethane elastomers. *Progress in Polymer Science* **1991,** *16* (5), 695-836.
23. Tam, H. Y.; Pun, C.-F. J.; Zhou, G.; Cheng, X.; Tse, M. L. V., Special structured polymer fibers for sensing applications. *Optical Fiber Technology* **2010,** *16* (6), 357-366.
24. Rodríguez Patino, J. M.; Pilosof, A. M. R., Protein–polysaccharide interactions at fluid interfaces. *Food Hydrocolloids* **2011,** *25* (8), 1925-1937.
25. Hardy, J. G.; Scheibel, T. R., Composite materials based on silk proteins. *Progress in Polymer Science* **2010,** *35* (9), 1093-1115.
26. Coyne, K. J.; Qin, X. X.; Waite, J. H., Extensible collagen in mussel byssus: a natural block copolymer. *Science* **1997,** *277* (5333), 1830-1832.
27. Magin, T. M.; Vijayaraj, P.; Leube, R. E., Structural and regulatory functions of keratins. *Experimental Cell Research* **2007,** *313* (10), 2021-2032.
28. Fuchs, E., Genetic disorders of keratins and their associated proteins. *Journal of Dermatological Science* **1996,** *13* (3), 181-192.
29. Shukla, R. K.; Tiwari, A., Carbohydrate polymers: Applications and recent advances in delivering drugs to the colon. *Carbohydrate Polymers* **2012,** *88* (2), 399-416.
30. Wei, Y.; Cheng, F., Synthesis and aggregates of cellulose-based hydrophobically associating polymer. *Carbohydrate Polymers* **2007,** *68* (4), 734-739.
31. Liu, H.; Xie, F.; Yu, L.; Chen, L.; Li, L., Thermal processing of starch-based polymers. *Progress in Polymer Science* **2009,** *34* (12), 1348-1368.
32. Wilson, W. A.; Hughes, W. E.; Tomamichel, W.; Roach, P. J., Increased glycogen storage in yeast results in less branched glycogen. *Biochemical and Biophysical Research Communications* **2004,** *320* (2), 416-423.
33. Szathmary, E., Why are there four letters in the genetic alphabet? *Nat Rev Genet* **2003,** *4* (12), 995-1001.
34. Martin, A. L.; Davies, M. C.; Rackstraw, B. J.; Roberts, C. J.; Stolnik, S.; Tendler, S. J. B.; Williams, P. M., Observation of DNA–polymer condensate formation in real time at a molecular level. *FEBS letters* **2000,** *480* (2), 106-112.
35. Rajamani, S.; Vlassov, A.; Benner, S.; Coombs, A.; Olasagasti, F.; Deamer, D., Lipid-assisted Synthesis of RNA-like Polymers from Mononucleotides. *Orig Life Evol Biosph* **2008,** *38* (1), 57-74.
36. Lu, Y.; Freeland, S., On the evolution of the standard amino-acid alphabet. *Genome biology* **2006,** *7* (1), 102.
37. Lu, Y.; Freeland, S. J., A quantitative investigation of the chemical space surrounding amino acid alphabet formation. *Journal of Theoretical Biology* **2008,** *250* (2), 349-361.
38. Weber, A.; Miller, S., Reasons for the occurrence of the twenty coded protein amino acids. *J Mol Evol* **1981,** *17* (5), 273-284.
39. Cox, D. L. N. a. M. M., *Lehninger Principles of Biochemistry* Fourth Edition ed.; 2004.
40. A., B. W., Origins of molecular chirality. *Ponnamperuma C (ed) Exobiology. North-Holland, Amsterdam, p 170* **1972**.
41. Nordén, B., The asymmetry of life. *J Mol Evol* **1978,** *11* (4), 313-332.
42. Brack, A.; Spach, G., β-structures of polypeptides with L- and D-residues. *J Mol Evol* **1980,** *15* (3), 231-238.
43. Richardson, J. S., The Anatomy and Taxonomy of Protein Structure. In *Advances in Protein Chemistry*, C.B. Anfinsen, J. T. E.; Frederic, M. R., Eds. Academic Press: 1981; Vol. Volume 34, pp 167-339.

44. Creighton, T. E., *Proteins : structures and molecular properties*. W.H. Freeman: New York, 1993.
45. Creighton, T. E., Experimental studies of protein folding and unfolding. *Progress in Biophysics and Molecular Biology* **1979,** *33* (0), 231-297.
46. Corey, R. B., X-Ray Studies of Amino Acids and Peptides. In *Advances in Protein Chemistry*, Anson, M. L.; John, T. E., Eds. Academic Press: 1948; Vol. Volume 4, pp 385-406.
47. Esposito, L.; Vitagliano, L.; Zagari, A.; Mazzarella, L., Pyramidalization of backbone carbonyl carbon atoms in proteins. *Protein science : a publication of the Protein Society* **2000,** *9* (10), 2038-2042.
48. Cozzone, A. J., Proteins: Fundamental Chemical Properties. In *eLS*, John Wiley & Sons, Ltd: 2001.
49. Ohgo, K.; Niemczura, W. P.; Ashida, J.; Okonogi, M.; Asakura, T.; Kumashiro, K. K., Heterogeneity in the Conformation of Valine in the Elastin Mimetic (LGGVG)6 as Shown by Solid-State 13C NMR Spectroscopy. *Biomacromolecules* **2006,** *7* (12), 3306-3310.
50. Guantieri, V.; Grando, S.; Pandolfo, L.; Tamburro, A. M., Synthetic fragments and analogues of elastin. I. The synthesis. *Biopolymers* **1990,** *29* (4-5), 845-854.
51. Karle, I. L.; Urry, D. W., Crystal structure of cyclic (APGVGV)2, an analog of elastin, and a suggested mechanism for elongation/contraction of the molecule. *Biopolymers* **2005,** *77* (4), 198-204.
52. Schmidt, P.; Dybal, J.; Rodriguez-Cabello, J. C.; Reboto, V., Role of Water in Structural Changes of Poly(AVGVP) and Poly(GVGVP) Studied by FTIR and Raman Spectroscopy and ab Initio Calculations. *Biomacromolecules* **2005,** *6* (2), 697-706.
53. Martino, M.; Tamburro, A. M., Chemical synthesis of cross-linked poly(KGGVG), an elastin-like biopolymer. *Biopolymers* **2001,** *59* (1), 29-37.
54. Spezzacatena, C.; Perri, T.; Guantieri, V.; Sandberg, Lawrence B.; Mitts, T. F.; Tamburro, Antonio M., Classical Synthesis of and Structural Studies on a Biologically Active Heptapeptide and a Nonapeptide of Bovine Elastin. *European Journal of Organic Chemistry* **2002,** *2002* (1), 95-103.
55. Urry, D. W., Free energy transduction in polypeptides and proteins based on inverse temperature transitions. *Progress in Biophysics and Molecular Biology* **1992,** *57* (1), 23-57.
56. Urry, D. W., Molecular Machines: How Motion and Other Functions of Living Organisms Can Result from Reversible Chemical Changes. *Angewandte Chemie International Edition in English* **1993,** *32* (6), 819-841.
57. Urry, D. W., Physical Chemistry of Biological Free Energy Transduction As Demonstrated by Elastic Protein-Based Polymers†. *The Journal of Physical Chemistry B* **1997,** *101* (51), 11007-11028.
58. Meyer, D. E.; Chilkoti, A., Quantification of the Effects of Chain Length and Concentration on the Thermal Behavior of Elastin-like Polypeptides. *Biomacromolecules* **2004,** *5* (3), 846-851.
59. Ghoorchian, A.; Holland, N. B., Molecular Architecture Influences the Thermally Induced Aggregation Behavior of Elastin-like Polypeptides. *Biomacromolecules* **2011,** *12* (11), 4022-4029.
60. Rodriguez-Cabello, J. C., Smart elastin-like polymers. *Adv Exp Med Biol* **2004,** *553*, 45-57.
61. Rodríguez-Cabello, J. C.; Alonso, M.; Guiscardo, L.; Reboto, V.; Girotti, A., Amplified Photoresponse of a p-Phenylazobenzene Derivative of an Elastin-like Polymer by α-

Cyclodextrin: The Amplified ΔTt Mechanism. *Advanced Materials* **2002,** *14* (16), 1151-1154.

62. Urry, D. W.; Peng, S. Q.; Hayes, L. C.; McPherson, D.; Xu, J.; Woods, T. C.; Gowda, D. C.; Pattanaik, A., Engineering protein-based machines to emulate key steps of metabolism (biological energy conversion). *Biotechnology and bioengineering* **1998,** *58* (2-3), 175-190.
63. Reiersen, H.; Clarke, A. R.; Rees, A. R., Short elastin-like peptides exhibit the same temperature-induced structural transitions as elastin polymers: implications for protein engineering. *Journal of Molecular Biology* **1998,** *283* (1), 255-264.
64. Rodríguez-Cabello, J. C.; Prieto, S.; Reguera, J.; Arias, F. J.; Ribeiro, A., Biofunctional design of elastin-like polymers for advanced applications in nanobiotechnology. *Journal of Biomaterials Science, Polymer Edition* **2007,** *18* (3), 269-286.
65. Arévalo, M. d. C. G. RECOMBINAMERS ELASTIN-LIKE FOR ADVANCED BIOMEDICAL APPLICATIONS: TISSUE ENGINEERING, GENE DELIVERY AND NANOVACCINES. Valladolid, Valladolid, 2012.
66. Carlos Rodríguez-Cabello, J.; Reguera, J.; Girotti, A.; Alonso, M.; Testera, A. M., Developing functionality in elastin-like polymers by increasing their molecular complexity: the power of the genetic engineering approach. *Progress in Polymer Science* **2005,** *30* (11), 1119-1145.
67. Urry, D. W.; Trapane, T. L.; Prasad, K. U., Phase-structure transitions of the elastin polypentapeptide–water system within the framework of composition–temperature studies. *Biopolymers* **1985,** *24* (12), 2345-2356.
68. Urry, D. W.; Peng; Xu, J.; McPherson, D. T., Characterization of Waters of Hydrophobic Hydration by Microwave Dielectric Relaxation. *Journal of the American Chemical Society* **1997,** *119* (5), 1161-1162.
69. Cook, W. J.; Einspahr, H.; Trapane, T. L.; Urry, D. W.; Bugg, C. E., Crystal structure and conformation of the cyclic trimer of a repeat pentapeptide of elastin, cyclo-(L-valyl-L-prolylglycyl-L-valylglycyl)3. *Journal of the American Chemical Society* **1980,** *102* (17), 5502-5505.
70. Urry, D. W.; Shaw, R. G.; Prasad, K. U., Polypentapeptide of elastin: Temperature dependence of ellipticity and correlation with elastomeric force. *Biochemical and Biophysical Research Communications* **1985,** *130* (1), 50-57.
71. Urry, D. W.; Trapane, T. L.; Iqbal, M.; Venkatachalam, C. M.; Prasad, K. U., Carbon-13 NMR relaxation studies demonstrate an inverse temperature transition in the elastin polypentapeptide. *Biochemistry* **1985,** *24* (19), 5182-5189.
72. Yamaoka, T.; Tamura, T.; Seto, Y.; Tada, T.; Kunugi, S.; Tirrell, D. A., Mechanism for the Phase Transition of a Genetically Engineered Elastin Model Peptide (VPGIG)40 in Aqueous Solution. *Biomacromolecules* **2003,** *4* (6), 1680-1685.
73. Urry, D. W.; Gowda, D. C.; Parker, T. M.; Luan, C.-H.; Reid, M. C.; Harris, C. M.; Pattanaik, A.; Harris, R. D., Hydrophobicity scale for proteins based on inverse temperature transitions. *Biopolymers* **1992,** *32* (9), 1243-1250.
74. Urry, D. W., Elastic molecular machines in metabolism and soft-tissue restoration. *Trends in Biotechnology* **1999,** *17* (6), 249-257.
75. Woods, T. C.; Urry, D. W., Controlled release of phosphorothioates by protein-based polymers. *Drug Deliv* **2006,** *13* (4), 253-9.
76. Urry, D. W.; Luan, C. H.; Parker, T. M.; Gowda, D. C.; Prasad, K. U.; Reid, M. C.; Safavy, A., Temperature of polypeptide inverse temperature transition depends on mean residue hydrophobicity. *Journal of the American Chemical Society* **1991,** *113* (11), 4346-4348.

77. Urry, D. W.; Haynes, B.; Zhang, H.; Harris, R. D.; Prasad, K. U., Mechanochemical coupling in synthetic polypeptides by modulation of an inverse temperature transition. *Proc Natl Acad Sci U S A* **1988,** *85* (10), 3407-11.
78. Reguera, J.; Lagarón, J. M.; Alonso, M.; Reboto, V.; Calvo, B.; Rodríguez-Cabello, J. C., Thermal Behavior and Kinetic Analysis of the Chain Unfolding and Refolding and of the Concomitant Nonpolar Solvation and Desolvation of Two Elastin-like Polymers. *Macromolecules* **2003,** *36* (22), 8470-8476.
79. Urry, D. W.; Urry, K. D.; Szaflarski, W.; Nowicki, M., Elastic-contractile model proteins: Physical chemistry, protein function and drug design and delivery. *Adv Drug Deliv Rev* **2010,** *62* (15), 1404-55.
80. Li, B.; Daggett, V., The molecular basis of the temperature- and pH-induced conformational transitions in elastin-based peptides. *Biopolymers* **2003,** *68* (1), 121-9.
81. Phlip, D., Supramolecular chemistry: Concepts and perspectives. By J.-M. Lehn, VCH, Weinheim 1995, x, 271 pp., softcover, DM 58.00, ISBN 3-527-2931 1-6. *Advanced Materials* **1996,** *8* (10), 866-868.
82. Whitesides, G. M.; Simanek, E. E.; Mathias, J. P.; Seto, C. T.; Chin, D.; Mammen, M.; Gordon, D. M., Noncovalent Synthesis: Using Physical-Organic Chemistry To Make Aggregates. *Accounts of Chemical Research* **1995,** *28* (1), 37-44.
83. Lawrence, D. S.; Jiang, T.; Levett, M., Self-Assembling Supramolecular Complexes. *Chemical Reviews* **1995,** *95* (6), 2229-2260.
84. Philp, D.; Stoddart, J. F., Self-Assembly in Natural and Unnatural Systems. *Angewandte Chemie International Edition in English* **1996,** *35* (11), 1154-1196.
85. Sauvage, J.-P.; Atwood, J. L.; Lehn, J. M., *Comprehensive supramolecular chemistry. Volume 9, Templating, self-assembly, and self-organization*. Pergamon: New York, 1996.
86. Olenyuk, B.; Whiteford, J. A.; Fechtenkotter, A.; Stang, P. J., Self-assembly of nanoscale cuboctahedra by coordination chemistry. *Nature* **1999,** *398* (6730), 796-799.
87. Whitesides, G. M.; Grzybowski, B., Self-Assembly at All Scales. *Science* **2002,** *295* (5564), 2418-2421.
88. Desiraju, G. R., *Crystal engineering: the design of organic solids*. Elsevier: 1989.
89. De Rosa, C.; Park, C.; Thomas, E. L.; Lotz, B., Microdomain patterns from directional eutectic solidification and epitaxy. *Nature* **2000,** *405* (6785), 433-437.
90. Aizenberg, J.; Black, A. J.; Whitesides, G. M., Control of crystal nucleation by patterned self-assembled monolayers. *Nature* **1999,** *398* (6727), 495-498.
91. Whitesides, G. M.; Boncheva, M., Beyond molecules: Self-assembly of mesoscopic and macroscopic components. *Proceedings of the National Academy of Sciences* **2002,** *99* (8), 4769-4774.
92. Shapiro, J. A., Thinking about bacterial populations as multicellular organisms. *Annu Rev Microbiol* **1998,** *52*, 81-104.
93. Jakubith, S.; Rotermund, H. H.; Engel, W.; von Oertzen, A.; Ertl, G., Spatiotemporal concentration patterns in a surface reaction: Propagating and standing waves, rotating spirals, and turbulence. *Physical Review Letters* **1990,** *65* (24), 3013-3016.
94. Ikkala, O.; ten Brinke, G., Hierarchical self-assembly in polymeric complexes: towards functional materials. *Chem Commun* **2004,** *7* (19), 2131-7.
95. Carlsen, A.; Lecommandoux, S., Self-assembly of polypeptide-based block copolymer amphiphiles. *Current Opinion in Colloid & Interface Science* **2009,** *14* (5), 329-339.
96. Bates, F. S.; Fredrickson, G. H., Block Copolymer Thermodynamics: Theory and Experiment. *Annual Review of Physical Chemistry* **1990,** *41* (1), 525-557.
97. Bates, F. S.; Fredrickson, G. H., Block Copolymers---Designer Soft Materials. *Physics Today* **1999,** *52* (2), 32-38.

98. Auschra, C.; Stadler, R., New ordered morphologies in ABC triblock copolymers. *Macromolecules* **1993,** *26* (9), 2171-2174.
99. Goldacker, T.; Abetz, V.; Stadler, R.; Erukhimovich, I.; Leibler, L., Non-centrosymmetric superlattices in block copolymer blends. *Nature* **1999,** *398* (6723), 137-139.
100. Abetz, V.; Goldacker, T., Formation of superlattices via blending of block copolymers. *Macromolecular Rapid Communications* **2000,** *21* (1), 16-34.
101. Hadjichristidis, N.; Pitsikalis, M.; Pispas, S.; Iatrou, H., Polymers with Complex Architecture by Living Anionic Polymerization. *Chemical Reviews* **2001,** *101* (12), 3747-3792.
102. Muthukumar, M.; Ober, C. K.; Thomas, E. L., Competing Interactions and Levels of Ordering in Self-Organizing Polymeric Materials. *Science* **1997,** *277* (5330), 1225-1232.
103. Adams, J.; Gronski, W., LC side chain AB-block copolymers with an amorphous A-block and a liquid-crystalline B-block. *Die Makromolekulare Chemie, Rapid Communications* **1989,** *10* (10), 553-557.
104. Fischer, H.; Poser, S., Liquid crystalline block and graft copolymers. *Acta Polymerica* **1996,** *47* (10), 413-428.
105. Stupp, S. I.; LeBonheur, V.; Walker, K.; Li, L. S.; Huggins, K. E.; Keser, M.; Amstutz, A., Supramolecular Materials: Self-Organized Nanostructures. *Science* **1997,** *276* (5311), 384-389.
106. Osuji, C.; Zhang, Y.; Mao, G.; Ober, C. K.; Thomas, E. L., Transverse Cylindrical Microdomain Orientation in an LC Diblock Copolymer under Oscillatory Shear. *Macromolecules* **1999,** *32* (22), 7703-7706.
107. Lee, M.; Cho, B. K.; Zin, W. C., Supramolecular structures from rod-coil block copolymers. *Chemical Reviews* **2001,** *101* (12), 3869-3892.
108. Jenekhe, S. A.; Chen, X. L., Self-Assembly of Ordered Microporous Materials from Rod-Coil Block Copolymers. *Science* **1999,** *283* (5400), 372-375.
109. Hamley, I. W., Nanotechnology with Soft Materials. *Angewandte Chemie International Edition* **2003,** *42* (15), 1692-1712.
110. Babloyantz, A., *Molecules, Dynamics and Life: An Introduction to Self-Organization of Matter*. John Wiley & Sons: New York, 1986.
111. Debelle, L.; Alix, A. J. P.; Wei, S. M.; Jacob, M.-P.; Huvenne, J.-P.; Berjot, M.; Legrand, P., The secondary structure and architecture of human elastin. *European Journal of Biochemistry* **1998,** *258* (2), 533-539.
112. Parks, W. C.; Pierce, R. A.; Lee, K. A.; Mecham, R. P., Elastin. In *Advances in Molecular and Cell Biology*, Bittar, E. E., Ed. Elsevier: 1993; Vol. Volume 6, pp 133-181.
113. Mithieux, S. M.; Weiss, A. S., Elastin. In *Advances in Protein Chemistry*, David, A. D. P.; John, M. S., Eds. Academic Press: 2005; Vol. Volume 70, pp 437-461.
114. Bellingham, C. M.; Keeley, F. W., Self-ordered polymerization of elastin-based biomaterials. *Current Opinion in Solid State and Materials Science* **2004,** *8* (2), 135-139.
115. Li, B.; Daggett, V., Molecular basis for the extensibility of elastin. *J Muscle Res Cell Motil* **2002,** *23* (5-6), 561-573.
116. Urry, D. W., On the molecular mechanisms of elastin coacervation and coacervate calcification. *Faraday Discussions of the Chemical Society* **1976,** *61* (0), 205-212.
117. Rodríguez-Hernández, J.; Chécot, F.; Gnanou, Y.; Lecommandoux, S., Toward 'smart' nano-objects by self-assembly of block copolymers in solution. *Progress in Polymer Science* **2005,** *30* (7), 691-724.

118. Riess, G., Micellization of block copolymers. *Progress in Polymer Science* **2003,** *28* (7), 1107-1170.
119. Förster, S.; Plantenberg, T., From Self-Organizing Polymers to Nanohybrid and Biomaterials. *Angewandte Chemie International Edition* **2002,** *41* (5), 688-714.
120. Register, R. A., Materials science: Continuity through dispersity. *Nature* **2012,** *483* (7388), 167-168.
121. Martin, L.; Arias, F. J.; Alonso, M.; Garcia-Arevalo, C.; Rodriguez-Cabello, J. C., Rapid micropatterning by temperature-triggered reversible gelation of a recombinant smart elastin-like tetrablock-copolymer. *Soft Matter* **2010,** *6* (6), 1121-1124.
122. Simnick, A. J.; Lim, D. W.; Chow, D.; Chilkoti, A., Biomedical and Biotechnological Applications of Elastin-Like Polypeptides. *Polymer Reviews* **2007,** *47* (1), 121-154.
123. Ribeiro, A. J. A. M. Functionality Development In Systems Based On Elastin-like Recombinamers: From Nano-objects To Macrogels. VALLADOLID, VALLADOLID-SPAIN, 2010.
124. Cappello, J.; Crissman, J.; Dorman, M.; Mikolajczak, M.; Textor, G.; Marquet, M.; Ferrari, F., Genetic engineering of structural protein polymers. *Biotechnology Progress* **1990,** *6* (3), 198-202.
125. Sinsheimer, R. L., Recombinant Dna. *Annual Review of Biochemistry* **1977,** *46* (1), 415-438.
126. Birnboim, H. C.; Doly, J., A rapid alkaline extraction procedure for screening recombinant plasmid DNA. *Nucleic Acids Res* **1979,** *7* (6), 1513-23.
127. Vogelstein, B.; Gillespie, D., Preparative and analytical purification of DNA from agarose. *Proceedings of the National Academy of Sciences* **1979,** *76* (2), 615-619.
128. Laemmli, U. K., Cleavage of Structural Proteins during the Assembly of the Head of Bacteriophage T4. *Nature* **1970,** *227* (5259), 680-685.
129. Lee, C.; Levin, A.; Branton, D., Copper staining: a five-minute protein stain for sodium dodecyl sulfate-polyacrylamide gels. *Anal Biochem* **1987,** *166* (2), 308-12.
130. Räder, H. J.; Spickermann, J.; Müllen, K., MALDI-TOF mass spectrometry in polymer analytics, 1. Monitoring the polymer-analogous sulfonation reaction of polystyrene. *Macromolecular Chemistry and Physics* **1995,** *196* (12), 3967-3978.
131. Nielen, M. W. F., Maldi time-of-flight mass spectrometry of synthetic polymers. *Mass Spectrometry Reviews* **1999,** *18* (5), 309-344.
132. Bahr, U.; Deppe, A.; Karas, M.; Hillenkamp, F.; Giessmann, U., Mass spectrometry of synthetic polymers by UV-matrix-assisted laser desorption/ionization. *Analytical Chemistry* **1992,** *64* (22), 2866-2869.
133. Gremlich, H. U.; Yan, B., *Infrared and Raman Spectroscopy of Biological Materials*. Marcel Dekker Incorporated: 2001.
134. Gaskell, S. J., Biomedical applications of spectroscopy. Edited by R. J. H. Clark and R. E. Hester. Advances in spectroscopy, volume 25. Wiley, Chichester 1996. ISBN 0-471-95918-9 Price £125. *Rapid Communications in Mass Spectrometry* **1996,** *10* (15), 2002-2002.
135. Jackson, M.; Moore, D. J.; Mantsch, H. H.; Mendelsohn, R., Vibrational Spectroscopy of Membranes. In *Handbook of Vibrational Spectroscopy*, John Wiley & Sons, Ltd: 2006.
136. Kalasinsky, V. F., Biomedical Applications of Infrared and Raman Microscopy. *Applied Spectroscopy Reviews* **1996,** *31* (3), 193-249.
137. Naumann, D., FT-INFRARED AND FT-RAMAN SPECTROSCOPY IN BIOMEDICAL RESEARCH. *Applied Spectroscopy Reviews* **2001,** *36* (2-3), 239-298.
138. Petrich, W., MID-INFRARED AND RAMAN SPECTROSCOPY FOR MEDICAL DIAGNOSTICS. *Applied Spectroscopy Reviews* **2001,** *36* (2-3), 181-237.

139. Kong, J.; Yu, S., Fourier transform infrared spectroscopic analysis of protein secondary structures. *Acta Biochim Biophys Sin* **2007,** *39* (8), 549-59.
140. Susi, H.; Michael Byler, D., Protein structure by Fourier transform infrared spectroscopy: Second derivative spectra. *Biochemical and Biophysical Research Communications* **1983,** *115* (1), 391-397.
141. Tamm, L. K.; Tatulian, S. A., Infrared spectroscopy of proteins and peptides in lipid bilayers. *Q Rev Biophys* **1997,** *30* (4), 365-429.
142. Krimm, S.; Bandekar, J., Vibrational spectroscopy and conformation of peptides, polypeptides, and proteins. *Adv Protein Chem* **1986,** *38*, 181-364.
143. Chirgadze, Y. N.; Fedorov, O. V.; Trushina, N. P., Estimation of amino acid residue side-chain absorption in the infrared spectra of protein solutions in heavy water. *Biopolymers* **1975,** *14* (4), 679-694.
144. Stuart, B. H., *Infrared spectroscopy: fundamentals and applications*. Wiley: 2004.
145. Barth, A., Infrared spectroscopy of proteins. *Biochimica et Biophysica Acta (BBA) - Bioenergetics* **2007,** *1767* (9), 1073-1101.
146. Lui, K.; Jackson, M.; Sowa, M. G.; Ju, H.; Dixon, I. M.; Mantsch, H. H., Modification of the extracellular matrix following myocardial infarction monitored by FTIR spectroscopy. *Biochim Biophys Acta* **1996,** *1* (2), 73-7.
147. Venyaminov, S. Y.; Kalnin, N. N., Quantitative IR spectrophotometry of peptide compounds in water (H2O) solutions. I. Spectral parameters of amino acid residue absorption bands. *Biopolymers* **1990,** *30* (13-14), 1243-1257.
148. Höhne, G.; Hemminger, W.; Flammersheim, H. J., *Differential scanning calorimetry: an introduction for practitioners*. Springer-Verlag: 1996.
149. Privalov, P. L.; Potekhin, S. A., Scanning microcalorimetry in studying temperature-induced changes in proteins. *Methods Enzymol* **1986,** *131*, 4-51.
150. DT, H., *Biological Thermodynamics*. Cambridge University Press: Cambridge, UK, 2008.
151. Haines PJ, R., M, Wilburn FW, Differential thermal analysis and differential scanning calorimetry. In *Handbook of Thermal Analysis and Calorimetry*, ME, B., Ed. Elsevier Science BV: The Netherlands, 1998; Vol. 1, pp 279 –361.
152. Danley, R. L., New heat flux DSC measurement technique. *Thermochimica Acta* **2002,** *395* (1–2), 201-208.
153. Zucca, N.; Erriu, G.; Onnis, S.; Longoni, A., An analytical expression of the output of a power-compensated DSC in a wide temperature range. *Thermochimica Acta* **2004,** *413* (1–2), 117-125.
154. Harding, S. E.; Chowdhry, B. Z., Differential scanning microcalorimetry. In *Protein-Ligand Interactions: Hydrodynamics and Calorimetry*, Cooper A, N. M., Walood A., Ed. Oxford University Press, Incorporated: 2001; pp 287–318.
155. Van Holde, K. K. E.; Johnson, W. C.; Ho, P. S., Thermodynamics and biochemistry. In *Principles Of Physical Biochemistry*, Pearson Education, Limited: 2006; pp 72–105.
156. A, C., Microcalorimetry of protein-DNA interactions. In *DNA-Protein Interactions*, Travers A, B. M., Ed. Oxford University Press: Oxford, UK, 2000; pp 125–139.
157. Brown, W.; Schillen, K.; Hvidt, S., Triblock copolymers in aqueous solution studied by static and dynamic light scattering and oscillatory shear measurements: influence of relative block sizes. *The Journal of Physical Chemistry* **1992,** *96* (14), 6038-6044.
158. Dorshow, R.; Briggs, J.; Bunton, C. A.; Nicoli, D. F., Dynamic light scattering from cetyltrimethylammonium bromide micelles. Intermicellar interactions at low ionic strengths. *The Journal of Physical Chemistry* **1982,** *86* (13), 2388-2395.

159. Schillen, K.; Brown, W.; Johnsen, R. M., Micellar Sphere-to-Rod Transition in an Aqueous Triblock Copolymer System. A Dynamic Light Scattering Study of Translational and Rotational Diffusion. *Macromolecules* **1994,** *27* (17), 4825-4832.
160. Chu, B., Laser Light Scattering. *Annual Review of Physical Chemistry* **1970,** *21* (1), 145-174.
161. Berne, B. J.; Pecora, R., Laser Light Scattering from Liquids. *Annual Review of Physical Chemistry* **1974,** *25* (1), 233-253.
162. Clark, N. A.; Lunacek, J. H.; Benedek, G. B., A Study of Brownian Motion Using Light Scattering. *American Journal of Physics* **1970,** *38* (5), 575-585.
163. Štěpánek, P.; Koňák, Č., Quasielastic light scattering from polymers, colloids and gels. *Advances in Colloid and Interface Science* **1984,** *21* (3–4), 195-274.
164. Berne, B. J.; Pecora, R., *Dynamic light scattering: with applications to chemistry, biology, and physics*. Wiley: 1976.
165. Buffle, J.; van Leeuwen, H. P., *Environmental particles*. Lewis Publishers: 1993.
166. Urban, C. Development of Fiber Optic Based Dynamic Light Scattering for a Characterization of Turbid Suspensions. Karlsruhe, Germany, 1999.
167. Kätzel, U.; Vorbau, M.; Stintz, M.; Gottschalk-Gaudig, T.; Barthel, H., Dynamic Light Scattering for the Characterization of Polydisperse Fractal Systems: II. Relation between Structure and DLS Results. *Particle & Particle Systems Characterization* **2008,** *25* (1), 19-30.
168. Pecora, R., Spectral Distribution of Light Scattered by Monodisperse Rigid Rods. *The Journal of Chemical Physics* **1968,** *48* (9), 4126-4128.
169. Siegert, A. J. F.; Laboratory, M. I. o. T. R., *On the Fluctuations in Signals Returned by Many Independently Moving Scatterers*. Radiation Laboratory, Massachusetts Institute of Technology: 1943.
170. Xu, A.-W.; Ma, Y.; Colfen, H., Biomimetic mineralization. *Journal of Materials Chemistry* **2007,** *17* (5), 415-449.
171. Calvert, P.; Rieke, P., Biomimetic Mineralization in and on Polymers. *Chemistry of Materials* **1996,** *8* (8), 1715-1727.
172. Perry, C. C.; Keeling-Tucker, T., Biosilicification: the role of the organic matrix in structure control. *J. Biol. Inorg. Chem.* **2000,** *5* (5), 537-550.
173. Campbell, A. A.; Nancollas, G. H., The mineralization of calcium phosphate on separated salivary protein films. *Colloids and Surfaces* **1991,** *54* (0), 33-40.
174. Peytcheva, A.; Cölfen, H.; Schnablegger, H.; Antonietti, M., Calcium phosphate colloids with hierarchical structure controlled by polyaspartates. *Colloid Polym Sci* **2002,** *280* (3), 218-227.
175. Benesch, J.; Mano, J. F.; Reis, R. L., Proteins and their peptide motifs in acellular apatite mineralization of scaffolds for tissue engineering. *Tissue Eng Part B Rev* **2008,** *14* (4), 433-45.
176. Raj, P. A.; Johnsson, M.; Levine, M. J.; Nancollas, G. H., Salivary statherin. Dependence on sequence, charge, hydrogen bonding potency, and helical conformation for adsorption to hydroxyapatite and inhibition of mineralization. *Journal of Biological Chemistry* **1992,** *267* (9), 5968-76.
177. Schwartz, S.; Hay, D.; Schluckebier, S., Inhibition of calcium phosphate precipitation by human salivary statherin: Structure-activity relationships. *Calcif Tissue Int* **1992,** *50* (6), 511-517.
178. Stayton, P. S.; Drobny, G. P.; Shaw, W. J.; Long, J. R.; Gilbert, M., Molecular Recognition at the Protein-Hydroxyapatite Interface. *Critical Reviews in Oral Biology & Medicine* **2003,** *14* (5), 370-376.

179. Combes, C.; Rey, C., Amorphous calcium phosphates: synthesis, properties and uses in biomaterials. *Acta Biomater* **2010,** *6* (9), 3362-78.
180. Schweizer, S.; Taubert, A., Polymer-controlled, bio-inspired calcium phosphate mineralization from aqueous solution. *Macromol Biosci* **2007,** *7* (9-10), 1085-99.
181. Kumta, P. N.; Sfeir, C.; Lee, D. H.; Olton, D.; Choi, D., Nanostructured calcium phosphates for biomedical applications: novel synthesis and characterization. *Acta Biomater* **2005,** *1* (1), 65-83.
182. Meyers, M. A.; Chen, P.-Y.; Lin, A. Y.-M.; Seki, Y., Biological materials: structure and mechanical properties. *Progress in Materials Science* **2008,** *53* (1), 1-206.
183. Patti, A., Molecular Modeling of Self-assembling Hybrid Materials (PhD Thesis). *arXiv preprint arXiv:1006.0945* **2010**.
184. Miller, S. A.; Ding, J. H.; Gin, D. L., Nanostructured materials based on polymerizable amphiphiles. *Current Opinion in Colloid & Interface Science* **1999,** *4* (5), 338-347.
185. Nesterova, M.; Moreau, J.; Banfield, J. F., Model biomimetic studies of templated growth and assembly of nanocrystalline FeOOH. *Geochimica et cosmochimica acta* **2003,** *67* (6), 1185-1195.
186. Cong, H.-P.; Yu, S.-H., Self-assembly of functionalized inorganic–organic hybrids. *Current Opinion in Colloid & Interface Science* **2009,** *14* (2), 71-80.
187. Cui, H.; Webber, M. J.; Stupp, S. I., Self-assembly of peptide amphiphiles: From molecules to nanostructures to biomaterials. *Peptide Science* **2010,** *94* (1), 1-18.
188. Lin, Y.; Mao, C., Bio-inspired supramolecular self-assembly towards soft nanomaterials. *Frontiers of materials science* **2011,** *5* (3), 247-265.
189. Hartgerink, J. D.; Beniash, E.; Stupp, S. I., Self-Assembly and Mineralization of Peptide-Amphiphile Nanofibers. *Science* **2001,** *294* (5547), 1684-1688.
190. Cölfen, H.; Yu, S.-H., Biomimetic Mineralization/Synthesis of Mesoscale Order in Hybrid Inorganic–Organic Materials via Nanoparticle Self-Assembly. *MRS bulletin* **2005,** *30* (10), 727-735.
191. Khoo, H. S.; Lin, C.; Huang, S.-H.; Tseng, F.-G., Self-assembly in micro-and nanofluidic devices: A review of recent efforts. *Micromachines* **2011,** *2* (1), 17-48.
192. Deshpande, A. S.; Beniash, E., Bio-inspired Synthesis of Mineralized Collagen Fibrils. *Cryst Growth Des* **2008,** *8* (8), 3084-3090.
193. Price, P. A.; Toroian, D.; Lim, J. E., Mineralization by inhibitor exclusion: the calcification of collagen with fetuin. *J Biol Chem* **2009,** *284* (25), 17092-101.
194. Weiner, S.; Wagner, H. D., THE MATERIAL BONE: Structure-Mechanical Function Relations. *Annual Review of Materials Science* **1998,** *28* (1), 271-298.
195. Nudelman, F.; Pieterse, K.; George, A.; Bomans, P. H. H.; Friedrich, H.; Brylka, L. J.; Hilbers, P. A. J.; de With, G.; Sommerdijk, N. A. J. M., The role of collagen in bone apatite formation in the presence of hydroxyapatite nucleation inhibitors. *Nat Mater* **2010,** *9* (12), 1004-1009.
196. Olszta, M. J.; Cheng, X.; Jee, S. S.; Kumar, R.; Kim, Y.-Y.; Kaufman, M. J.; Douglas, E. P.; Gower, L. B., Bone structure and formation: A new perspective. *Materials Science and Engineering: R: Reports* **2007,** *58* (3), 77-116.
197. Fantner, G. E.; Hassenkam, T.; Kindt, J. H.; Weaver, J. C.; Birkedal, H.; Pechenik, L.; Cutroni, J. A.; Cidade, G. A.; Stucky, G. D.; Morse, D. E., Sacrificial bonds and hidden length dissipate energy as mineralized fibrils separate during bone fracture. *Nature materials* **2005,** *4* (8), 612-616.
198. Smith, B. L.; Schäffer, T. E.; Viani, M.; Thompson, J. B.; Frederick, N. A.; Kindt, J.; Belcher, A.; Stucky, G. D.; Morse, D. E.; Hansma, P. K., Molecular mechanistic origin of the toughness of natural adhesives, fibres and composites. *Nature* **1999,** *399* (6738), 761-763.

199. Giachelli, C. M.; Steitz, S., Osteopontin: a versatile regulator of inflammation and biomineralization. *Matrix Biology* **2000,** *19* (7), 615-622.
200. Oyane, A.; Kim, H. M.; Furuya, T.; Kokubo, T.; Miyazaki, T.; Nakamura, T., Preparation and assessment of revised simulated body fluids. *J Biomed Mater Res A* **2003,** *65* (2), 188-95.
201. Tao, J.; Pan, H.; Zeng, Y.; Xu, X.; Tang, R., Roles of amorphous calcium phosphate and biological additives in the assembly of hydroxyapatite nanoparticles. *J Phys Chem B* **2007,** *111* (47), 13410-8.
202. Ji, H.; Ponton, C. B.; Marquis, P. M., Microstructural characterization of hydroxyapatite coating on titanium. *J Mater Sci: Mater Med* **1992,** *3* (4), 283-287.
203. Olszta, M. J.; Cheng, X.; Jee, S. S.; Kumar, R.; Kim, Y.-Y.; Kaufman, M. J.; Douglas, E. P.; Gower, L. B., Bone structure and formation: A new perspective. *Materials Science and Engineering: R: Reports* **2007,** *58* (3–5), 77-116.
204. Rey, C.; Shimizu, M.; Collins, B.; Glimcher, M. J., Resolution-enhanced fourier transform infrared spectroscopy study of the environment of phosphate ion in the early deposits of a solid phase of calcium phosphate in bone and enamel and their evolution with age: 2. Investigations in thev 3 PO4 domain. *Calcif Tissue Int* **1991,** *49* (6), 383-388.
205. Gadaleta, S. J.; Paschalis, E. P.; Betts, F.; Mendelsohn, R.; Boskey, A. L., Fourier transform infrared spectroscopy of the solution-mediated conversion of amorphous calcium phosphate to hydroxyapatite: New correlations between X-ray diffraction and infrared data. *Calcif Tissue Int* **1996,** *58* (1), 9-16.